
POLITECNICO DI TORINO

Master of Science Program Energy and Nuclear Engineering



Master Thesis

Innovative technique to estimate the performance of a photovoltaic generator using the parameters of the single diode model equivalent circuit

Supervisors:

Prof. Filippo Spertino

Prof. Vicente Munoz

Ing. Gabriele Malgaroli

Prof. Slawomir Gulkowski

Ing. Alessandro Ciocia

Candidate:

Andrea Scaiola

July 2019

Academic year 2018/2019.

Ringrazio il Prof. Filippo Spertino, l'Ing. Alessandro Ciocia, l'Ing. Gabriele Malgaroli, il Prof. Vicente Munoz e il Prof. Slawomir Gulkowski per avermi assistito in questo lavoro con grande pazienza e disponibilità. In particolare ringrazio Gabriele per aver sopportato i miei vocali infiniti e Vicente per avermi accolto calorosamente a Jaen non facendomi sentire la nostalgia di casa. Ringrazio i miei amici che mi sono stati vicini e con i quali ho potuto distrarmi e rilassarmi, durante la mia lunga carriera universitari. Ringrazio mio fratello per il quale spero di poter essere un buon esempio per il futuro. Ringrazio le mie due nonne al quale spero di dare una grande soddisfazione laureandomi. Un ringraziamento speciale va anche ai compagni dei miei genitori Giovanni e Lorenza i quali mi hanno sempre trattato come un figlio. E soprattutto un ringraziamento di cuore va ai miei genitori i quali mi hanno sempre sostenuto emotivamente, e soprattutto economicamente durante questo periodo universitario, sicuramente senza il vostro aiuto non sarei riuscito ad arrivare fino a qui.

Contents

1	Introduction to semiconductor physics.....	1
1.1	Electronic band structure	1
1.2	Insulators, Metals, and Semiconductors	2
1.2.1	Semiconductor Material.....	3
1.2.2	Silicon	4
1.3	Doping of semiconductors	6
1.3.1	V group dopant atoms.....	6
1.3.2	III group dopant atoms.....	8
1.4	Drift Current.....	9
1.5	Diffusion current	11
1.6	Current balance in a semiconductor	12
1.7	P-n Junction.....	12
1.8	Recombination.....	13
1.9	Diode.....	13
2	Photovoltaic generation system	15
2.1	Solar cell, operating principles.....	15
2.2	PV Solar Cells State Of the Art.....	16
2.3	I-V Curve	19
2.4	Fill Factor	21
2.5	Equivalent circuit.....	22
2.5.1	Effect of parameters variation on I-V curve	26
2.5.2	Overview of the alternative SDM equivalent circuits:	28

2.5.3	Explicit form of transcendental equation using Lambert function	30
2.6	Solar cell power and efficiency	31
2.7	Causes of energy losses in a solar cell	31
2.8	Variation of the PV performances with G and T_c	33
2.9	Solar Cells connected in series and in parallel	35
2.10	Mismatch.....	36
2.10.1	Mismatch of cells connected in series.....	36
2.10.2	Mismatch of cells connected in parallel	40
2.11	PV module structure	42
2.12	STC-Standard Test Conditions.....	43
2.13	NOCT, Nominal Operating Cell Temperature	44
2.13.1	Data given by the manufacturer.....	44
2.14	Power and efficiency of a PV module	45
2.15	Evaluation of PV performance in STC and Osterwald Model.....	47
3	Description of the experimental set up	50
3.1	Politecnico di Torino Energetic Department Measurement System	51
3.1.1	Measurement uncertainty of the data collected at DENERG Laboratory at Politecnico d Torino	56
3.2	Laboratory of the IDEA Solar Energy Research Group at University of Jaen. 57	
3.2.1	Measurement uncertainty of the data collected at IDEA research group laboratory	63
4	Parameters Extraction	65
4.1	Parameter extraction procedure.....	68
4.1.1	Pre-processing of the IV curves	70

4.1.2	Politecnico di Torino curve fitting optimization algorithm	73
4.1.3	University of Jaen curve fitting optimization algorithm.....	82
4.1.4	Parameter Validation	95
4.1.5	Weighted reduction of the I-V curve points.....	95
5	Analysis of the obtained results	97
5.1	Experimental campaigns	97
5.1.1	Politecnico di Torino experimental campaign	97
5.1.2	UJA experimental campaign	98
5.2	Parameter extraction results and estimation of the correlations.....	100
5.2.1	Politecnico di Torino Nonlinear Regression Results.....	104
5.2.2	University of Jaen Nonlinear Regression Results	118
5.3	Estimation of the maximum power at different cell temperatures and irradiances.....	130
5.3.1	Politecnico di Torino estimation of maximum power results	131
5.3.2	University of Jaen estimation of power peak results	137
5.3.3	University of Jaen estimation of energy results	142
6	Conclusion	144
7	References.....	146
8	Appendix.....	150
8.1	Monocrystalline Trina Solar TSM-DD05A.08-P300	150
8.1.1	Electrical data at STC	150
8.1.2	Cell temperature coefficients α , β , γ and NOCT	150
8.1.3	Specifications	150
8.1.4	$I-V$ curves provided by manufacturers.....	152
8.2	Polycrystalline JA-Solar JAP60S01 -P280.....	153
8.2.1	Electrical data at STC	153

8.2.2	Cell temperature coefficients α , β , γ and NOCT	153
8.2.3	Specifications	153
8.2.4	I - V curves provided by manufacturers.....	154
8.3	Monocrystalline Luxor LX-100M -P100.....	156
8.3.1	Electrical data at STC	156
8.3.2	Cell temperature coefficients α , β , γ and NOCT	156
8.3.3	Specifications	156

List of Figures

Figure 1-1: 2 and N-atoms Energy band structures.	1
Figure 1-2 : Valence Band, Energy Gap, Conduction Band.	2
Figure 1-3: 3D structure of unit cell of Si (monocrystalline).	4
Figure 1-4: 2D representation of a Si crystalline lattice.	5
Figure 1-5: Creation of a hole electron pair.	5
Figure 1-6: n-type semiconductor (doped with an element of the V group). ...	7
Figure 1-7: p-type semiconductor (semiconductor doped with a III group atom).	8
Figure 1-8: Separation surface between two zones with different concentrations of charge carriers.	11
Figure 1-9: diffusion current density as the gradient changes of the charge carriers.	11
Figure 1-10: Diode I - V curve	14
Figure 2-1: Schematic representation of a PV solar cells connected with a load.	15
Figure 2-2: Schematic representation of the transversal section of a Solar Cell.	17
Figure 2-3: Schematic representation of the section of a Thin-Film solar cell.	18
Figure 2-4: Schematic representation of the section of a multijunction solar cell.	18
Figure 2-5: I - V curve and P - V curve with most important points.	19
Figure 2-6: complete I - V Curve with Breakdown and Hot Spot limits.	20

Figure 2-7: Schematic representation of the I-V curve at the Fill Factor variation.	21
Figure 2-8: Ideal PV equivalent circuit with 3 parameters.	22
Figure 2-9: Ideal PV equivalent circuit IV curve.	23
Figure 2-10: 5 parameters equivalent circuit.	23
Figure 2-11: $I-V$ curve with R_{sh} finite value.	24
Figure 2-12: $I-V$ curve taking into account the effect of R_s (different from 0).	24
Figure 2-13: $I-V$ curve varying I_{ph}	26
Figure 2-14: $I-V$ curve at the variation of $n e I_{SD} = I_0$	27
Figure 2-15: I-V curves at the varying of the parameters R_S and R_{sh}	27
Figure 2-16: 7 parameters equivalent circuit models.	28
Figure 2-17: 10 parameters equivalent circuit model.	29
Figure 2-18: $J=f(V)$ and $P_u=f(V)$	31
Figure 2-19: G variation effect on the $I-V$ curves.	33
Figure 2-20: T_c variation effect on the $I-V$ curves.	34
Figure 2-21: Construction of an $I-V$ curve of a module from the $I-V$ curves of the individual cells.	36
Figure 2-22: Mismatch of two cells connected in series.	37
Figure 2-23: Series connection with bypass diode.	38
Figure 2-24: Action of a bypass diode on a connection of two cells in series.	39
Figure 2-25: Mismatch of cells connected in parallel.	40

Figure 2-26: Parallel connection of blocking diode.....	41
Figure 2-27: Action of a blocking diode on a connection of two cells in parallel.	42
Figure 2-28: Representation of the generic structure of a photovoltaic module.	43
Figure 3-1 Measuring circuit at Laboratory of DENERG at Politecnico di Torino.	51
Figure 3-2: differential voltage probes Sapphire model, used to measure the voltage at Politecnico di Torino DENERG laboratory.....	51
Figure 3-3: Current probe DC / AC LEM-HEME PR30 da 30 Apk, used to measure the current at Politecnico di Torino DENERG laboratory.	52
Figure 3-4: Electrolytic capacitor used to record the <i>I-V curve</i> at Politecnico di Torino DENERG laboratory.	52
Figure 3-5: Cell temperature probe used to measure the cell temperature of the PV module at Politecnico di Torino.	53
Figure 3-6: Voltage power supply used to pre-charge negatively the electrolytic capacitor at Politecnico di Torino DENERG laboratory.	53
Figure 3-7: Pyranometer used at Politecnico di Torino to measure the irradiance.	54
Figure 3-8: PV module with metal support, pyranometer, solar cell, used at Politecnico di Torino DENERG laboratory.....	54
Figure 3-9: A/D converter DAQ-NI USB-6251 BNC, used to convert the data from analogue to digital at Politecnico di Torino DENERG laboratory.	55
Figure 3-10: Digital oscilloscope Labview graphic interface, used to manage the measurement system at Politecnico di Torino DENERG laboratory.	55

Figure 3-11: Flowchart and instruments controlled by the Labview™ program of the Laboratory of the IDEA Solar Energy Research Group at University of Jaen.....	57
Figure 3-12: 2-axes solar tracker on the flat roof of the Higher Technical College where the measures were taken.....	58
Figure 3-13: Schematic of $I-V$ curve tracer implemented at University of Jaen	58
Figure 3-14: $v(t)$ characteristic during the charge transient.	59
Figure 3-15: Capacitive load circuit designed by the University of Jaen. The internal capacitor by RIFA has a capacitance of 4.7mF.....	60
Figure 3-16: Digital multimeters Agilent™34411A.....	60
Figure 3-17: Data-logger Agilent™ 34970A and measurement card model 3401A which includes 20 voltage channels.....	61
Figure 3-18: Technical features for the Pyranometer CMP11 by model Kipp and Zonnen™	61
Figure 3-19: Image of the Pt-100 Temperature probe used at University of Jaen to measure the temperature of the module under test.	62
Figure 3-20: Interface of Labview programs used at University of Jaen to manage the measurement system.	63
Figure 4-1: flowchart which summarises the whole process carried out to extract the SDM parameters from an experimental $I-V$ curve. This procedure is applied for each measured G and T_c conditions.	69
Figure 4-2: Flowchart of the Combined Analytical and Numerical Method implemented on Matlab for the extraction of the initial parameters.	73
Figure 4-3: Flowchart of the Levenberg Marquardt Method computed in Matlab for the extraction of Parameter.....	80
Figure 4-4: Boltzman (or Gibbs) pdf.	83

Figure 4-5: Schematic representation of Metropolis Algorithm.	85
Figure 4-6: Flowchart of the Metropolis Simulated Annealing algorithm implemented in University of Jaen procedure for the extraction of the SDM parameters.....	87
Figure 4-7: reflection of a three points simplex.....	90
Figure 4-8: expansion of a three points simplex.....	91
Figure 4-9: contraction of a three points simplex.....	91
Figure 4-10: Shrink of a three points simplex.....	92
Figure 4-11: Flowchart of the Nelder-Mead Method computed in Octave for the extraction of the Parameters.....	93
Figure 5-1: nonlinear regression results for I_{ph} monocrystalline by Trina Solar. The blue line is the estimated correlation function for I_{ph} . The red dots represent the extracted points.	105
Figure 5-2: nonlinear regression results for I_{ph} for monocrystalline by Trina Solar. The blue line is the estimated correlation function for I_{ph} . The red dots represent the extracted points.....	105
Figure 5-3: monocrystalline by Trina Solar nonlinear regression results for I_0 . The blue line is the estimated correlation function for I_0 . The red dots represent the extracted points.	106
Figure 5-4: nonlinear regression results for n for monocrystalline by Trina Solar. The blue line is the estimated correlation function for n . The red dots represent the extracted points.....	107
Figure 5-5: nonlinear regression results for R_s for monocrystalline by Trina Solar. The blue line is the estimated correlation function for R_s . The red dots represent the extracted points.....	108
Figure 5-6: nonlinear regression results for R_s for monocrystalline by Trina Solar. The blue line is the estimated correlation function for R_s . The red dots represent the extracted points.....	108

Figure 5-7: nonlinear regression results for R_{sh} for monocrystalline by Trina Solar. The blue line is the estimated correlation function for R_{sh} . The red dots represent the extracted points.....	109
Figure 5-8: nonlinear regression results for I_{ph} for polycrystalline by JA-Solar. The blue line is the estimated correlation function for I_{ph} . The red dots represent the extracted points.	112
Figure 5-9: nonlinear regression results for I_0 for polycrystalline by JA-Solar. The Blue line is the estimated correlation function for I_0 . The red dots represent the extracted points.	113
Figure 5-10: nonlinear regression results for n for polycrystalline by JA Solar. The blue line is the estimated correlation function for n . The red dots represent the extracted points	114
Figure 5-11: nonlinear regression results for R_s for polycrystalline by JA Solar. The blue line is the estimated correlation function for R_s . The red dots represent the extracted points.	115
Figure 5-12: nonlinear regression results for R_s for polycrystalline by JA Solar. The blue line is the estimated correlation function for R . The red dots represent the extracted points.	115
Figure 5-13: nonlinear regression results for R_{sh} for polycrystalline by JA Solar. The blue line is the estimated correlation function for R_{sh} . The red dots represent the extracted points.....	116
Figure 5-14: nonlinear regression results for I_{ph} for polycrystalline by Luxor. Blue line is the correlation function for I_{ph} . The red dots are the I_{ph} . Extracted using Politecnico di Torino procedure (LM).	120
Figure 5-15: nonlinear regression results for I_{ph} for polycrystalline by Luxor. Blue line is the correlation function for I_{ph} . The red dots are the I_{ph} . Extracted using University of Jaen procedure (SA-NM).	120
Figure 5-16: nonlinear regression results for I_0 for polycrystalline by Luxor. Blue line is the correlation function for I_0 . The red dots are the I_0 . extracted using Politecnico di Torino procedure (LM).	121

Figure 5-17: nonlinear regression results for I_0 for polycrystalline by Luxor. Blue line is the correlation function for I_0 . The red dots are the I_0 extracted using University of Jaen procedure (SA-NM).	122
Figure 5-18: nonlinear regression results for n for polycrystalline by Luxor. Blue line is the correlation function for n . The red dots are the n extracted using Politecnico di Torino procedure (LM)	123
Figure 5-19: nonlinear regression results for n for polycrystalline by Luxor. Blue line is the correlation function for n . The red dots are the n extracted using University of Jaen procedure (SA-NM).	123
Figure 5-20: nonlinear regression results for R_s for polycrystalline by Luxor. Blue line is the correlation function for R_s . The red dots are the R_s extracted using Politecnico di Torino procedure (LM)	124
Figure 5-21: nonlinear regression results for R_s for polycrystalline by Luxor. Blue line is the correlation function for R_s . The red dots are the R_s extracted using University of Jaen procedure (SA-NM).	125
Figure 5-22: nonlinear regression results for R_s for polycrystalline by Luxor. Blue line is the correlation function for R_s . The red dots are the R_s extracted using Politecnico di Torino procedure (LM)	125
Figure 5-23: nonlinear regression results for R_s for polycrystalline by Luxor. Blue line is the correlation function for R_s . The red dots are the R_s extracted using University of Jaen procedure (SA-NM).	126
Figure 5-24: nonlinear regression results for R_{sh} for polycrystalline by Luxor. Blue line is the correlation function for R_{sh} . The red dots are the R_{sh} extracted using Politecnico di Torino procedure (LM).	127
Figure 5-25: nonlinear regression results for R_{sh} for polycrystalline by Luxor. Blue line is the correlation function for R_{sh} . The red dots are the R_{sh} extracted using University of Jaen procedure (SA-NM).	127
Figure 5-26: $I-V$ curves experimentally measured and $I-V$ curves estimated with the correlations for Trina Solar Monocrystalline TSM-DD05A.08 (300W).....	131

Figure 5-27: comparison of maximum power estimated by correlations and by OM for a wide range of irradiances (0 1200 W), for the monocrystalline by Trina Solar (300 W).....	133
Figure 5-28: $I-V$ curves experimentally measured and $I-V$ curves estimated with the correlations for JA-Solar Polycrystalline JAP60S01 (280W).....	134
Figure 5-29: comparison of maximum power estimated by correlations and by OM for a wide range of irradiances (0 1200 W), for polycrystalline by JA Solar (280 W).....	136
Figure 5-30: $I-V$ curves experimentally measured, estimated with the Politecnico di Torino model and with the University of Jaen model for Luxor monocrystalline (280W).....	138
Figure 5-31: comparison among the maximum power estimated: by Politecnico di Torino model, by OM and experimental one for monocrystalline by Luxor (100 W).....	140
Figure 5-32: comparison among the maximum power estimated: by Politecnico di Torino model, by University of Jaen model and experimental one for monocrystalline Luxor (100W).....	140
Figure 8-1: Transversal and frontal views for Trina SolarTSM-DD05A.08-P300.....	151
Figure 8-2: $I-V$ curves at different irradiance values for Trina SolarTSM-DD05A.08-P305.....	152
Figure 8-3: P-V curves dependence on irradiance for Trina SolarTSM-DD05A.08-P305.....	152
Figure 8-4: transversal and frontal for the two sides (front and back) views for Polycrystalline JA-Solar JAP60S01 -P280.....	154
Figure 8-5: $I-V$ curves at different irradiance values for JA-Solar JAP60S01 -P270.....	154
Figure 8-6: $I-V$ curves at different cell temperature values for JA-Solar JAP60S01 -P270	155

Figure 8-7: P-V curves dependence on irradiance for JA-Solar JAP60S01 -P270	155
Figure 8-8: Frontal views of the two sides (front and back) for Luxor LX-100M -P100	157

List of Tables

Table 1-1: Most important semiconductor Energy Gap [eV].....	4
Table 2-1: Monocrystalline, Polycrystalline, Thin Films.	16
Table 2-2: Temperature coefficient to report the parameters from the STC to the real conditions.	35
Table 3-1: Source of uncertainty associated to each measurands together with the value of the expanded uncertainty in percentage.	64
Table 4-1: Table of the pre-processing steps adopted by the two methods in order to filtered the $I-V$ curves before the curve fitting procedure.	71
Table 4-2: Coefficient of simplex algorithm applied in the extraction procedure for the SDM parameters by the University of Jaen. Applied in the Eq.(4-38), Eq.(4-39), Eq.(4-40), Eq.(4-41), Eq.(4-42) and Eq.(4-43) explained in the previous section.....	94
Table 5-1: Cell temperature and irradiance ranges of the TRINA solar monocrystalline experimental campaign performed at Turin Polytechnique.....	98
Table 5-2: Cell temperature and irradiance ranges of the JA solar polycrystalline experimental campaign performed at Politecnico di Torino.....	98
Table 5-3: Range of measurements of cell temperature, irradiance, and wind speed for the Luxor monocrystalline experimental campaign performed at University of Jaen.....	99
Table 5-4: SDM parameters extracted for monocrystalline PV module TSM-DD05A.08 by Trina Solar using the Politecnico extraction procedure, irradiance, cell temperature, and percentage error on the maximum power.....	104
Table 5-5: Coefficients of the proposed correlations for TSM-DD05A.08 PV module by Trina Solar evaluated performing the nonlinear regression.	110
Table 5-6: Percentage Relative Standard Deviation calculated between extracted points and correlation points for monocrystalline by Trina Solar.	110

Table 5-7: SDM parameters extracted for polycrystalline by JA-Solar using the Politecnico extraction procedure, irradiance, cell temperature, and percentage error on the maximum power.	111
Table 5-8: Coefficients of the proposed correlations evaluated performing the nonlinear regression for polycrystalline by JA-Solar.....	117
Table 5-9: Percentage Relative Standard Deviation between extracted points and correlation points of Polycrystalline JA-Solar.	117
Table 5-10: SDM parameters extracted for monocrystalline by Luxor using the Politecnico di Torino (LM) extraction procedure, irradiance, cell temperature, and percentage error on the maximum power.	118
Table 5-11: SDM parameters extracted for monocrystalline by Luxor using the University of Jaen (SA-NM) extraction procedure, irradiance, cell temperature, and percentage error on the maximum power.	119
Table 5-12: Coefficients of monocrystalline by Luxor (100W), evaluated from the nonlinear regression for the Politecnico di Torino and University of Jaen extracted parameters.....	128
Table 5-13: PRSD for the nonlinear regression for the two methods for monocrystalline by Luxor (100W).....	128
Table 5-14: Comparison of the mean values of the convergence time, of the error on the maximum power at different irradiance ranges, and of the of the resnorm resulted from the application of the two algorithms.	129
Table 5-15: Comparison between Maximum power and errors (absolute and %) on maximum power with respect the experimental data. Respectively estimated using correlations and OM for monocrystalline by Trina Solar (300 W), reported together with G, T _c and experimental maximum power values.....	132
Table 5-16: Maximum power and errors (absolute and %) on maximum power with respect the experimental data estimated using correlations and OM for polycrystalline by JA Solar (280 W), reported together with G, T _c and experimental maximum power values.....	135

Table 5-17: Comparison between Maximum power and errors (absolute and %) on maximum power with respect the experimental data, respectively estimated using Politecnico di Torino model and University of Jaen model for monocrystalline by Luxor (100 W), reported together with G, T_c and experimental maximum power values..... 139

Table 5-18: Energy produced during the experimental campaign of 20 days: estimated by Politecnico di Torino correlations, estimated by University of Jaen correlations, estimated by OM and experimentally measured..... 143

Table 8-1: Main features for Trina SolarTSM-DD05A.08-P300 150

Table 8-2: NOCT and cell temperature coefficients for Monocrystalline Trina SolarTSM-DD05A.08-P300. 150

Table 8-3: Main specifications for Trina SolarTSM-DD05A.08-P300 150

Table 8-4: Main features for Polycrystalline JA-Solar JAP60S01 -P280..... 153

Table 8-5: NOCT and cell temperature coefficients for Polycrystalline JA-Solar JAP60S01 -P280 153

Table 8-6: Main specifications for Trina SolarTSM-DD05A.08-P300 153

Table 8-7: Main features for Luxor LX-100M -P100..... 156

Table 8-8: NOCT and cell temperature coefficients for Luxor LX-100M -P100 156

Table 8-9: Main specifications for Luxor LX-100M -P100..... 156

Introduction

Nowadays, the fossil fuels still represent the largest energy source exploited for energy production. However, the combustion of fossil fuels leads to harmful environmental effects like the emission of CO₂, which causes the global warming and the increase of atmospheric pollution. Moreover, the fossil fuel resources are depleting and they are not uniformly distributed all over the World. Renewable Energy Sources (RES) are expected to be the green response to the above described issues. In particular, PhotoVoltaic (PV) solar energy seems to be a promising choice of clean and inexhaustible source, directly converting the solar energy into DC electricity without rotating machinery or other mechanical parts. PV installed capacity has rapidly grown in the last two decades, increasing from ≈ 9 GW (2007) to ≈ 480 GW (2018).

The present work has been performed at Politecnico di Torino and at the University of Jaen. The rated power of a PhotoVoltaic (PV) module is provided by the manufacturer in Standard Test Conditions (STC), corresponding to cell temperature $T_c=25$ °C and irradiance $G=1000$ W/m². However, PV generators generally work in very different conditions and, in order to assess their performance, several models have been developed in literature. The Osterwald Model (OM) is the most used, in which, generated power is proportional to irradiance and dependent on temperature by the γ coefficient, provided by the manufacturer. Even if this model is one of the most accurate, it presents a not negligible error regarding the estimation of the maximum power and the productivity of a PV module (3%-6%). However, other models are required for a more accurate evaluation. The performance of a PV module can be described by several electrical equivalent circuits. In this work, the Single Diode Model (SDM) is considered for completely irradiated modules. The SDM is described by five parameters: the photovoltaic current I_{ph} , the saturation current I_0 , the non ideality factor n , the series resistance R_s , and the shunt resistance R_{sh} .

In the first part of the thesis, at Politecnico di Torino, the parameters of SDM for two PV modules (monocrystalline and polycrystalline silicon) are extracted starting from experimental I-V curves by a curve fitting procedure based on Levenberg-Marquardt (LM) algorithm. Then, correlations are identified, which describe the dependence of the parameters with respect to irradiance and cell temperature. These equations are obtained modifying the coefficients of

correlations already present in literature by a nonlinear regression of the extracted parameters. Correlations are used to estimate the maximum power in measurement conditions and the obtained results are compared with experimental data and the results from OM.

In the second part of the thesis, at the University of Jaen, the above described analysis is performed on another monocrystalline silicon PV module. The results are compared with the ones obtained from a different extraction procedure based on two numerical methods (Simulated-Annealing e Nelder-Mead, SA-NM). Finally, the energy produced by the module during 20 days of measurements is estimated with the two models and with OM.

In future, this technique will be implemented to performed the real time diagnostics of a PV generator. In particular, the state of health of the PV modules will be checked by comparing reference parameters, evaluated by the proposed correlations in real operating conditions, with experimental parameters.

1 Introduction to semiconductor physics

1.1 Electronic band structure

The theory of electronic band structure, is founded on quantum mechanics, and it establishes the possible or prohibited values of energy that an electron can assume inside a crystal lattice of a macroscopic solid ($\sim 10^{22}$ atoms) and homogeneous (uniform chemical composition). This concept is at the base of the functioning of all semiconductor devices (Ex. Diodes, Transistors, Solar Cells, Integrated Circuits). In the structure of a macroscopic and homogenous solid the orbitals overlap each other moreover the energy levels of each atom are not a unified but appear with a small difference in energy. In this way if the number of atoms or molecules within the lattice is very large ($N \sim 10^{22}$) the energetic levels are very close and follow each other continuously. A group of energy levels is called Energy Band (or Electronic Band). The bands can be separated by an energy interval, or have their energy levels partially overlapped with the neighboring energy bands creating wider bands.

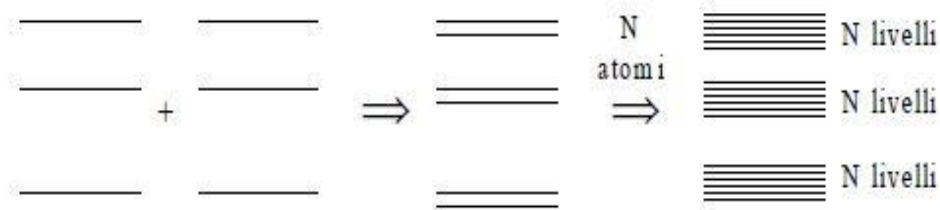


Figure 1-1: 2 and N-atoms Energy band structures.

The bands with energy too high to be occupied by electrons (empty bands furthest from nuclei) and the lowest energy bands, stable and always completely occupied (inert bands, composed of the orbitals closest to the nuclei) do not participate neither in the formation of bonds nor in electronic conduction. The Fermi Energy Level is the energy value corresponding to the highest level occupied

(partially or totally) by electrons, at an absolute temperature of 0 K. The most interesting energy bands in the semiconductor physics are close to that energy level:

- Valence Band (E_v), it is the electronic band with the greater energy among which occupied, partially (or totally) by valence electrons. The valence electrons participate in the formation of the chemical bonds but are not free to move inside the crystal lattice because are strongly attracted by the nucleus.
- Conduction Band (E_c), it is the electronic band with the lower energy that could be occupied by free electrons that are able to move inside the crystal structure conducting energy.
- Band Gap (o banda proibida), conduction band and valence band are separated from a prohibited band which is made by the energy levels that an electron can't assume (All the values between E_c and E_v). The width of this band is called Energy Gap:

$$E_g = E_c - E_v \quad \text{Eq.(1-1)}$$

Where:

- E_g [eV] → Energy Gap.
- E_c [eV] → Energy of the conduction band.
- E_v [eV] → Energy of the valence band.

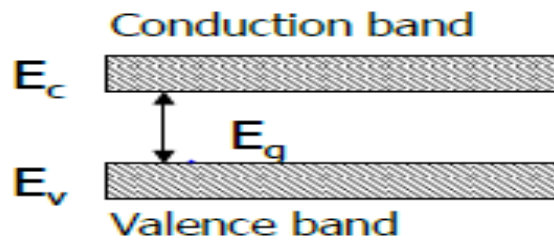


Figure 1-2 : Valence Band, Energy Gap, Conduction Band.

1.2 Insulators, Metals, and Semiconductors

To understand the meaning of valence band, conduction band and forbidden band it is necessary to analyse these concepts with respect to the different classes of solid. An exhaustive classification divides the solids into three classes:

- **Metal (o Conductor)**, valence band and conduction band are partially or totally overlapped (the Fermi level cross the conduction band). They are excellent current conductors because the electrons could easily pass to the conduction band generating an high number of free electrons.
- **Insulator**, the conduction band is completely occupied and separate by the valence band from a large Energy Gap E_g (Es. SiO_2 , ossido di silicio $E_g=8\text{eV}$, diamante $E_g=6\text{eV}$) for this reason the transition is highly improbable. The bonds between the atoms are too strong to be broken and to deliver an electron.
- **Semiconductor**, the energy gap that separates the valence band and the conduction band has an intermediate values ($0.2 < E_g < 2\text{eV}$) so it is possible to supply a valence electron with an amount of energy that allows it to reach conduction band. The covalent bond can be broken by generating a free electron capable of conducting current. For all temperatures higher than 0K , some electrons have sufficient energy to overcome the gap and reach the conduction band, which gradually fills with the increasing of the temperature.

1.2.1 Semiconductor Material

The semiconductor materials are mainly:

- IV group element: Germanium (Ge), Silicon (Si).
- Compounds of 2 elements of the III-V group: Gallium Arsenide (GaAs), Indium phosphide (InP).
- Compounds of 2 elements of the II-VI group: Cadmium tellurium (CdTe), Cadmium sulfide (CdS).
- Compounds of 3 (ternari) or of 4 (quaternari) elements: Aluminium and Gallium Arsenide (GaAlAs), Indium Arsenide and Gallium Phosphide (GaInAsP), Indium and Copper Diselenide (Cu-In-Se).

Table 1-1: Most important semiconductor Energy Gap [eV].

Crystalline Silicon (c-Si)	1,12
Amorphous Silicon (a-Si)	1,75
Germanium (Ge)	0,67
Gallium Arsenide (GaAs)	1,42
Indium Phosphide (InP)	1,34
Copper Indium Diselenide (CuInSe)	1,05
Cadmium Telluride (CdTe)	1,45
Cadmium Sulfide (CdS)	2,4

1.2.2 Silicon

Chemical element with atomic number $Z = 14$ belongs to the 4th group of the periodic table of the elements. It is the second most common element in nature after oxygen, the earth's crust is 27.7% by weight composed of Si. In any case, its pure form is artificially obtained through industrial processes, which use as starting elements all the composts in which the Si is contained, such as silica (SiO_2) and silicates ($\text{Si} + \text{O} + \text{other elements such as metals}$). The Si crystal lattice is composed by atoms that shares their 4 valence electrons through 4 covalent bonds with the 4 contiguous Si atoms. Si atoms occupy the space disposing themselves at the vertices of a perfectly symmetrical structure of tetrahedral shape. The tetrahedra joined together will form the crystal. Si atom, in the lattice, shares its 4 valence electrons through 4 covalent bonds with the 4 contiguous Si atoms. Si atoms occupy the space disposing themselves at the vertices of a perfectly symmetrical structure of tetrahedral shape. The elementary cell of the lattice of a silicon crystal is cubic in shape, and is composed of the union of several tetrahedrons.

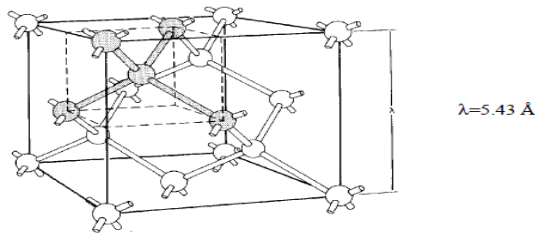


Figure 1-3: 3D structure of unit cell of Si (monocrystalline).

The 2D model is able to well describe the properties of the chemical bonds for this reason, even if it doesn't able to represent the crystallographic structure is one of the most common models to represent the crystalline lattice of a semiconductor.

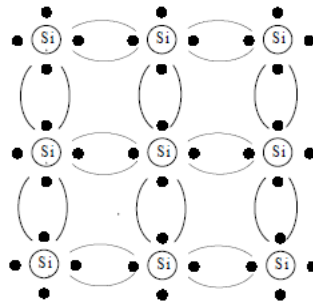


Figure 1-4: 2D representation of a Si crystalline lattice.

The 2D representation shows the way in which each Si atom shares the 4 valence electrons with which every of the 4 neighbour atoms. The circles correspond to the nucleus of the Si atoms and the electrons to the inner orbitals nearer to the nucleus. The black filled spots symbolize the valence electrons and the line that connect them are represent the covalent bonds. At the absolute Temperature of 0K the valence electrons are completely employed in the formation of the covalent bonds with the neighbour atoms, there are no one free electrons on conduction band able to conduct electricity. The crystal behaves like an insulator. At the increase of the Temperature $T > 0$ K the atoms broke the bonds releasing free electrons (the broken of a bond in the 2D model is equivalent to the passage of one electron from valence band to the conduction band). The energy necessary to break a covalent bond is equal to the Energy gap. In the point where was the electron a hole is generated this process could be view as an ionization of the atom, even if the crystal even if the crystal remain neutral (A hole in the 2D model is equal to a lack of electron in the Energy bands model).

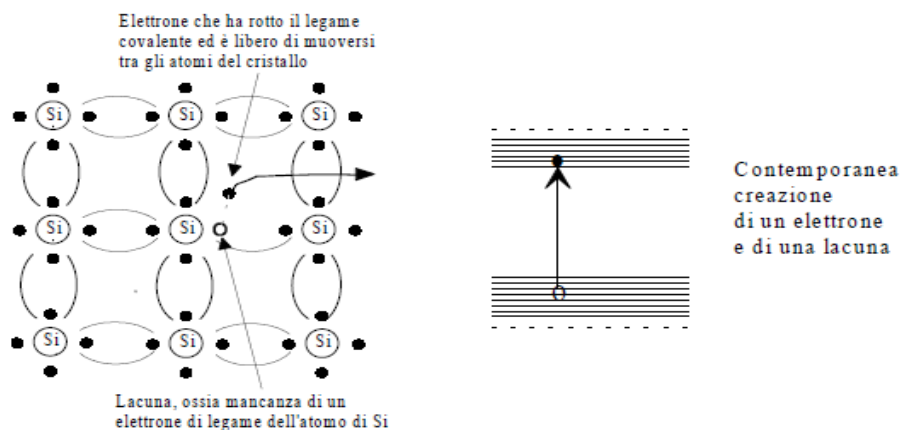


Figure 1-5: Creation of a hole electron pair.

The Si is the more common used semiconductor in the electronic application (diodes, transistors, solar cells), it could exist under three different allotropic forms:

- **Monocrystalline Silicon**, the crystalline lattice is continuous, uninterrupted and free of grain boundaries.
- **Polycrystalline Silicon**, the crystalline lattice is composed from a lot of small and microscopic crystals of different forms dimensions and different orientations called crystallites.
- **Amorphous Silicon**, is the non-crystalline allotropic form of Si, the atoms forms a disordered lattice forming a continuous random network.

1.3 Doping of semiconductors

An intrinsic semiconductor is an extremely pure material with low percentages of non-semiconductor contaminating elements. In this case the presence of charge carriers is due only to the thermal excitation. The amount of charge carriers present in the lattice of the semiconductor material can be increased by inserting neutral atoms of other elements into the lattice of the crystal, this technological solution takes the name of doping. The chemical elements used as dopants belong to 2 different groups of the periodic table, each of one has a specific effect on the semiconductor:

- Elements of the V group of the periodic table.
- Elements of the SECOND group of the periodic table.

1.3.1 V group dopant atoms

The atoms belong to the V group are defined donors because thanks to their electronic structure they are able to deliver an electron on the conduction band. Their electronic structure is characterized by the presence of 5 electrons in the valence energy band. If one this atom is added to the Si lattice one of that electrons presents in the valence band remain not strongly bounded to the crystal. The energy needed to transfer an electron to the conduction band is really smaller than the energy needed for a common electron employed in a Si covalent bonds. (Ex. For the P-Phosphorus inside a Si lattice the $E_g = 44\text{meV}$ with respect to $E_g = 1.1\text{eV}$ employed in the covalent bound from Si atoms). Often the thermal energy is sufficient to ionize the electrons. (Ex. For the P-phosphorous inside the Si lattice at $T=150\text{K}$ all the electrons not engaged in a covalent bound are completely ionized).

The crystal is globally neutral but two local regions are generated inside the lattice, a positive charge near to the ionized atom and a negative charge in another region. This process not generate holes but only free electrons. The doping with V group atoms allow to add the desired amounts of free electrons to the conduction band. A region doped with a V group atom is defined “n-type” and the electrons are the majority carriers and the holes are the minority carriers. The most common dopants belonging to the V group are As-Arsenic, P-Phosphorous and Sb-Antimony.

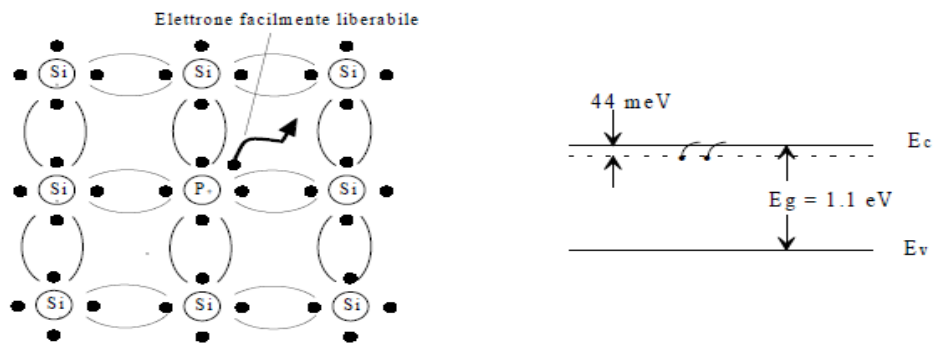


Figure 1-6: n-type semiconductor (doped with an element of the V group).

1.3.2 III group dopant atoms

The atoms belong to the III group are defined acceptors because they are able to accept an electron inside their structure generating a hole inside the lattice. The hole is defined as a covalent bond not saturated inside the Si lattice. Inside the Si crystal the 3 valence electrons form 3 covalent bounds with the Si atoms that surround it meanwhile the not saturated bond tends to attract the near electrons employed in the covalent bounds. it can happen only if a small amount of energy is given to the crystal because losing an electron the Si atom would assume a positive charge generating a force that attract the electron. This effect is attenuated from the crystal structure and for that reason the energy needed to supply to the Silicon is low. (Ex. For the B-Boron and Si-Silicon structure the energy needed to create an hole is of only 45 meV, the only thermal energy could allow to ionize all the acceptors). Two local charges are generated inside the Si lattice, the acceptors become negatively charged and the donors become positively charged but the crystal is globally neutral. The adding of dopant of the III group allow to add the desired amount of vacancies. A region doped with an atom of the III group is defined “p-type”. In this region the holes are the majority carriers and the free electrons are the minority carriers. The more common elements of the III group are B-boron, Al-Aluminium e Ga-gallium.

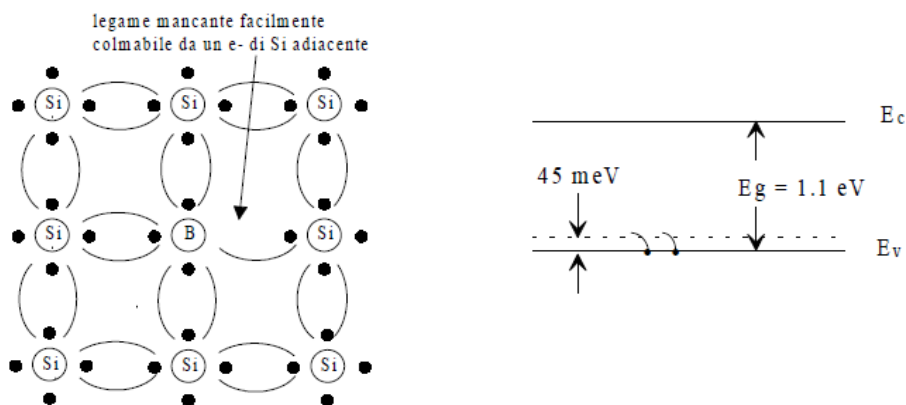


Figure 1-7: p-type semiconductor (semiconductor doped with a III group atom).

1.4 Drift Current

The conduction current is due to the shifting of the movable charges, which accelerate subjected to the action of an electric field E . The drift current in a semiconductor is derived from an analogy between the motion of the particles and a model with dry impacts, the resulting relation, which defines the surface density of the drift current, is as follows:

$$J = q * (n * \mu_n + p * \mu_p) * E \quad \text{Eq.(1-2)}$$

Where :

- E [V/m] → Electric field intensity.
- q [C] → Unit of charge .
- n [m^{-3}] → Doping n, concentration of n dopant atoms..
- p [m^{-3}] → Doping p, concentration of p dopant atoms.
- V_n [m/s] → Drift speed electrons.
- V_p [m/s] → Drift speed holes.
- μ_n [$cm^2/m/s$] → electrons mobility.
- μ_p [$cm^2/m/s$] → Holes mobility.

The Mobility of an electric charge is a parameter that indicates how easily a charge carrier moves in the crystal lattice, it coincides with the ratio between the electric field and the average speed with which the particle moves between two successive shocks.

$$\mu = \frac{\overline{V_m}}{\overline{E}} \quad \text{Eq.(1-3)}$$

Indicates the speed at which a charge carrier moves per unit of applied electric field, and the higher it is, the easier it is for a charge carrier to move. Mobility of electrons and gaps in silicon with respect to reference conditions, dopant Doping \cong $[(10) \wedge 14 \div 10 \wedge 17]$ [$cm^{(-3)}$] and $T=298.15$ K [1]:

- Electrons mobility → $\mu_n = 400[cm^2/V/s]$
- Holes mobility → $\mu_p = 1300[cm^2/V/s]$

From the formula of the surface density of current we can obtain the formula that allows to obtain the current:

$$I = q * S * J \quad \text{Eq.(1-4)}$$

In addition, starting from Eq.(1-2) you can highlight the contributions depending on the type of doping of the material, in consideration:

- For a p-type material ($p \gg n$)

$$J_p = q * n * \mu_p * E \quad \text{Eq.(1-5)}$$

- For n-type material ($n \gg p$)

$$J_n = q * n * \mu_n * E \quad \text{Eq.(1-6)}$$

Generally, for a semiconductor doped by acceptors and donors (also called p-n junction) the two contributions are added together because a single field produces opposite flows in the direction of opposite charges:

$$J = J_n + J_p \quad \text{Eq.(1-7)}$$

Moreover, it is possible to define the conductivity of the semiconductor which coincides with the coefficient of proportionality between the electric field E and the current density J:

$$\sigma = q * (n * \mu_n + p * \mu_p) \quad \left[\frac{1}{\Omega cm} \right] \quad \text{Eq.(1-8)}$$

The resistivity is the inverse of conductivity:

$$\rho = \frac{1}{q * (n * \mu_n + p * \mu_p)} \quad [\Omega cm] \quad \text{Eq.(1-9)}$$

The electrical resistance of a material:

$$R = \rho * \frac{L}{S} \quad [\Omega] \quad \text{Eq.(1-10)}$$

Where:

- L → length of the material.
- S → Trasversal (to the current) surface of the material.

We can also express Ohm's law as a function of current density or normalizing the latter with respect to L and S:

$$J = \frac{E}{\rho} \quad \text{Eq.(1-11)}$$

1.5 Diffusion current

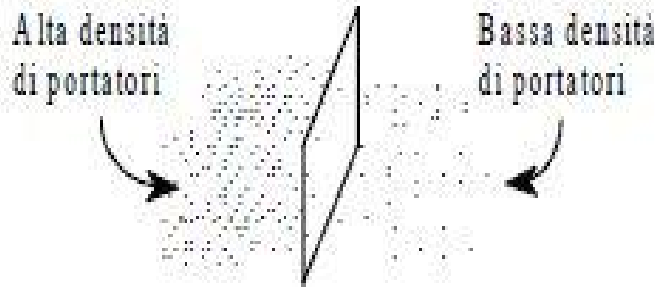


Figure 1-8: Separation surface between two zones with different concentrations of charge carriers.

Current generated as a result of the presence of a concentration gradient of semiconductor charge carriers, which coincides with a net transfer of carriers from the area with the highest density to the area with the lowest density. This flow of charges is generated by the thermal movement of the individual carriers, which is continuous, random and comparable in all directions. Considering a surface, permeable to the carriers, that separates the zones with different densities, the most probable direction of crossing the membrane will be the one that coincides with the passage of carriers from the zone with the highest concentration towards the zone with the lowest concentration. This problem can be analysed in analogy with the law of diffusion in gas molecules, expressed by Fick's law.

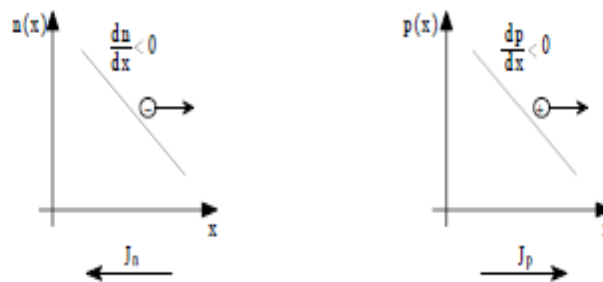


Figure 1-9: diffusion current density as the gradient changes of the charge carriers.

The two addendums have an opposite trend in that the same gradient produces flows of concurrent charge carriers that correspond to opposite currents:

$$J = J_n + J_p = q * (D_n * \nabla(n) - D_p * \nabla(p)) \quad \text{Eq.(1-12)}$$

Where :

- $D_p \rightarrow$ Diffusion coefficient of holes in the semiconductor.
- $\nabla(p) \rightarrow$ Holes gradient in the semiconductor.
- $D_n \rightarrow$ Diffusion coefficient of free electrons in the semiconductor.
- $\nabla(n) \rightarrow$ electrons gradient in the semiconductor.

1.6 Current balance in a semiconductor

In the semiconductor are present simultaneously the two current contributions, that is, the diffusion current, due to the concentration gradients of the charge carriers inside the semiconductor and the drift current, due to the action of the electric field. The total current circulating in the semiconductor is therefore the sum of the 2 contributions; analysing separately the contributions in the one-dimensional case we can define:

$$J_{tot} = J_p + J_n \quad \text{Eq.(1-13)}$$

$$J_n = q * n * \mu_n * E + q * D_n * \frac{\partial n}{\partial x} \quad \text{Eq.(1-14)}$$

$$J_p = q * p * \mu_p * E - q * D_p * \frac{\partial p}{\partial x} \quad \text{Eq.(1-15)}$$

1.7 P-n Junction

This term indicates the separation surface between a zone of type n, and a zone of type p generated as a result of doping of a semiconductor material with different materials. A diffusion phenomenon is triggered, it is due to the concentration gradients of the charge carriers, electronic current moves from zone n to zone p, vice versa, a current of gaps moves from zone p to zone n. The zone n charges positively, due to the loss of electrons vice versa, the zone p charges negatively due to the acquisition of electrons. The two initially neutral zones tend to acquire locally, charged with opposite sign, generating an electric field. The mobile carriers move away from the junction "emptying it", so the area around the junction is called the region of emptying. The effect of the electric field acts on the carriers generating a drift current, opposite in direction to the diffusion current. In the absence of an

external electric field, in the emptying region, a dynamic equilibrium is established, in which the flow of the charge carriers is completely balanced.

1.8 Recombination

The electrons belonging to the conduction band are in a metastable state, which tends to stabilize at lower energy levels; the closest levels coincide with the energy levels belonging to the valence band. When an electron passes from the conduction band to the valence band, a phenomenon of annihilation of the electron gap pair occurs, which is called recombination. When a recombination occurs, a release of energy from the system to the outside takes place, this energy can lead to the generation of a photon (Radiative Recombination) or thermal energy. A fundamental parameter to evaluate this effect is the Recombination Rate, that is the number of recombination processes that occur in the unit of time. The recombination rate is influenced by numerous factors such as the concentration of minority and majority carriers, the presence of defects in the crystalline lattice, the type of material (depending on whether it is Direct or Indirect Band) and the Temperature.

1.9 Diode

The diode is a passive non-linear electronic unit with two terminals (bipolar), which allows the flow of electrical current in one direction and blocks it in the opposite direction. The physical principle behind a diode is exactly the same of the p-n junction. In the presence of an external electric field applied to the ends of the diode, two configurations are possible:

- **Direct Bias** (zone type N connected to the negative electrode and zone type P connected to the positive electrode), the external and the junction electric field are opposite, the intensity of the junction electric field and the amplitude of the emptying zone are reduced. Through the junction a diffusion current is conducted. The diode is ON.
- **Reverse bias.** (zone type P connected to the negative electrode and zone type N connected to the positive electrode), the external electric field and the junction electric field are coherent. The intensity of the electric field and the amplitude of the emptying region increase. Only a negligible diffusion current is conducted

through the junction. The diode is OFF. The physical behaviour of the diode is described by Shockley Equation:

$$I = I_0 * \left(e^{\frac{q*V}{n*k*T}} - 1 \right) \quad \text{Eq.(1-16)}$$

Where:

- $I_0 \rightarrow$ Saturation current [A]
- $V \rightarrow$ Voltage applied to the dode [V]
- $k \rightarrow$ Boltzman costant $1.38064852 \left[\frac{J}{K} \right]$
- $T \rightarrow$ Diode temperature[K]
- $n \rightarrow$ Diode ideality factor.
- $q \rightarrow$ Electronic charge (unit ofcharge) $1.6e^{-19}[C]$

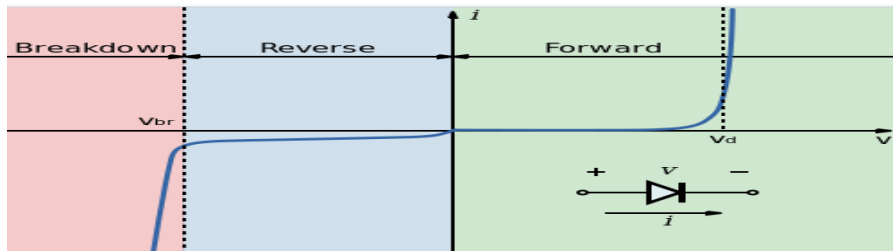


Figure 1-10: Diode I - V curve .

It is possible to express this equation also in the form:

$$I = I_0 * \left(e^{\frac{V}{V_{th}*n}} - 1 \right) \quad \text{Eq.(1-17)}$$

Where:

- $V_{th} [V] \rightarrow$ Thermal voltage $V_{th} = \frac{k*T}{q}$

2 Photovoltaic generation system

2.1 Solar cell, operating principles

The most important component in a photovoltaic generation system is the solar cell, it is nothing more than a p-n junction, see section 1.7, connected to an external electrical circuit by two electrodes. The current circulating in the external electrical circuit is generated through the photoelectric effect.

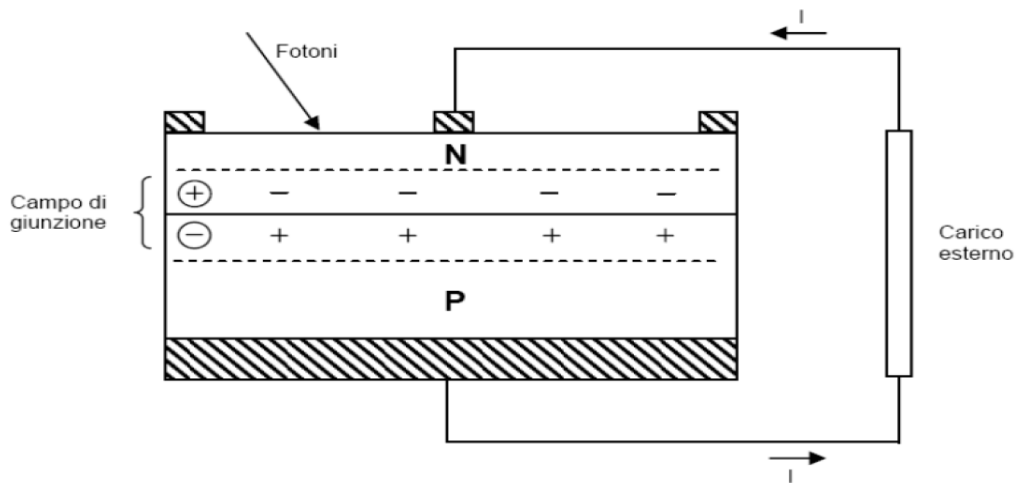


Figure 2-1: Schematic representation of a PV solar cells connected with a load.

The photoelectric effect is the phenomenon that occurs when an electron passes from the valence band to the conduction band because of the energy absorption of a photon of light. This could happen only if the photon has energy greater than or equal to the energy gap E_g . Knowing the equation that characterizes the energy of the photon it is possible to express this relationship in analytical terms:

$$E_{ph} = h * \nu = h * \frac{c}{\lambda} \quad \text{Eq.(2-1)}$$

Where:

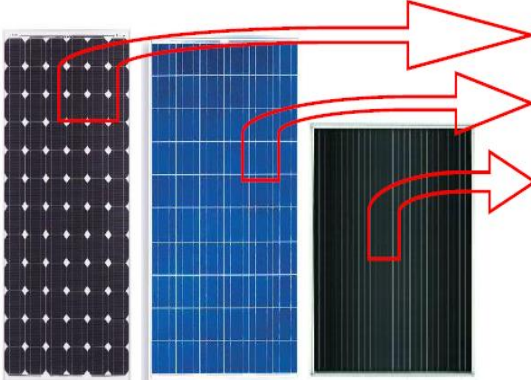
- $E_{ph} \rightarrow$ Light photon energy [J] o [eV]
- $h \rightarrow$ Plank’s constant $6.626e-34$ [j*s].
- $\nu \rightarrow$ light frequency [Hz].
- $C \rightarrow$ speed of light in the vaacum $2.9979e5$ [m/s].
- $\lambda \rightarrow$ wawelength of light [m]

$$E_{ph} \geq E_g \quad \text{Eq.(2-2)}$$

In the presence of the electric field that is established through the junction, the conduction electrons are pushed towards the region n and the gaps towards the region p. If the circuit is closed, a current I is conducted through the external electric circuit, if the open circuit occurs, the photovoltaic current induces a reduction in the electric field, and a consequent increase in the diffusion current, in this case the two diffusion and drift currents counterbalance each other. This happes when no photons of light reaches the cell, in Dark Conditions, when the cell behaves likes a diode.

2.2 PV Solar Cells State Of the Art

Table 2-1: Monocrystalline, Polycrystalline, Thin Films.



Technology	Efficiency
m-Si ; m-Si/a-Si	15-22 %
p-Si	14-16 %
a-Si ; a-Si/ μ C	6-10 %
CIS/CIGS	11-13 %
CdTe/CdS	13-15 %

The main photovoltaic cells technologies that are available on the market today are:

- **Silicon solar cells (polycrystalline or monocrystalline),** polycrystalline silicon cells are the first cells to be developed and are the cells that achieve an high efficiency, reaching in some cases values higher than 20%. Two different allotropic forms of

silicon are contained in monocrystalline and polycrystalline cells (See paragraph 1.2.2). These two typologies of cells are generated through different manufacturing processes, because of that, at the end of the processes the cells have different shapes. The polycrystalline cell is square while the monocrystalline cell is pseudo-square, as the corners of the square are rounded. Some changes are arranged on the normal configuration of the cells in order to increase their efficiency. For example in the All Back Contact cells, the contacts of the electrodes are moved to the back part of the cell and the front surface undergoes texturing procedures. This is done for increase the useful surface allowable for solar reception increasing also the efficiency.

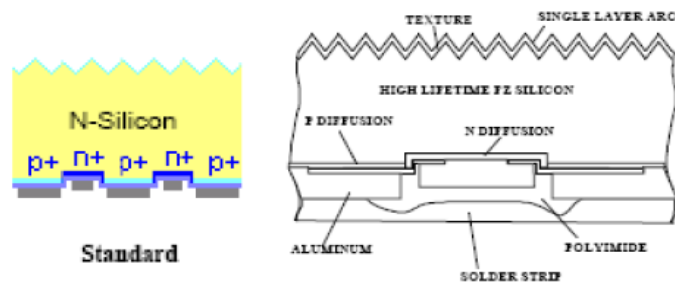


Figure 2-2: Schematic representation of the transversal section of a Solar Cell.

- **Thin-film solar cell (o thin-film)**, normally the material used to build these cells are: CIS, indium-copper di-selenide, CdTe/CdS, cadmium telluride/cadmium sulphide and a-Si/ μc , amorphous Si/microcrystalline Si. In order to create that cells one or more thin layers (or films) is deposited on a plastic, metal or glass substrate. This deposited layer is very thin, it could has a thicks included in a range between a few nanometers to tens of micrometers. This cells are largely utilized for the PV building integrations thanks to the properties of the thin film. The best properties of this material are its high flexibility and high transparency to light. Generally, these cells are cheaper than silicon cells but at the same moment they have a lower efficiency.

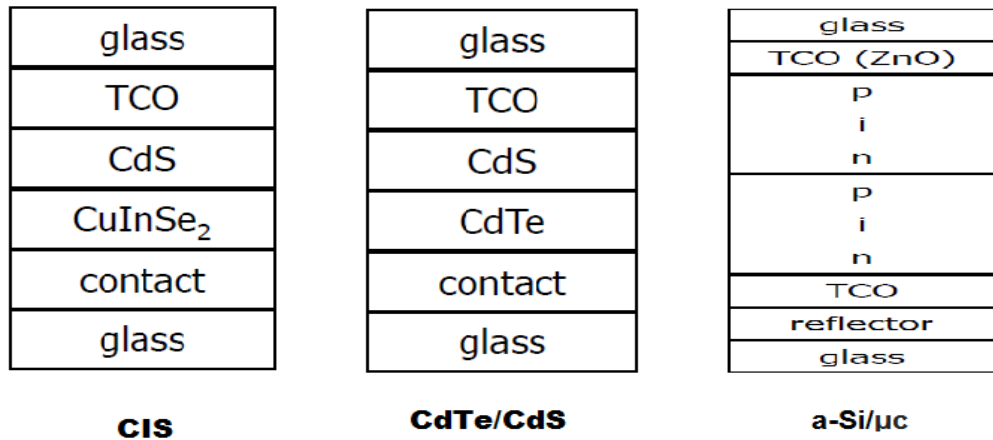


Figure 2-3: Schematic representation of the section of a Thin-Film solar cell.

- **Multijunction solar cell**, that are composed of p-n junctions of different semiconductor materials. Each semiconductor material is associated to a certain energy gap. It allow a current to be generated over a wide wavelength range of the incident sunlight. These cells allow a large spectrum of solar radiation to be absorbed. They achieve very high efficiencies (40%).

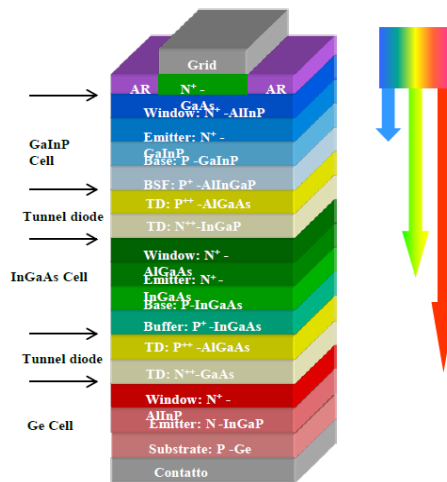


Figure 2-4: Schematic representation of the section of a multijunction solar cell.

2.3 I-V Curve

An exhaustive way to describe the behaviour of a PV cell (or also of a PV module) for fixed values of irradiance $G[\frac{W}{m^2}]$ and temperature $T_c[^\circ C]$ is through the characteristics:

- I - V curve
- P - V curve

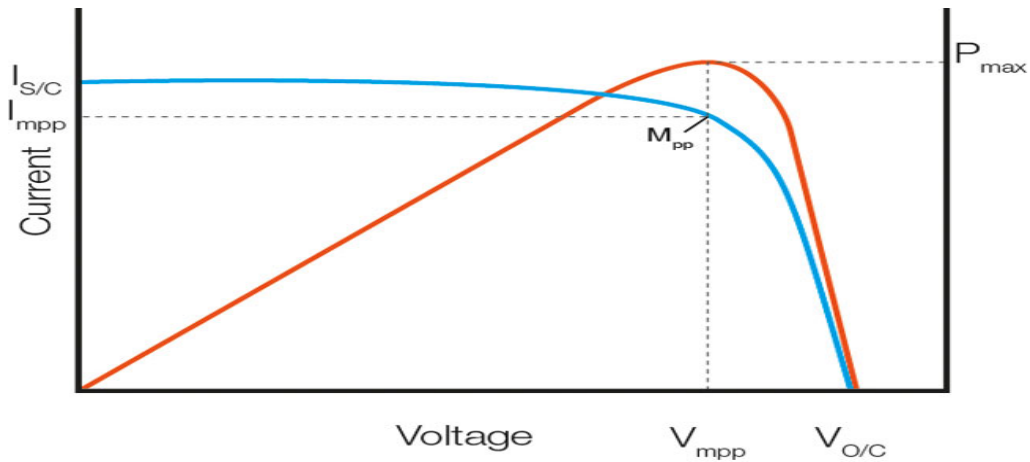


Figure 2-5: I - V curve and P - V curve with most important points.

It is possible identify three points on that curves that are related at three different operating conditions; they are respectively:

- $OC(0, I_{SC})$, Short Circuit point, condition in which the load is null and so the voltage across the cell is equal to 0 and the current is maximum.
- $OC(V_{OC}, 0)$, Open Circuit point, condition in which the current is null because the load is soo high.
- $MPP(V_{MPP}, I_{MPP})$, Maximum Power Point. It is the point on the curve in which the power produced from the cell is maximum. It can be calculated analytically calculating the maximum value of P expressed through the equation:

$$P = I * V \quad \text{Eq.(2-3)}$$

$$\frac{dP}{dV} = \frac{d(I*V)}{dV} = V * dI + I * dV \quad \text{Eq.(2-4)}$$

$$\frac{dP}{dV} = 0 \rightarrow \frac{I}{V} = -\frac{dI}{dV} \quad \text{Eq.(2-5)}$$

The real I - V curve occupies also the II and the IV quadrant of the graph. In particular conditions (shadowing and mismatch) the solar cell behaves like a load. In these situations, it is likely that faults occur leading to a bad functioning of the cell and to an increase of the losses. When the cells behave like a load it can assume negative voltage or negative current values. This is the reason because the I - V curve is present also in the II and IV quadrants.

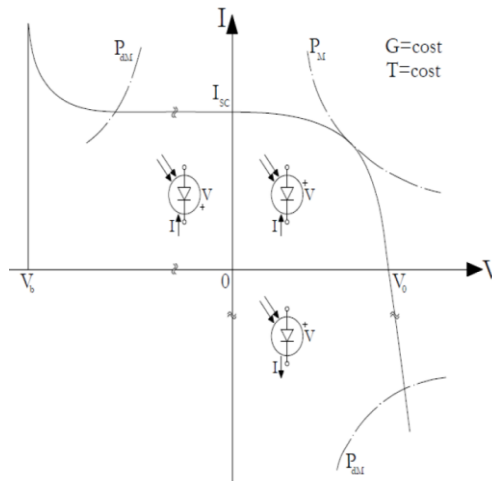


Figure 2-6: complete I - V Curve with Breakdown and Hot Spot limits.

In particular it is possible to identify part of the curve in the:

Quadrant IV: When the curve is included in quadrant IV, the cell assumes a positive voltage and a negative current ($V>0$ & $I<0$). By acting like a load, instead of generating electrical power, the cell dissipates power in the form of heat by heating up itself. If the cell temperature rises excessively and a certain limit is passed, the EVA material faults. The limit generally consists of $T \approx 85^{\circ}\text{C}$ for silicon modules. This type of failure is called Hot Spot, and is highlighted by the point of intersection between the I - V curve and

a branch of hyperbola $I \cdot V = \text{COST}$, which represents the power needed to heat the cell beyond the limit the failure occurs.

- II quadrant, when the curve is included in quadrant II, the cell has a negative voltage and a positive current ($V < 0$ & $I > 0$). In this situation, a failure can occur for high reverse voltages, in which the limit known as breakdown voltage is passed. The cell is forced to dissipate a high amount of thermal energy, this causes its failure, generating a short circuit. For silicon cells this limit coincides with a few dozen Volts. In addition, even in this case there may be hot spot phenomena represented by the intersection of the hyperbola with the $I-V$ curve.

2.4 Fill Factor

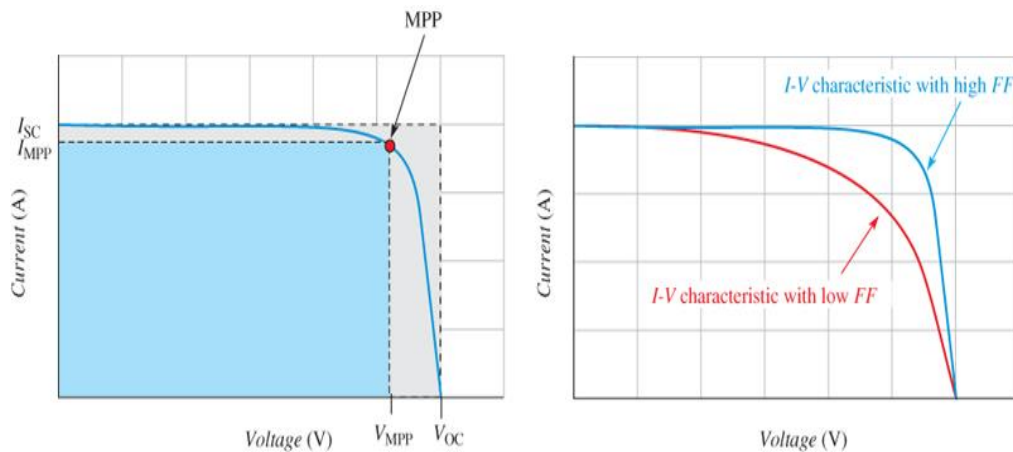


Figure 2-7: Schematic representation of the I-V curve at the Fill Factor variation.

A parameter of fundamental importance in determining the performance of a solar cell (or module) is the Fill Factor:

$$FF = \frac{I_{MPP} \cdot V_{MPP}}{I_{sc} \cdot V_{oc}} \quad \text{Eq.(2-6)}$$

Higher is the FF higher is the solar cell quality. If the FF is equal to 1 we are in the ideal case in which the solar cells behaves like an ideal current source. The I-V curve is square and the maximum power produced is equal to the product between the open circuit voltage and the short circuit current. For the crystalline silicon FF takes values included between (0.5, 0.86).

2.5 Equivalent circuit

In the purely ideal case, the cell can simply be represented by a current generator that generates a current equal to the photovoltaic current I_{ph} , disposed in parallel with a diode through which the current I_j (Junction current) flows. I_{ph} is proportional to the cell surface and irradiance G .

$$I_{ph} = G * S * K \quad \text{Eq.(2-7)}$$

Where K is a coefficient that depends on the solar cell. The diode functioning can be described from the Shokley Equation, Eq.(1-17)

$$I_j = I_0 * \left(e^{\frac{q*V}{n*k*T}} - 1 \right) \quad \text{Eq.(2-8)}$$

In this model we can identify three parameters that determine the behaviour of the circuit (I_{ph}, I_0, n).

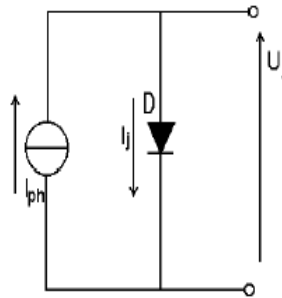


Figure 2-8: Ideal PV equivalent circuit with 3 parameters.

In this condition the $I-V$ curve can be represented by the subsequent characteristic presented in Figure 2-9. Where the curve in the OC and SC regions is completely straight.

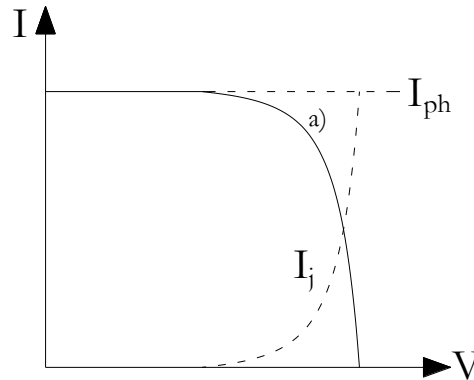


Figure 2-9: Ideal PV equivalent circuit IV curve.

The real behaviour of a cell or module, instead, can be described through a model that represents an equivalent electric circuit containing also resistors, arranged in series and/or in parallel. The I - V curve can be obtained, through the application of different models, each of which describes the behaviour of the cell with a good accuracy depending on the operating conditions in which the PV cell works. these models will be analysed in details in the next section, while, in this, we will focus on the analysis of the most common model that coincides with the 5 parameters equivalent circuit model, also called single diode circuit (SDM, Single Diode Model).

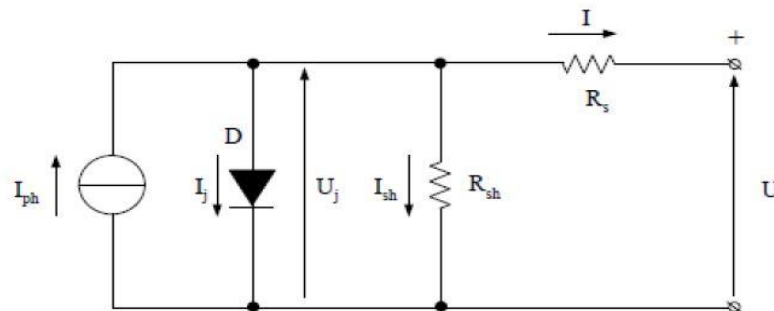


Figure 2-10: 5 parameters equivalent circuit.

SDM included 2 resistances:

- R_{sh} → Shunt Resistance, a resistor placed in parallel to the rectifier diode and the current generator, crossed by the current I_{sh} . This resistance takes into account the lateral current losses of the cell, simulated by the I_{sh} current. In the I - V curve presented in Fig 2-9 the effect of R_{sh} is neglected ($R_{sh} \rightarrow \infty$). If R_{sh} is taken into account and the lateral leakage of current is considered (R_{sh} assumes a finite value) the I - V curve becomes that in Fig.2-11 in which the

part of the curve closest to the OC is no more vertical but it is a little bit sharp.

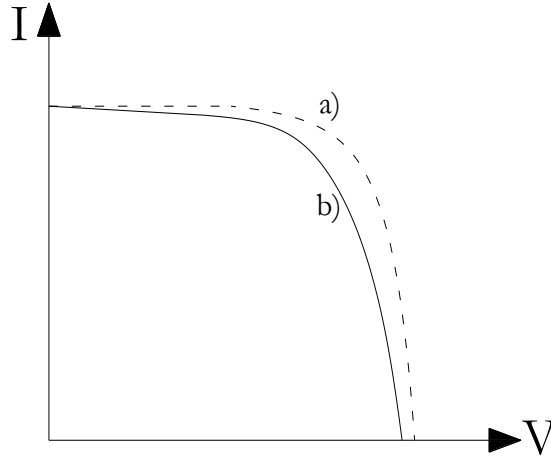


Figure 2-11: I - V curve with R_{sh} finite value.

- $R_s \rightarrow$ Resistance series, a resistance placed in series to the current generator and rectifier diode, crossed by current I (current transmitted to the load). This resistance takes into account all ohmic energy losses due to electrical contacts on the front side of the module. In Fig.2-9 and Fig.2-11 it is neglected. Taking into account its effect the I - V curve become more sharp in the area closest to the SC and the characteristic will be the next presented in Fig.2-12.

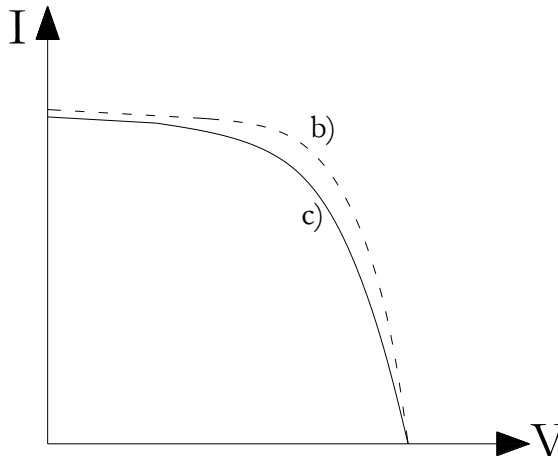


Figure 2-12: I - V curve taking into account the effect of R_s (different from 0).

In this case the parameters that determine the behaviour of the circuit are five ($I_{ph}, I_0, n, R_s, R_{sh}$). The transcendental equation that describes the behaviour of the

circuit, is obtained by applying Kirchhoff's law at the SD Fig.2-10. For the currents results:

$$I = I_{ph} - I_j - \frac{V_j}{R_{sh}} \quad \text{Eq.(2-9)}$$

For the Voltage results:

$$V = V_j - R_s * I \quad \text{Eq.(2-10)}$$

From the previous equations it is possible to derive the values of V_j e I_j

$$V_j = \frac{n*k*T_c}{q} * \ln\left(\frac{I_j+I_0}{I_0}\right) \quad \text{Eq.(2-11)}$$

$$I_j = I_{ph} - I - \frac{V_j}{R_{sh}} \quad \text{Eq.(2-12)}$$

Between the two resistances, $R_{sh} \gg R_s$ because of that $\frac{V_j}{R_s} \approx 0$ and from the 2 equations we can calculate the term V_j

$$V_j = \frac{n*k*T_c}{q} * \ln\left(\frac{I_{ph}-I+I_0}{I_0}\right) \quad \text{Eq.(2-13)}$$

Substituting in Eq.(2-10)

$$V = \frac{n*k*T_c}{q} * \ln\left(\frac{I_{ph}-I+I_0}{I_0}\right) - R_s * I \quad \text{Eq.(2-14)}$$

From which is possible calculate V_{OC} , imposing $V=V_{OC}$ when $I=0$:

$$V_{OC} = \frac{n*k*T_c}{q} * \ln\left(\frac{I_{ph}+I_0}{I_0}\right) \quad \text{Eq.(2-15)}$$

By replacing it is possible to obtain the transcendental equation of the equivalent circuit:

$$I = I_{ph} - I_0 * \left(e^{\frac{V+R_s*I}{V_{th}*n}} - 1 \right) - \frac{V+IR_s}{R_{sh}} \quad \text{Eq.(2-16)}$$

From which imposing $V=0$ it is possible determinatethe equation for I_{sh} :

$$I_{sc} = I_{ph} - I_0 * \left(e^{\frac{q*R_s*I}{n*k*T}} - 1 \right) - \frac{I*R_s}{R_{sh}} \quad \text{Eq.(2-17)}$$

Being the therm $R_s * I$ negligible, because $R_s \ll 1$ from Eq.(2-16):

$$I_{sc} \approx I_{ph} \quad \text{Eq.(2-18)}$$

2.5.1 Effect of parameters variation on I-V curve

In this section we will show how the I - V curves vary with the variation of the individual parameters of the circuit. In the following figures the impact of the variation of each parameter of the single diode circuit is varied within a certain range of values, while the other parameters are kept constant.

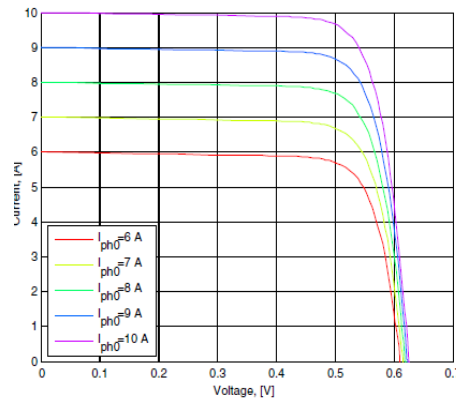


Figure 2-13: I - V curve varying I_{ph} .

How is evident from the previous equations (section 2.5) the effects generated by a I_{ph} variation:

- A larger effect, linked to a proportional variation of I_{SC} Eq.(2-17), that increase at the increasing of I_{ph} .
- A lower effect, V_{OC} grows as logarithmic trend at the increasing of I_{ph} eq(2-14)

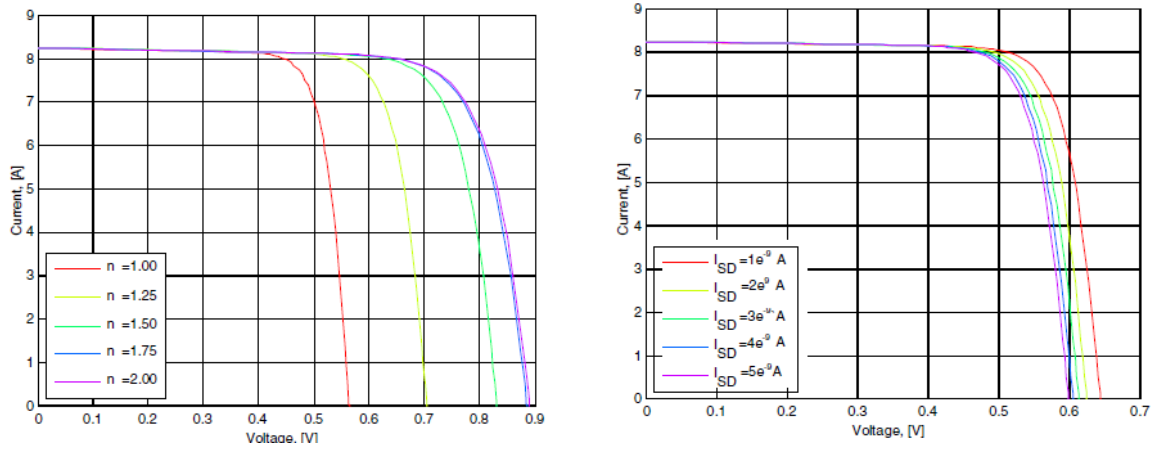


Figure 2-14: I - V curve at the variation of n e $I_{SD} = I_0$.

From Fig.2-10 it is possible notice that:

- The variation of n and I_0 parameters, not effects the position of SC, while it affects a lot the position of MPP, and on open circuit voltage V_{OC} .
- At the increasing of n the open circuit voltage increase and the point MPP moves towards right, because V_{MPP} increase, while I_{MPP} remain constant.
- At the growing of I_0 , decrease V_{OC} , and the point MPP moves towards left, because growing I_0 decrease V_{MPP} while I_{MPP} remain constant.

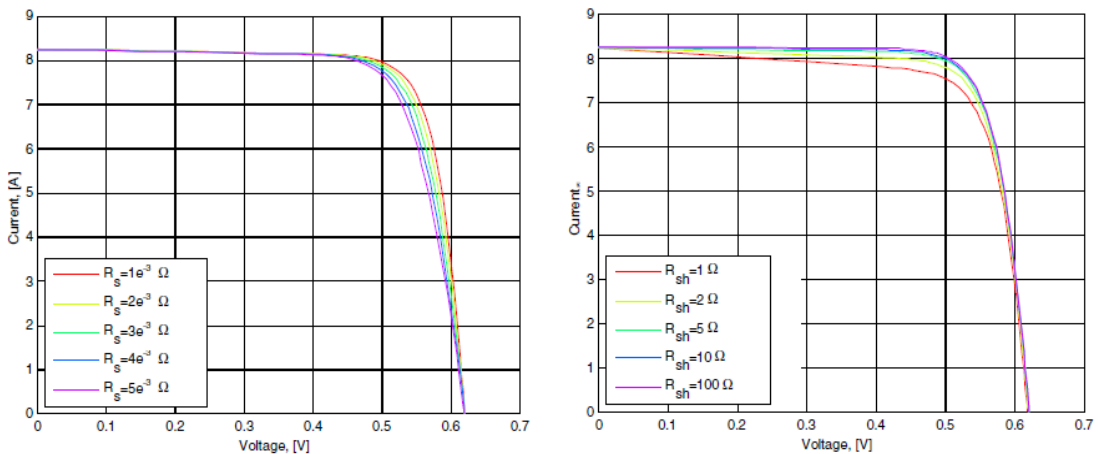


Figure 2-15: I - V curves at the varying of the parameters R_S and R_{sh} .

Finally, it is possible to analyse how the I - V curves vary with the variation of R_S e R_{sh} . These variations:

- Not affect I_{SC} and V_{OC} , that remain constants. While MPP moves because of the variation of both I_{MPP} and V_{MPP} .
- The R_s variation varies the slope of the curve in the area ner to the OC (Where the $I-V$ curve is approximated to a row with a negative angular coefficient), when $I=0$. At the increasing of R_s lthe sharp decrease, and so the point MPP is always moved towards low-left direction, because both I_{MPP} and V_{MPP} decrease.
- The R_{sh} variation allows to vary the slope of the curve in SC (Where the $I-V$ curve is approximated to a row with a negative angular coefficient) when $V=0$. At the increasing of R_{sh} the slope decrease, and so MPP moves towards up to the right, because both I_{MPP} and V_{MPP} increase.

2.5.2 Overview of the alternative SDM equivalent circuits:

In addition to the single diode model, there are other equivalent circuit models that allow to adequately simulate the behaviour of a cell. The most important equivalent circuit models in the literature will be listed and discussed in the following chapter. The most used model is the double diode model with seven parameters.

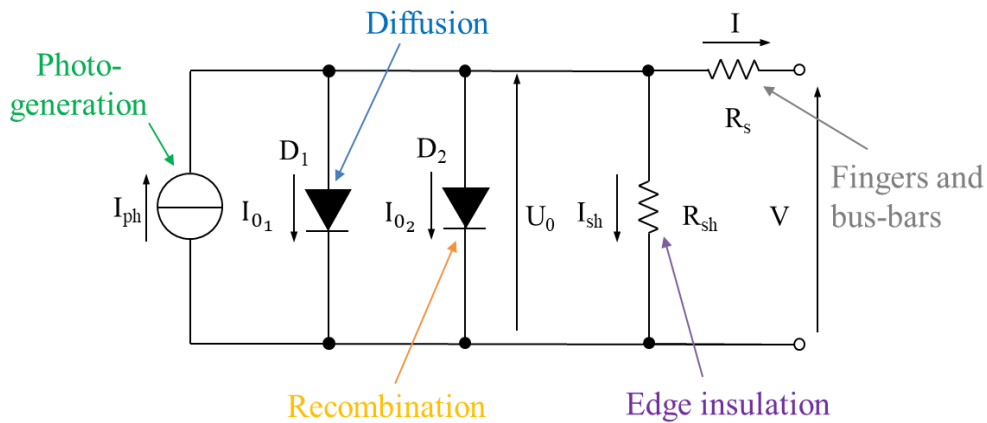


Figure 2-16: 7 parameters equivalent circuit models.

The 7 parameters equivalent circuit has higher accuracy than the single diode model in fact allows to simulate separately, the phenomena of diffusion and recombination in the junction of a photovoltaic cell. In the single-diode model, a single ideality factor is used to take into account recombination and diffusion within

the junction. The value of the ideality factor varies with the variation of the voltage, at high voltages dominates the diffusion, while

The ideality factor of the diode varies with the variation of the voltage. When the voltage is high, the diffusion phenomena dominate, while when the voltage is low, the recombination phenomena dominate (section 1-8). The use of a double-diode model allows to separate the effects of diffusion and recombination. The two diodes are connected in parallel. The first simulate the diffusion and has an ideality factor of about 1, the second simulate the recombination with an ideality factor of about 2. The transcendental equation of the 7-parameter model is as follows:

$$I = I_{ph} - I_{01} \cdot \left(e^{\frac{q(V+R_S \cdot I)}{n_1 \cdot kT}} - 1 \right) - I_{02} \cdot \left(e^{\frac{q(V+R_S \cdot I)}{n_2 \cdot kT}} - 1 \right) - \frac{(V+R_S \cdot I)}{R_{sh}} \quad \text{Eq.(2-19)}$$

When the photovoltaic cell works like a load, in case of mismatch you need to use another equivalent circuit model that allows the phenomenon of breakdown to be simulated. This model is the 10-parameters equivalent circuit model that allows the behaviour of the cell to be described even in case of high negative turns due to shading phenomena.

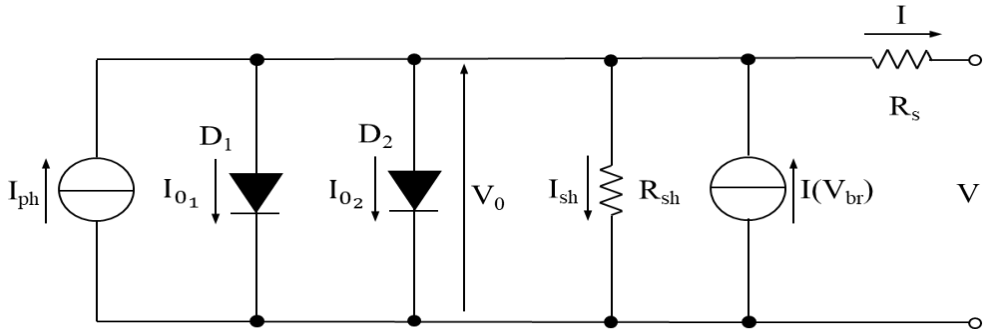


Figure 2-17: 10 parameters equivalent circuit model.

The transcendental equation that allows the 10-parameter model to be deciphered is as follows:

$$I = I_{ph} - I_{01} \cdot \left(e^{\frac{q(V+R_S \cdot I)}{n_1 \cdot kT}} - 1 \right) - I_{02} \cdot \left(e^{\frac{q(V+R_S \cdot I)}{n_2 \cdot kT}} - 1 \right) - \frac{(V+R_S \cdot I)}{R_{sh}} - a \cdot (V + R_S \cdot I) \cdot \left(1 - \frac{V+R_S \cdot I}{V_{br}} \right)^{-m} \quad \text{Eq.(2-20)}$$

Where the three terms added with respect the DD model are:

- $m \rightarrow$ exponent of the breakdown avalanche.

- $V_{br} \rightarrow$ breakdown voltage limit associated to a certain cell.
- $a \rightarrow$ portion of current Ohmic avalanche involved in break down

Some of the criteria that justify the choice of a model are related to the procedure of the extraction of parameters (which will be explained in the following paragraphs) are the computational cost, which increases as the number of parameters increases (increases the number of unknowns) and the accuracy of the model compared to the experimental data. In this chapter, the 5-parameter, single-diode model is analysed. It is a good trade-off between the accuracy of the results compared to experimental data and the computational effort in parameter extraction.

2.5.3 Explicit form of transcendental equation using Lambert function

In the section 2-4 is introduced the transcendental equation, Eq.(2-16), which is the equation that describes the SDM. This equation is an implicit equation, because the current cannot be expressed in an explicit form. It possible to say that, because the current variable is present both in linear and in exponential form into the equation. In order to make explicitly the transcendental equation Eq.(2-16) is possible to use the Lambert function. The Lambert Function, which is the function LambertW of independent variable z for which the subsequent equation is verified.

$$z = LambertW(z) * e^{LambertW(z)} \quad \text{Eq.(2-21)}$$

Using the Lambert function into the transcendental equation Eq.(2-16), it becomes:

$$I = -\frac{U}{R_s} + \left(-LambertW \left(\frac{R_s * I_0 * R_{sh} * e^{\frac{R_s * I_{ph} + R_s * I_0 + U}{n * U_{th} * (R_s + R_{sh})}}}{n * U_{th} * (R_s + R_{sh})} \right) * \frac{n * U_{th}}{R_s} + \frac{R_{sh} * (R_s * I_{ph} + R_s * I_0 + U)}{n * U_{th} * (R_s + R_s)} \right) \quad \text{Eq.(2-22)}$$

The equation passing from implicit form to the explicit form some there are several advantages, especially for the extraction parameters problem which will be explain in the next sections. For that reason often, in these types of problem the equation is computed in its explicit form using the Lambert function [2, 3].

2.6 Solar cell power and efficiency

The conversion efficiency referred to a solar cell can be expressed through the subsequent formulation:

$$\eta = \frac{P_{MPP}}{G * A} \quad \text{Eq.(2-23)}$$

Where:

- P_{MAX} [W] → It is the maximum power that the cell is able to produce when it works at MPP.
- G [W/m^2] → It is the irradiance on the surface S of the solar cell.
- A [m^2] → Surface of the solar cell.

Today solar cells available on the market can reach efficiency $\approx 23\%$. **Errore. L'origine riferimento non è stata trovata.** 8 shows a typical profile of the current density J the $J = \frac{I}{S}$ and of the useful power density produced $p_u = \frac{P_u}{S}$ for a solar cell of surface S express as a function of voltage V .

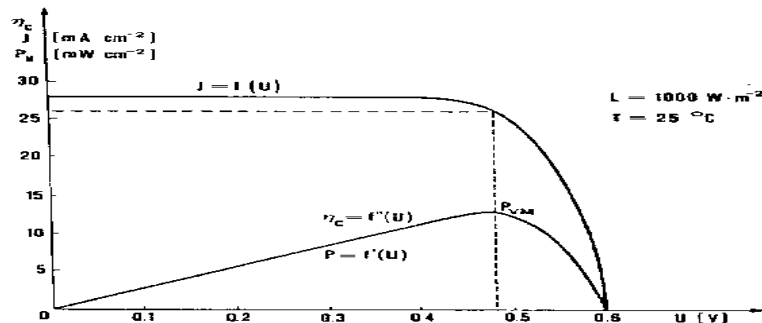


Figure 2-18: $J=f(V)$ and $P_u=f(V)$

Conversion efficiency and useful power density curve have the same shape, given a precise geographical site imposed climatic and environmental conditions and type of module the product $G * A$ remains constant.

2.7 Causes of energy losses in a solar cell

The Power Losses are always present in a real system, and also in the solar cells they can be reduced but not completely eliminated:

- *Reflection and covering*, It constitutes the 10% of the total amount of power losses. They are the losses due to the radiation that is reflected or that doesn't reach the solar cell because of the contacts over the frontal surface. So, to minimize these power leakages, an anti-reflective layer is applied to the frontal surface moreover the surface of the frontal contacts is reduced to the minimum.
- *Energetic Surplus*, they happens when the photons that hit the solar cell have an energy much more higher than the energy gap of the semiconductor. The amount of energy in excess is lost under the form of heat. They constitute about the 25% of the total amount of losses.
- *Insufficient energy of incident photons*, this phenomenon happens when the photons that hit the solar cell surface have less energy than the energy gap of the semiconductor. Their energy is not used and is dispersed in heat These losses constitute about 20% of the total amount of losses.
- *Recombination factor*. This losses occurs in presence of the recombination of the electrons holes pairs inside the p-n junction. The recombination becomes more likely when there are defect inside the material. It can constitute the 2% of the total amount of energy losses.
- *Fill Factor losses*, Losses due to leakage of current at the sides of the cell and due to the ohmic resistance of the electrical contacts. They are modelled in the equivalent circuit by R_{sh} and R_s . Generally this is the reason why the I-U curve assumes a distorted and not rectangular shape, and therefore the FF is not equal to 1. These losses represent about 20% of the total amount of energy losses.

2.8 Variation of the PV performances with G and T_c

As previously stated, the I - V curves refer to precise conditions of irradiance G and temperature of the T_c , as these operating parameters change the performance of the cell vary, generating significant changes in the I - V curves. The variations of the I - V curves with respect to the variation of T_c and G are shown in the following graphs, analysing separately the effect of the variation of each of the two parameters.

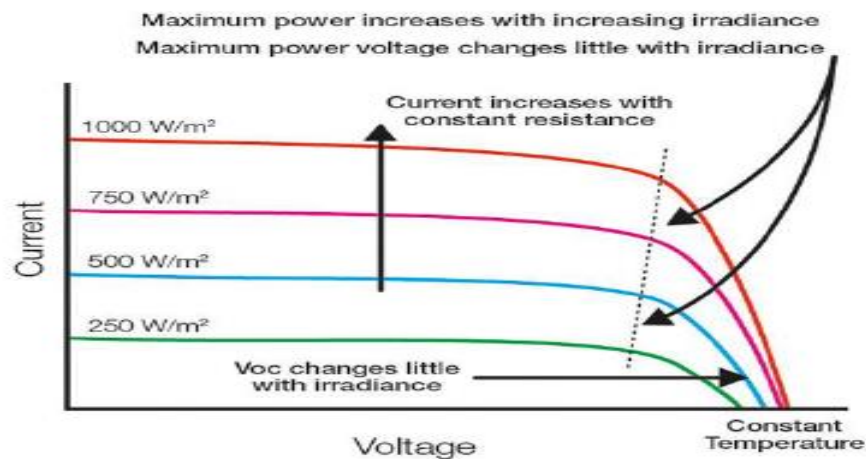


Figure 2-19: G variation effect on the I - V curves.

With the variation of G and keeping constant T_c the following effects occur:

- The short-circuit current and the I_{sc} and the I_{MPP} vary in a way that is proportional to the variation of the irradiance, growing with the growth of G .

$$I_{sc} \propto G \quad \& \quad I_{MPP} \propto G \quad \text{Eq.(2-24)}$$

- The short circuit voltage U_{oc} decreases with decreasing irradiance. It is possible to demonstrate that U_{oc} varies directly proportional to the logarithm of G , in fact with a good approximation:

$$U_{oc} \approx \frac{n \cdot k \cdot T}{q} \ln \left(\frac{I_{ph}}{I_0} \right) \quad \text{Eq.(2-25)}$$

$$U_{oc} \propto \ln(G) \quad \text{Eq.(2-26)}$$

The variations of U_{OC} are very small, so much so that U_{OC} is almost constant, while it assumes significant variations for very low values of irradiance ($G \leq 50 \text{ W/m}^2$). In the formulas that report the parameters from the standard condition this variation is often neglected and the parameters are considered constant.

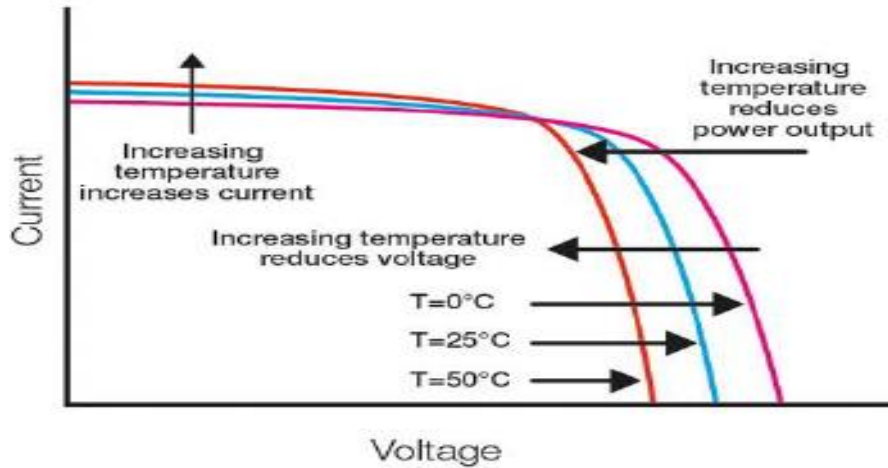


Figure 2-20: T_c variation effect on the $I-V$ curves.

With the variation of T_c and keeping constant G the following effects occur:

- I_{SC}, I_{MPP} they vary very little, decreasing as the T_c grows, in any case this decrease is almost negligible and the parameters can be considered almost constant. In the formulas that report the parameters from the standard condition is expressed a proportional relationship that relates I_{SC}, I_{MPP} to T_c . The proportionality coefficient is a very small negative constant, in the order of $[\mu\text{A}/^\circ\text{C}/\text{cm}^2]$. U_{oc} e U_{MPP} vary strongly as the T_c varies proportionally, growing as the T_c increases.

As result, the maximum power decrease proportionally with the increasing of the cell temperature with respect to the STC. This gradient for the silicon cell is more or less $-0.45 \frac{\%P_{MPPSTC}}{^\circ\text{C}}$. This coefficient depends on the technologies.

Table 2-2: Temperature coefficient to report the parameters from the STC to the real conditions.

dJ_{sc}/dT	+10 $\mu A/(cm^2 \cdot ^\circ C)$
dU_{oc}/dT	-2,2 mV/ $^\circ C$
$dP_M/P_M/dT$	-0,45 %/ $^\circ C$

2.9 Solar Cells connected in series and in parallel

A single silicon cell can be generated in optimal load conditions:

- $V \approx (0.5 \div 0.6)V$ (Independently from the frontal surface of the cell)
- $J_{SC} \approx (25 \div 35) \left[\frac{mA}{cm^2} \right]$ that means, $I_{SC} \approx (4 \div 5)[A]$ for square cells with side of 12,5 [cm] o $I_{SC} \approx (6 \div 8) [A]$ for square cells with side of 15.6 [cm].

The connection of an higher number of cells is necessary to supply the requests of current and voltage of the load, that normally are much larger than the aforementioned values.

- Cells connected in series, The connection of N_s cells in serie is called string. In order to connect N_s cells in series, it is needed to directly connect the the positive electrode of one cell with the negative electrode of the next cell. The same current I is conducted through the string, while the voltages across the string heads can be calculated summing the voltage of each cells. If mismatch problems (that will be explained in the next chapter) not sussists:

$$V = \sum_{i=1}^{N_s} V_i \quad \text{Eq.(2-27)}$$

$$I_i = I_{i+1} = I = cost. \quad \text{Eq.(2-28)}$$

- Cells connected in parallel, In order to connect N_p cells in parallel it is necessary to connect togheter the N_p electrodes of the same sign. When a certain number of strings are connected in parallel the voltage across the string heads is the same for each string,

while the current associated to the connection can be calculated summing the current of each string. If mismatch problems doesn't occur:

$$I = \sum_{i=1}^{N_s} I_i \quad \text{Eq.(2-29)}$$

$$V_i = V_{i+1} = V = cost. \quad \text{Eq.(2-30)}$$

Generally in a module the cells are connected in series in order to maximize the voltage at the heads of the PV module.

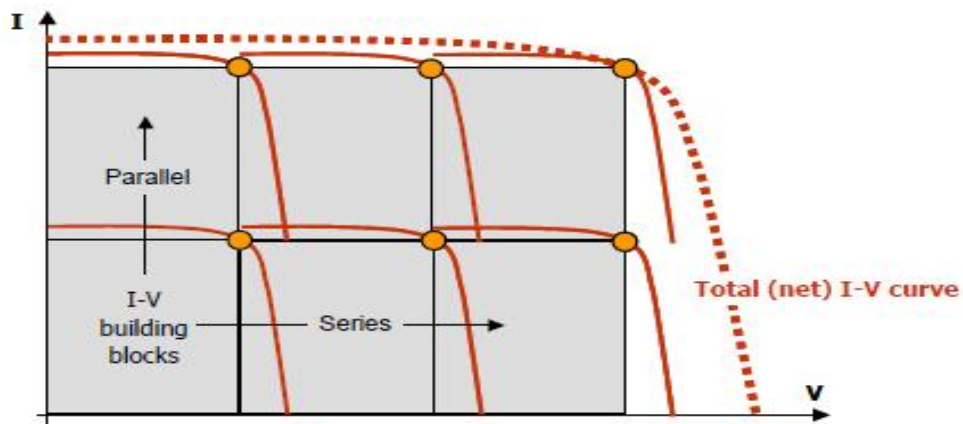


Figure 2-21: Construction of an $I-V$ curve of a module from the $I-V$ curves of the individual cells.

These effects are graphically visible because the $I-V$ curve of a $N_s \times N_p$ cells connection can be obtained by summing the graphs of each single $I-V$ curve.

2.10 Mismatch

When the $I-V$ curves of two connected cells are different from each other, a phenomenon called mismatch occurs. These differences between two identical cells connected together may exist due to the presence of manufacturing defects within some cells belonging to the connection, or even to a partial shading phenomena.

2.10.1 Mismatch of cells connected in series

If in a string of N_s equal cells connected in series there is one cell that has an $I-V$ curve different from the others, the global $I-V$ curve of the string will be obtained by summing, for each current value, the identical voltages V belonging to the (N_s-1) cells with the same $I-V$ curve plus the voltage V of the different cell. This is a

common condition of mismatch, that can be due to the shading effects or manufacturing defects.

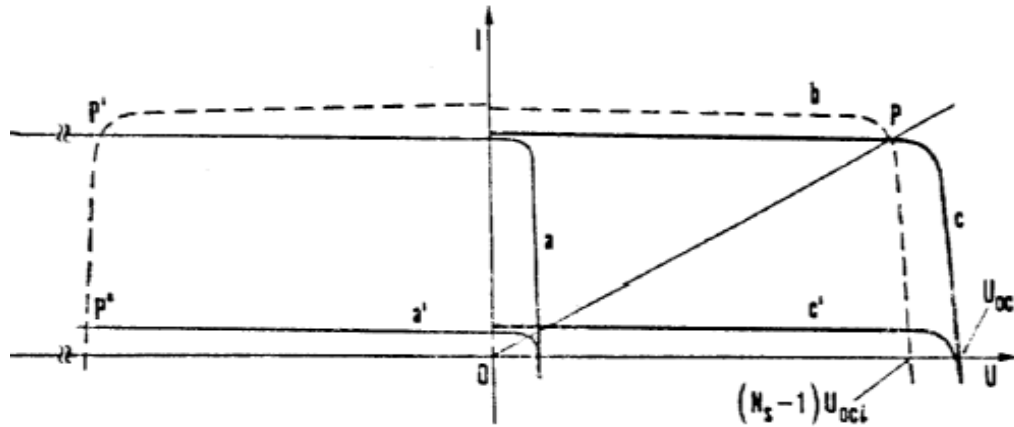


Figure 2-22: Mismatch of two cells connected in series.

Watching the Fig.2-22 it easy to understand that:

- a-curve: defected $I-V$ curve ;
- a'-curve: shaded $I-V$ curve;
- c-curve: $I-V$ curve calculated summing of the good cells with the defected a-curve
- c'-curve: $I-V$ curve calculated summing of the good cells with the shaded a'-curve
- b-curve: I-V curve curve calculated summing the $I-V$ curves of the N_s-1 good cells.

It is clear that in both cases the MPP of the string undergoes a significant reduction compared to the equivalent curve that can be obtained with our cells operating under conditions of complete irradiance and not defective cells. In particular, the shaded cell effect is the worst for the power produced by the system. Looking at the graph it is possible to observe that the V_{OC} is equal to the sum of all the individual V_{OC}, while the short-circuit current is equal to the minimum value of the short-circuit current of the cells of the string.

$$V_{OC} = \sum_{i=1}^{N_s} V_{OC_i} \quad \text{Eq.(2-31)}$$

$$I_{SC} \cong (I_{SC})_{MIN} \quad \text{Eq.(2-32)}$$

For a totally shaded cell, the resulting I_{SC} is zero, $(I_{SC})_{MIN}=0$, and the cell behaves like a very high resistive load (tends to infinity), while, if a-curve or a'-curve do not differ much from the good cell curves, the reduction I_{SC} is low and so, also the reduction of the power produced by the string. If the load resistance is so low that the intersection between the load and the $I-V$ curve occurs in an operating point lower than P, the cell (a) assumes a load behavior and a negative voltage occurs at the heads of the cell. The most harmful situation occurs in short circuit conditions; in this case, the defective cell (a) (or shaded cell (a')) behaves like a load dissipating power, at the heads of the cell is applied a negative voltage equal to $(N_s-1)*V$ which corresponds to the sum of the voltages of the fully radiated cells. This operating condition is represented in the figure by the points P' and P'' respectively for, cell with manufacturing defects and shaded cell. In these conditions the dissipated power by the defective cell is very large, hot spot or break down phenomena can arise leading to cell failure. Normally the values of the negative voltage associated to the Break Down failure for crystalline silicon cells are $V_{breakdown} \approx (25\div 50)$ V, since a cell averages 0.5 V, a number between 50 and 100 cells can lead to instantaneous failures for cell break down. The best way to avoid mismatch problems is to insert a protection diode, connected in parallel to the ends of each cell. Figure 1-15 shows the configuration of a string in the presence of a diode, which cancels the current flow if the cell behaves like a load with negative voltage. In the figure, the cells are represented as ideal current generators.

2.10.1.1 Bypass diode

In order to avoid the mismatch problems in a series connection of cells a protection diode can be connected in parallel to the heads of each cell. Figure 2-23 shows the configuration of the string with the application of the diodes (D_p); it stops the flow of current when the cell behaves like a load with negative voltage. In the figure, the cells are represented as ideal current generators.

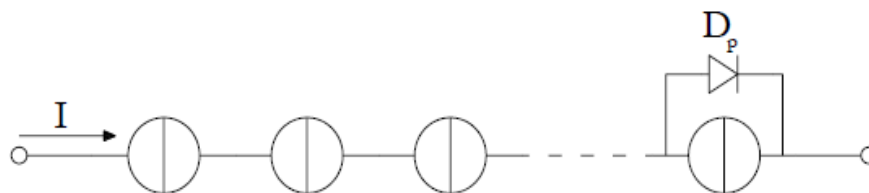


Figure 2-23: Series connection with bypass diode.

The Bypass diode is connected to the cell in order to operate in this way:

- Normal operating conditions of the cell, the cell behaves like a current generator. In this condition the diode is OFF and operates in reverse bias, D_p remains closed and the current flows through the cell. The cell produces electrical power.
- Mismatch operating condition of the cell, the cell behaves like a load with reverse voltage. At the heads of D_p a reverse voltage occurs, D_p works in a direct bias, the diode is ON and is able to conduct current. In this way the current does not pass from the cell, instead it passes through the diode. In this way the cell does not dissipate power. The minimum I_{sc} is no longer equal to the current of the defected cell but is equal to the I_{sc} of the cells that operate in normal operating conditions. The only energy loss now is the power that the cell bypassed from the current is no longer able to produce.

The application of one D_p for each cell is very expensive and not always is convenient from the economical point of view. This type of configuration is adopted only in aerospace applications. For common terrestrial applications a good compromise is to connect a bypass diode to strings of a group of cells. Generally, the strings at which the diode is connected are composed of 18-24 or 36 cells. So if a mismatch occurs, the string is disconnected. The graphical action of a bypass diode of a cell inside a string composed of two cells connected in series is shown in Fig.2-24.

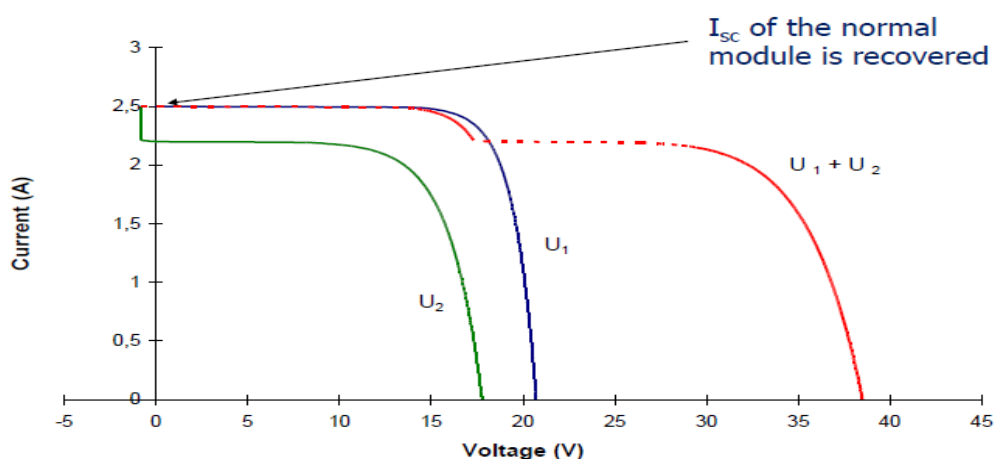


Figure 2-24: Action of a bypass diode on a connection of two cells in series.

2.10.2 Mismatch of cells connected in parallel

If in a group of N_p equal strings connected in parallel there is one cell that has an $I-V$ curve different from the others, the global $I-V$ curve of the parallel connection will be obtained by summing, for each voltage value, the identical current conducted through the (N_p-1) string composed by cells with a normal $I-V$ curve plus the current I of the string containing the defected cell. This is a common condition of mismatch, that can be due to the shading effects or manufacturing defects.

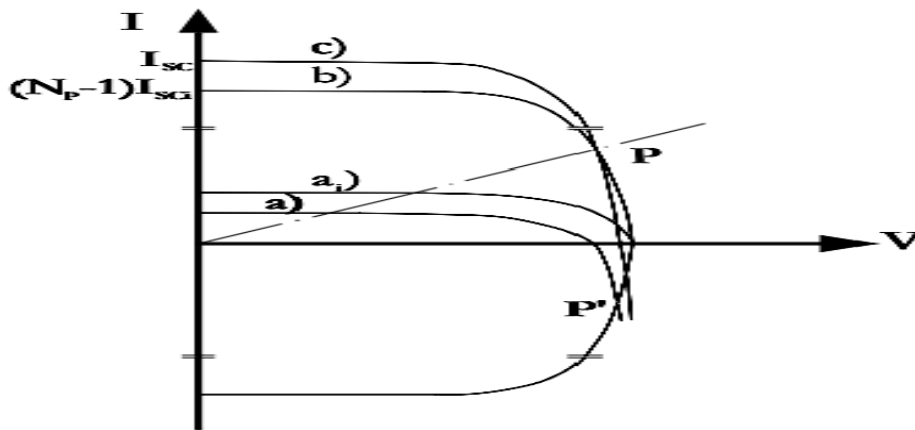


Figure 2-25: Mismatch of cells connected in parallel.

In Figure 2-25 it is possible to observe the different $I-V$ curves of the cells connected in parallel:

- a-curve: $I-V$ curve of a string of cells containing the defected cell;
- a'-curve: $I-V$ curve of a string of good cells;
- c-curve: $I-V$ curve calculated summing of the good strings with the one that contains the defected cell;
- b-curve: $I-V$ curve calculated summing the $I-V$ curves of the N_s-1 good string of cells.

The short circuit current of the resultant $I-V$ curve is given by the sum of the values of the short circuit currents of each strings, both those completely irradiated and operating under correct operating conditions string, and also the string that contains

the defective cell. The value of the open circuit voltage V_{OC} is equal to the value of the cell with minimum open circuit voltage.:

$$I_{SC} = \sum_{i=1}^{N_s} I_{SC_i} \quad \text{Eq.(2-33)}$$

$$V_{OC} \cong (V_{OC})_{MIN} \quad \text{Eq.(2-34)}$$

If The worst case is in open circuit conditions, in this case the string that contains the defective cell operates as a load that emits reverse current, dissipating power, and it absorb the current $(N_p-1)*I$ from all other strings that are composed from cells that operate correctly. If the power dissipation is too high, the cell heats up too much and the temperature reaches values too high that can lead to failure for Hot Spot.

2.10.2.1 Blocking diode

In order to solve this problem a blocking diode is connected in series to each string, so as to prevent a string of the parallel connection from behaving like a reverse current load.

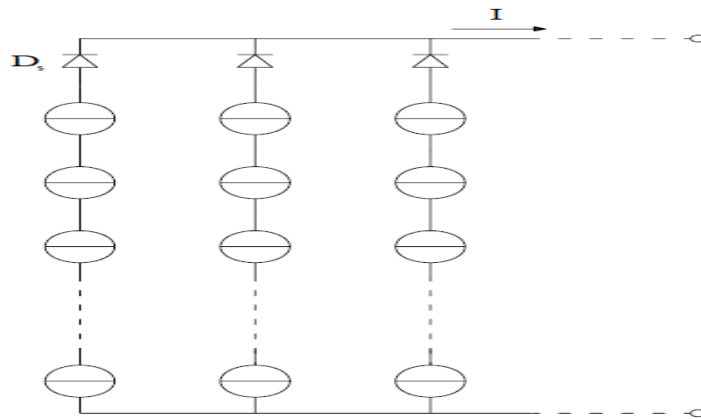


Figure 2-26: Parallel connection of blocking diode.

The diode is applied in order to allow:

- For normal operative conditions, all the cells behaving like a current generator, the diode is ON. It operates by direct polarization, allows the passage of current and the generation of power.

- For mismatch conditions, when at least one cell behaving like a load, at the heads of D_p occurs a negative voltage. D_p is connected by reverse polarization, the diode is OFF and does not allow the passage of current. The current coming from the whole string is blocked and is not transmitted to the node. In this way, the V_{oc} of the series connection no longer corresponds to the minimum V_{oc} of the defective cell, but is equal to the V_{oc} of the correctly connected and fully radiated cells. The reduction in power lies exclusively in the loss of the of energy produced by the string containing the defective cell, which does not produce power.

II The graphic result on the $I-V$ curve of the action of a bypass diode on a cell belonging to a connection of two cells in series is shown in the figure below.

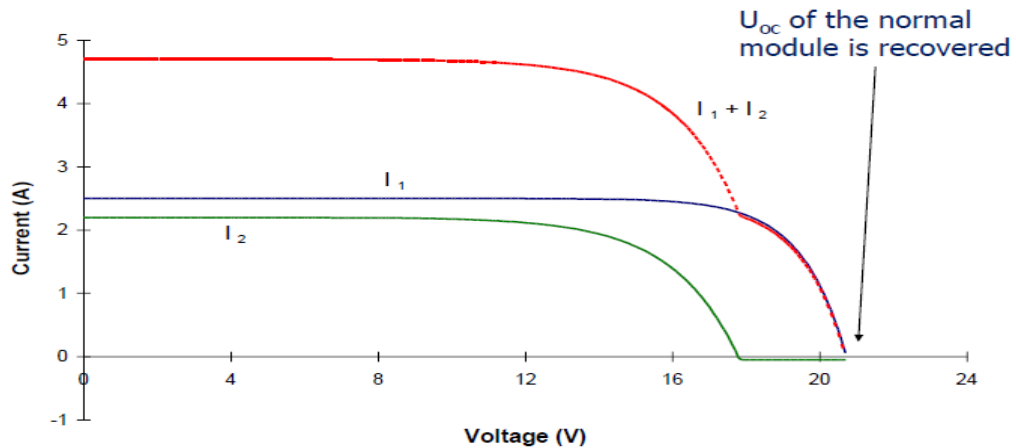


Figure 2-27: Action of a blocking diode on a connection of two cells in parallel.

2.11 PV module structure

The conventional structure of a module for ground power generation in photovoltaic power plants is shown in the following figure.

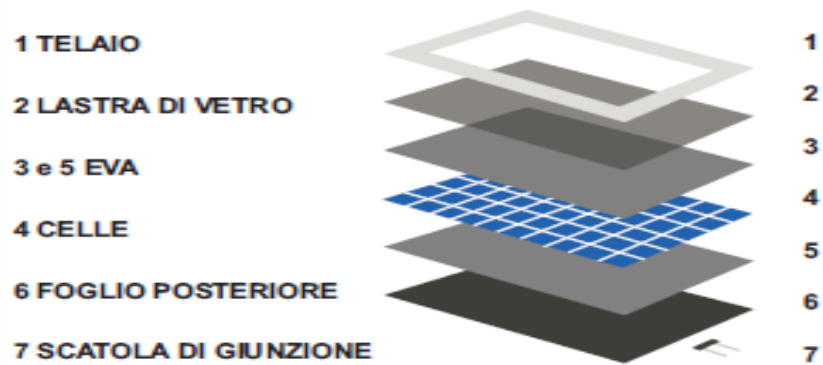


Figure 2-28: Representation of the generic structure of a photovoltaic module.

A module must withstand numerous environmental agents from outside (e.g. wind, dust, snow, hail, rain, humidity, etc.). For this reason, the module is covered with high transmittance glass in order to ensure a high irradiance to the active surface made up of cells. The solar cells are contained within a structure of EVA or Vinyl Ethylene Acetate. EVA is a thermoplastic polymer, transparent to light and unalterable over time, which has the purpose of electrically insulating the cells, and prevent the entry of moisture. The main problem of this material is that it does not tolerate high temperatures. it is the main cause of the phenomenon of the Hot Spot. There are other plastic materials with better performance but EVA is the most economical solution. The process of encapsulation of the cells within the EVA takes place through a vacuum lamination process at 140-150 °C, in which two sheets of EVA are fused together by encapsulating the cells within them. The flat rear surface can be made of Tedlar, mylar or glass. The module is mechanically supported and fixed to the ground by means of an aluminium frame. The junction box contains the bypass diodes and ends with two cables through which to connect the module to an external circuit or another module.

2.12 STC-Standard Test Conditions

The PV module features are often provided by the manufacturers in STC, as it complies with the IEC/EN60904 standard:

- Irradiancia $G=1000 \left[\frac{W}{m^2} \right]$.
- Air Mass $AM=1.5$.
- Cell Temperature $T_c=25 \left[^\circ C \right]$.

2.13 NOCT, Nominal Operating Cell Temperature

“NOCT (Nominal Operating Cell Temperature), is the value of the cell temperature at which the module is stable in open circuit conditions. It is evaluated under the following operating conditions”:

- Irradiance $\rightarrow G=800 \left[\frac{W}{m^2} \right]$.
- Wind Speed $\rightarrow w=1 \left[\frac{m}{s} \right]$.
- Ambient temperature $\rightarrow T_a=20 [^{\circ}C]$

NOCT allows the T_c cell temperature to be calculated under different operating conditions (typical values are between $(42 \div 50) ^{\circ}C$). Assuming that, at irradiance G and at room temperature T_a , the temperature difference (T_c-T_a) depends linearly on irradiance G , as express in the subsequent equation:

$$T_c = T_a + \frac{NOCT-20}{0,8} * G \left[\frac{kW}{m^2} \right] \quad \text{Eq.(2-35)}$$

2.13.1 Data given by the manufacturer

Each module needs a legible and indelible license plate where the following data have to be provided:

- Name and symbol of the manufacturer;
- Type and model number;
- Serial number;
- Polarity of terminals or conductors;
- Maximum operating voltage of the module;
- Module class of use;
- Class II symbol (for class A modules);
- Open-circuit voltage V_{oc} in STC conditions;
- Short-circuit current I_{sc} in STC conditions;

- Rated power P_{rated} in STC conditions and indications on production tolerances;
- Maximum power voltage V_{mpp} in STC conditions;
- Maximum power current I_{mpp} in STC conditions;
- Maximum rated current of devices that protect the module against overcurrents (usually fuses);
- Cell temperature in nominal operating conditions (NOCT);
- Maximum tolerable reverse current;
- α_{Isc} , short-circuit current temperature coefficient expressed in $\left[\frac{\%}{^{\circ}\text{C}}\right]$ or $\left[\frac{\text{A}}{^{\circ}\text{C}}\right]$;
- β_{Uoc} , open-circuit voltage temperature coefficient expressed in $\left[\frac{\%}{^{\circ}\text{C}}\right]$ or $\left[\frac{\text{V}}{^{\circ}\text{C}}\right]$;
- γ_{Pm} , power temperature coefficient expressed in $\left[\frac{\%}{^{\circ}\text{C}}\right]$ or $\left[\frac{\text{W}}{^{\circ}\text{C}}\right]$

Usually the maximum power P_{rated} is expressed in $[\text{W}_p]$, just to indicate briefly that considered condition is maximum power condition. However, the module can produce more than P_{rated} if the irradiance on the surface is higher than $1000 \left[\frac{\text{W}}{\text{m}^2}\right]$, in particular if cell temperature is lower than 25°C .

2.14 Power and efficiency of a PV module

For a certain fixed environment condition of irradiance G and ambient temperature T the power of the sun that hit the surface A is:

$$P_s = G \cdot A \quad \text{Eq.(2-36)}$$

Considering P_{MPP} the maximum power that the PV module is able to produce in a certain ambient condition (G,T), the conversion efficiency is calculated through:

$$\eta_M = \frac{P_M}{G \cdot A} \quad \text{Eq.(2-37)}$$

The global efficiency of a module is generally lower than the efficiency of the single cell because it depends on different factors that are contained in the concept of the module. In order to identify the different factors is possible to represent the efficiency of the module as a product of different efficiencies:

$$\eta_M = \eta_P \cdot \eta_{EC} \cdot \eta_{IM} \quad \text{Eq.(2-38)}$$

where:

- $\eta_M \rightarrow$ global efficiency of the photovoltaic module;
- $\eta_P \rightarrow$ is *filling* efficiency, it takes into account all the unactive surface contained in the frontal surface. They don't allow all the module surface to be exploited for the direct conversion of the solar energy of the module in electricity. This efficiency can be calculated as the ratio between the frontal surface and the active part that constitutes the frontal surface. Its value is around 85%.
- $\eta_{EC} \rightarrow$ encapsulation efficiency, it can be calculated as the product of three terms:

$$\eta_{EC} = \eta_C \cdot \eta_T \cdot \eta_{MIS} \quad \text{Eq.(2-39)}$$

where:

- η_C is the conversion efficiency of the cell without the presence of the EVA and the cover glass;
- η_T it considers the effect of absorption from the resin and from the glass cover materials and its value is around 95%.

- η_{MIS} The efficiency considers the effects of mismatch and the joule losses due to the connections. Its value is around 95%.
- $\eta_{IM} \rightarrow$ not homogeneous irradiance efficiency, it considers the fact that the irradiance that hit the PV module is not homogeneously distributed. Its value is around 98%.

2.15 Evaluation of PV performance in STC and Osterwald Model

The basic data of a module are often provided from the manufacturer datasheet, in STC conditions. For this reason, correlations to calculate the value of these data under different conditions of irradiance and cell temperature have been defined. Generally, the manufacturers provide three coefficients percentage temperature coefficient of I_{SC} , defined as $\alpha_{\%}$, percentage temperature coefficient of I_{SC} defined as $\beta_{\%}$ and percentage temperature coefficient of power at MPP defined as $\gamma_{\%}$.

Proportional correlation for I_{SC} , expresses the short-circuit current value as a function of cell temperature (weakly) and irradiance (strongly).

$$I_{SC}(G, T) = I_{SC}(STC) * \frac{G \left[\frac{W}{m^2} \right]}{1000} * \left(1 + \frac{\alpha_{\%} * I_{SC}}{100} * \Delta T_C \right) \quad \text{Eq.(2-40)}$$

$$\Delta T_C = T_c [^{\circ}C] - 25^{\circ}C \quad \text{Eq.(2-41)}$$

Dove:

- $I_{SC}(STC) \rightarrow$ Short-circuit current under STC conditions [A].
- $I_{SC}(G, T_C) \rightarrow$ Short-circuit current under irradiance conditions $G \left[\frac{W}{m^2} \right]$ e cell temperature $T_c [^{\circ}C]$.
- $\alpha_{\%} \rightarrow$ percentage variation coefficient of I_{SC} with $T_c \left[\frac{\%}{^{\circ}C} \right]$, the temperature coefficient $\left[\frac{A}{^{\circ}C} \right]$ may be expressed as:

$$\alpha_{I_{SC}} = \frac{I_{SC}}{100} * \alpha_{\%} \quad \text{Eq.(2-42)}$$

- Proportional correlation V_{oc} , expresses the value of the no-load voltage as a function of cell temperature, neglecting the dependence of the latter on irradiance (see section 2.3)

$$V_{OC}(G, T) = V_{OC}(STC) * \left(1 + \frac{\beta_{\%} * V_{OC}}{100} \Delta T_C\right) \quad \text{Eq.(2-43)}$$

$$\Delta T_C = T_c [^{\circ}C] - 25^{\circ}C \quad \text{Eq.(2-44)}$$

Dove:

- $V_{OC}(STC) \rightarrow$ Open circuit voltage in STC [V].
- $V_{OC}(G, T_c) \rightarrow$ Open circuit voltage in conditions of irradiance $G \left[\frac{W}{m^2}\right]$ e Temperature $T_c [^{\circ}C]$.
- $\beta_{\%} \rightarrow V_{OC}$ variation percentage coefficient with $T_c \left[\frac{\%}{^{\circ}C}\right]$, the temperature coefficient can be expressed as $\left[\frac{V}{^{\circ}C}\right]$:

$$\beta_{U_{OC}} = \frac{V_{OC}}{100} * \beta_{\%} \quad \text{Eq.(2-45)}$$

- Osterwald Model (OM) [4], expresses the value of the nominal power P_{MPP} of the module as a function of cell temperature, and irradiance (see section 2.3):

$$P_{MPP}(G, T) = P_{MPP}(STC) * \frac{G \left[\frac{W}{m^2}\right]}{1000} * \left(1 + \frac{\gamma_{\%} * P_{MPP}}{100} \Delta T_C\right) \quad \text{Eq.(2-46)}$$

$$\Delta T_C = T_c [^{\circ}C] - 25^{\circ}C \quad \text{Eq.(2-47)}$$

Dove:

- $P_{MPP}(STC) \rightarrow$ Nominal power or power in STC [W].
- $P_{MPP}(G, T_c) \rightarrow$ Maximum power produced from the module at value of maximum $G \left[\frac{W}{m^2}\right]$ and cell temperature $T_c [^{\circ}C]$.
- $\gamma_{\%} \rightarrow P_{MPP}$ percentage variation coefficient with $T_c \left[\frac{\%}{^{\circ}C}\right]$, the temperature coefficient $\left[\frac{W}{^{\circ}C}\right]$ can be calculated as:

$$\gamma = \frac{P_{MPP}}{100} * \gamma_{\%} \quad \text{Eq.(2-48)}$$

Proportional correlation η , expresses the value of the module efficiency as a function of cell temperature, and irradiance (see section 2.3):

$$\eta_{MPP}(G, T) = \frac{P_{MPP}(G, T_c)}{G * A} = \frac{P_{MPP}(STC)[W]}{1000} * \left(1 + \frac{\gamma_{\%} * P_{MPP}[W]}{100} * \Delta T_c \right) \quad \text{Eq.(2-49)}$$

$$\Delta T_c = T_c [^{\circ}C] - 25^{\circ}C \quad \text{Eq.(2-50)}$$

Dove:

- $\eta_{MPP}(STC) \rightarrow$ normal efficiency in STC [A].
- $\eta_{MPP}(G, T_c) \rightarrow$ efficiency in fixed conditions of $G \left[\frac{W}{m^2} \right]$ and cell Temperature $T_c [^{\circ}C]$ [A].
- $\gamma_{\%} \rightarrow$ percentage coefficient of variation of P_{MPP} with $T_c \left[\frac{\%}{^{\circ}C} \right]$, the temperature coefficient $\left[\frac{W}{^{\circ}C} \right]$ can be expressed as:

$$\gamma = \frac{P_{MPP}}{100} * \gamma_{\%} \quad \text{Eq.(2-51)}$$

3 Description of the experimental set up

It is very important to accurately measure the I - V curve because it describes the electrical response of a PV module. The experimental method to measure the I - V curve is an ongoing topic according to the previous works available in the literature. The key point, in the measurements of the I - V curves, is to read the current and voltage when the output impedance connected to the PV modules varies from short circuit to the open circuit conditions. The most common technique in order to force that variation is by a capacitive load. In the following sections the experimental measurement systems used to perform the experimental campaigns necessary to conduct this study will be explained. Two laboratories have taken part in this research:

- The Measurement System of Politecnico di Torino (Energetic Department).
- The Laboratory of the IDEA Solar Energy Research Group at University of Jaen.

3.1 Politecnico di Torino Energetic Department Measurement System

The I - V curves are recorded by means of a capacitor charging method. The measuring circuit is represented in Figure 3-1.

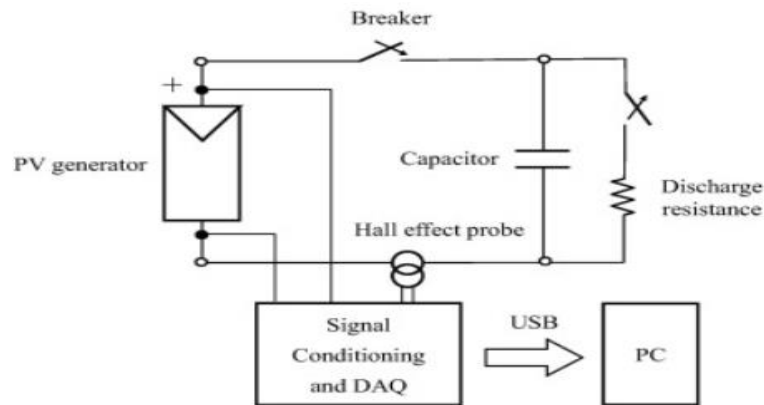


Figure 3-1 Measuring circuit at Laboratory of DENERG at Politecnico di Torino.

A direct measure of the voltage is performed at the PV generator terminals by differential probes for voltage measurements, *Sapphire model* (attenuation ratio 20:1 for PV model).



Figure 3-2: differential voltage probes Sapphire model, used to measure the voltage at Politecnico di Torino DENERG laboratory.

The current is measured through current probes for DC/AC measurements based on Hall effect.



Figure 3-3: Current probe DC / AC LEM-HEME PR30 da 30 Apk, used to measure the current at Politecnico di Torino DENERG laboratory.

The capacitor is an electrolytic and has a capacitance of 10 mF, the capacitor is contained inside a unique box in which there is also the power breaker and a discharge resistance. Through the power breaker it is possible to open and close manually the charge and the discharge circuit.

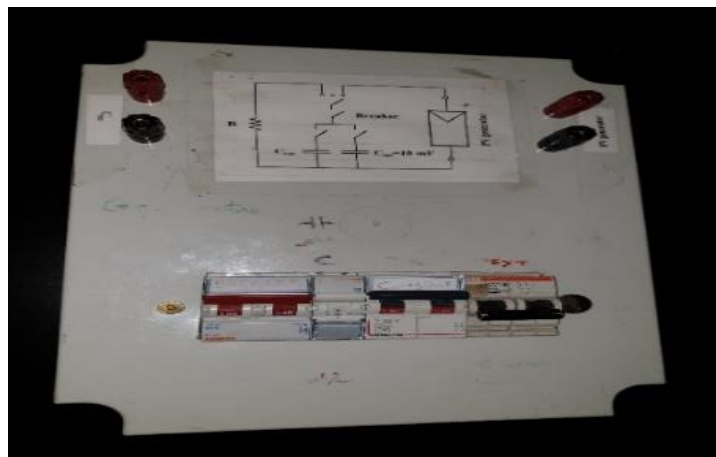


Figure 3-4: Electrolytic capacitor used to record the $I-V$ curve at Politecnico di Torino DENERG laboratory.

The temperature of the cell is measured through a Pt-100 sensors that is connected to the rear surface of the module in contact with the cell. By exchanging the heat for conduction it allows to measure the temperature of the cell that is read on the display.



Figure 3-5: Cell temperature probe used to measure the cell temperature of the PV module at Politecnico di Torino.

A voltage power supply is connected to the capacitor before starting the measurement operations to provide an initial negative voltage. In this way, you will be sure to consider in the transient also the short circuit configuration ($V=0$, voltage zero).



Figure 3-6: Voltage power supply used to pre-charge negatively the electrolytic capacitor at Politecnico di Torino DENERG laboratory.

The irradiance is measured by a pyranometer, that measures the global radiation (direct radiation + diffuse radiation + reflected radiation) by emitting a voltage signal that is detected and read on the display of a multimeter.



Figure 3-7: Pyranometer used at Politecnico di Torino to measure the irradiance.

In order to measure the solar radiation perpendicular to the surface of the photovoltaic panel the axis of the cell and pyranometer must be exactly parallel to the surface of the module, for this, a metal support bar is mounted on the frame of the module; pyranometer and cell are fixed to the bar.



Figure 3-8: PV module with metal support, pyranometer, solar cell, used at Politecnico di Torino DENERG laboratory.

A fundamental rule inside the measurement circuit is assumed from the A/D converter (16 bit-resolution and sampling rate 1.25 MSa/s) DAQ model NI USB-6251 BNC. It allows to record voltage and current pairs at the same time and convert the signal from analogue to digital, in this way it can be managed on a PC.



Figure 3-9: A/D converter DAQ-NI USB-6251 BNC, used to convert the data from analogue to digital at Politecnico di Torino DENERG laboratory.

A Labview software allow to use the ADAS like a storage oscilloscope in which is set a trigger to capture the current and voltage curve with respect the time during the transient capacitor. Here below is reported the interface that the user used to manage the ADAS from the PC. The program provides a simple graphical interface, which groups the main information into a single screen.

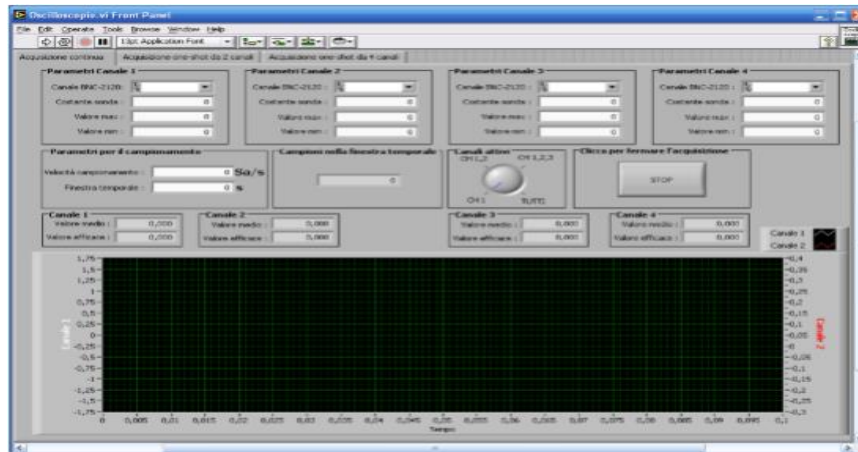


Figure 3-10: Digital oscilloscope Labview graphic interface, used to manage the measurement system at Politecnico di Torino DENERG laboratory.

3.1.1 Measurement uncertainty of the data collected at DENERG Laboratory at Politecnico di Torino

The uncertainty related to the measurement system available at Laboratory of DENERG at Politecnico di Torino in accordance with the values reported in [5, 6] are respectively:

- for the values of the irradiance measured by pyranometer the uncertainty in terms of absolute error is $\pm 20 \text{ W/m}^2$,
- for the cell temperature measured by the temperature probe the absolute uncertainty is $\pm 2 \text{ C}$;
- for the short circuit current I_{sc} measured by the Current probe DC / AC LEM-HEME PR30 the percentage relative uncertainty is $\pm 1\%$
- for open-circuit voltage V_{oc} measured by the differential voltage probes Sapphire, the percentage relative uncertainty is $\pm 0.1\%$;
- for the power the percentage relative uncertainty is $\pm 1\%$.

3.2 Laboratory of the IDEA Solar Energy Research Group at University of Jaen.

The laboratory of IDEA Solar Energy Research Group at University of Jaen has implemented an automatic measurement system able to sequentially record the $I-V$ curve of up to 4 PV modules together with the weather conditions. In Figure3-1 is shown a flowchart with the steps taken by the measurements system to trace the $I-V$ curve as well as the instruments involved in the process.

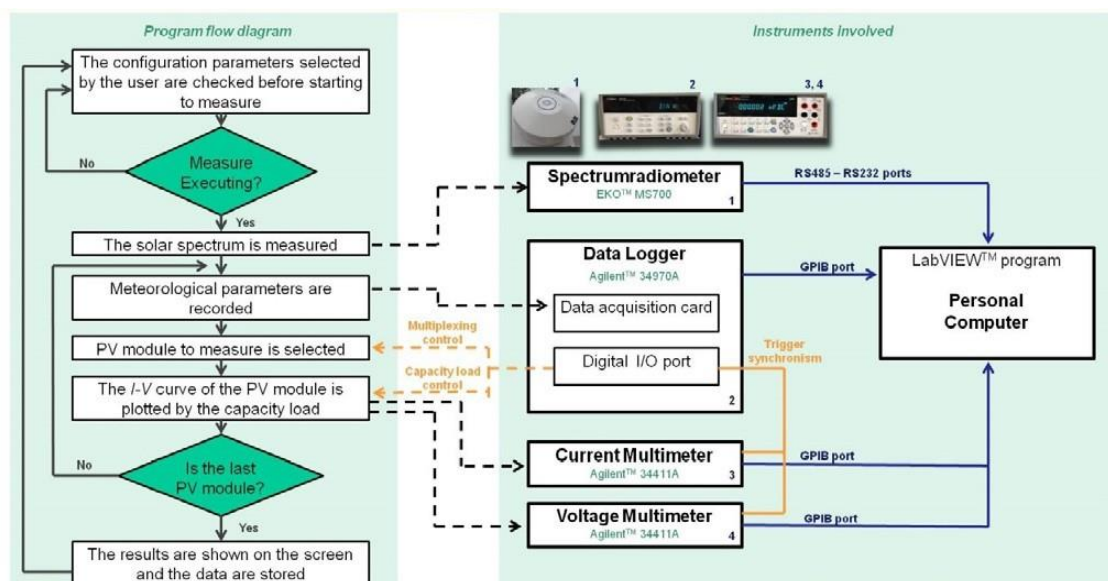


Figure 3-11: Flowchart and instruments controlled by the Labview™ program of the Laboratory of the IDEA Solar Energy Research Group at University of Jaen.

The experimental set up can automatically and continuously measure the $I-V$ curves of 4 modules, with the possibility of setting the lapse of time between each measurement. The system has some constrains regarding the maximum current and the maximum voltage that is capable of measuring. These limits are due to the SSR (solid-state relay) switches used to control the the capacitive load circuit. They are able to endure a maximum voltage of 100 V and a maximum current of 12 A.



Figure 3-12: 2-axes solar tracker on the flat roof of the Higher Technical College where the measures were taken.

PV modules are arranged on a PV tracker (Figure 3-2) with a misalignment error less than 0.5° avoiding in this way the angular effects. The tracker structure is placed on the roof-terrace of the Higher Technical College of the University of Jaen. The 2-axes solar tracker system is auto-regulated, hosts the modules and moves them tracking the sun to carry out the measurements. The $I-V$ curve is plot by means of a capacitive load designed and built up by the IDEA research group. The capacitive load circuit, which schematic is shown in Figure 3-3 is basically composed basically of a capacitor, SSR (solid state relay) switches, a voltage power supply aimed to conduct a negative power pre-charge and a resistance to dissipate the charge of the capacitor and rearm the system.

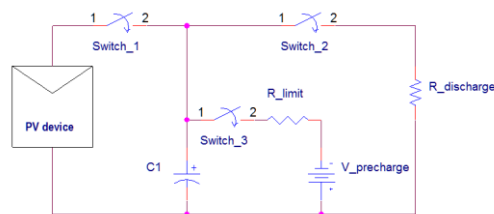


Figure 3-13: Schematic of $I-V$ curve tracer implemented at University of Jaen

The principle of operation of a capacitive load can be easily summarised by means of the description of three chained processes which take place when the $I-V$ curve of a PV device is plotted. First stadium corresponds to the negative pre-charge and occurs when switches SW1 and SW2 (Figure 1) are open and

SW3 is closed. This process is necessary to start the voltage swept from negative values in order to record the short circuit current (I_{sc}) of the device under test during the next stage. The following stage is the charge of the capacitor which takes place when SW2 and SW3 will be open and SW1 will be closed. The charging process consists of a variation of the voltage at the terminal of the capacitor from the negative voltage reached in the pre-charge to a value close to open circuit voltage (V_{oc}). The $i(t)$ and $V(t)$ curves represent the variation of current and voltage during the charging transient, Figure 3-4. The evolution of voltage and current are asymptotic processes, so theoretically speaking, the capacitor will never reach the V_{oc} . For this reason, a condition is generally imposed for the value of the voltage at the end of the transient. The most common condition is to consider the transient completed when the voltage reaches a percentage equal to 99.33% of V_{oc} .

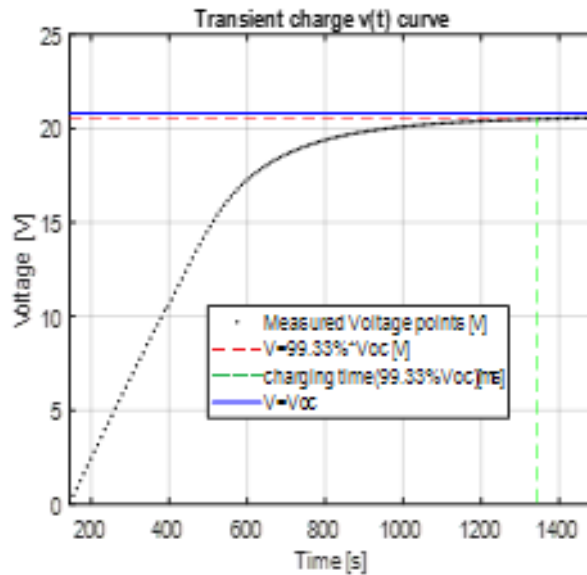


Figure 3-14: $v(t)$ characteristic during the charge transient.

Finally, the discharge process. The charge stored in the capacitor must be dissipated through a resistor in order to rearm the system and release it for re-starting the whole process again. Only switch SW2 keeps closed while the remaining ones will be open during the discharge stage. The capacitor used in the measurement circuit has a capacitance of 4.7 mF. An image of the capacitive load utilized at University of Jaen is shown in Figure 3-5.

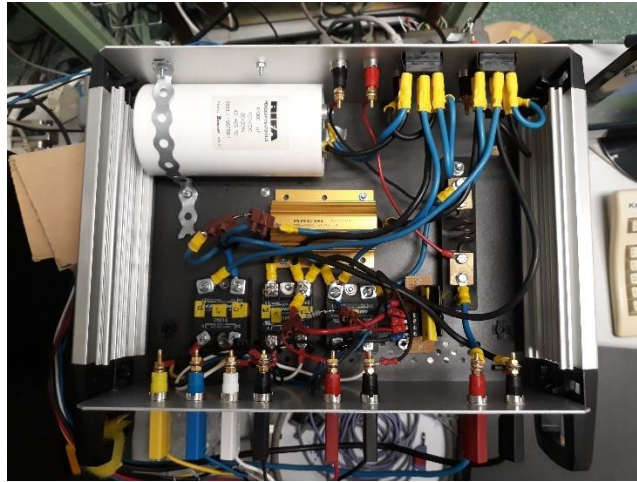


Figure 3-15: Capacitive load circuit designed by the University of Jaen. The internal capacitor by RIFA has a capacitance of 4.7mF.

Two digital multimeters Agilent™34411A which work simultaneously are used to record the points of the I - V curve. One of them directly measures the voltage, while the other reads the current through the indirect measurement of the voltage drop across a calibrated shunt resistor.



Figure 3-16: Digital multimeters Agilent™34411A.

An Agilent™ 34970A data-logger Figure 3-6 is also utilised. This is multipurpose device and has three slots that can be equipped with different cards depending on the type of data to acquire or action to execute. The data logger allows measurements from multimeters to be synchronised. The synchronisation is provided by a TTL pulse (Transistor- Transistor Logic) that allow triggering and synchronising the multimeters. This pulse is performed by a digital input/output card (card model 134407A) that is installed in one of the three available slots. This card allows also the solid-state relay to be controlled. The installation of two acquisition cards (model 34401A, Figure 3-7) that occupy the other two slots of the data-logger,

allows a large number of meteorological data (relative humidity, ambient temperature, etc.) to be measured by a wide range of sensor installed in a weather station. The data from this weather station are also recorded every 5 minutes and saved in the same file together with the $I-V$ curve.



Figure 3-17: Data-logger Agilent™ 34970A and measurement card model 3401A which includes 20 voltage channels.

Among them, there are three environmental parameters which must be deeply described:

- Irradiance. This parameter is measured by a pyranometer model Kipp and Zonnen™ CMP11. Two of these devices are used at University of Jaen, one of them measures the horizontal global irradiance ($Gh(0)$) and the other, the on-plane global irradiance ($Gh(a,b)$). The technical features of the instrument are reported in Fig.3-8.

Spectral range (50% points)	285 to 2800 nm
Sensitivity	7 to 14 $\mu V/W/m^2$
Response time	< 5 s
Zero offset A	< 7 W/m^2
Zero offset B	< 2 W/m^2
Directional response (up to 80° with 1000 W/m^2 beam)	< 10 W/m^2
Temperature dependence of sensitivity (-10 °C to +40 °C)	< 1 %
Operational temperature range	-40 °C to +80 °C
Maximum solar irradiance	4000 W/m^2
Classification to ISO 9060:2018	Spectrally Flat Class A



Figure 3-18: Technical features for the Pyranometer CMP11 by model Kipp and Zonnen™.

- Temperature of the module. This parameter is measured by a Pt-100 sensor (0.00385, under 4-wires configuration). It is of rectangular shape with a dimensions: 40mm x 14mm with a

thickness of 7mm (maximum). It works into a temperature operating range included between -50°C to 150°C at the tip.



Figure 3-19: Image of the Pt-100 Temperature probe used at University of Jaen to measure the temperature of the module under test.

- A Young TM 05305VM anemometer is used to measure the velocity of the wind. The measurement of the temperature of the module accuracy depends on the velocity of the wind. In literature there are many references that says that the wind speed (WS) must be lower than 5 m/s in order to be taken into account for the study [5].

The weather station, the multimeters and the data logger are controlled by a LabView™ program. This program can be managed by the users through an interface where is possible to set different measurement options:

- The lapse between the measurements can be defined.
- The measurements can be filtered depending on the irradiance.

Thanks to the use of this program the measurement system is totally autonomous and unify all the measurements in a single file.

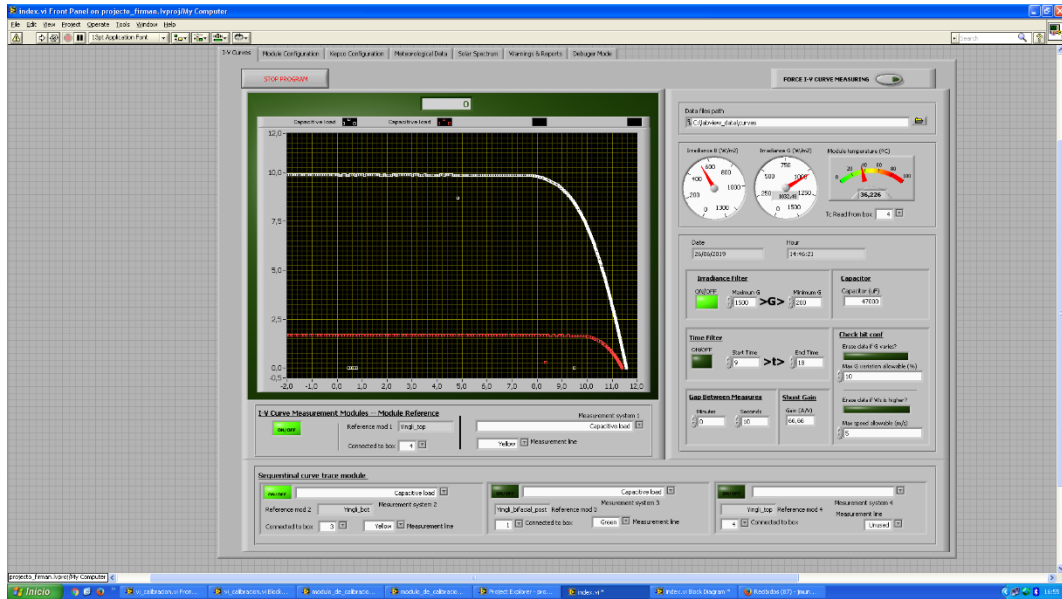


Figure 3-20: Interface of Labview programs used at University of Jaen to manage the measurement system.

3.2.1 Measurement uncertainty of the data collected at IDEA research group laboratory

The uncertainties related to the measurements collected during the experimental campaign are discussed in this section. It is really important to perform this analysis because it allows to conduct a comparison between the studied theoretical model and the real experimental results. The error between the experimental model and the ideal one could be compared with the uncertainties in order to quantify the accuracy of the results. The Guide to the Expression of the Uncertainty in Measurement is followed in order to evaluate the uncertainty of the equipment used [6]. The sources of uncertainty associated to each measurement and the uncertainty linked to the worst scenario $U_{x,worst}$ are displayed in Table 3-1. The term worst means that the uncertainty is computed for the worst scenario in terms of measurement range of the Agilent™ 34970A data-logger, the Agilent™ 34411A multimeters and the reading for the measurand under study. The manufacturer provides the relative standard uncertainty for Agilent™ 34970A data-logger and for Agilent™ 34411A multimeters. The multimeter records directly the voltage so that measurements are only affected by the uncertainty of the device. The maximum value of the expanded uncertainty is reached when the multimeter input range is set between 0 and 100 V and the measured voltage is maximum, that is 22.20 V (maximum

measured V_{OC} of the module under test). On the other hand, the current is indirectly measured by the voltage drop across a Kainos™ precision shunt resistor, because of that, the measure is affected by the multimeter and the resistor uncertainties. The maximum value of the expanded uncertainty is reached when the current is maximum, equal to 5.62 A.(maximum measured I_{SC} of the module under test) The measurements of the environmental factors ($G_h(0)/G_h(a,b)$, T_c and WS) are affected by two sources of uncertainty due to the measurement sensor for each factor (Kipp & Zonnen™ CMP11 pyranometer, Pt100 temperature probe and a Young™ 05305VM anemometer), and uncertainties by the multipurpose Agilent™ 34970A data-logger respectively by which measurements are recorded. The worst condition for the weather anemometer takes place when the wind speed is maximum, 5 m/s (maximum value of measured wind speed that is taken into account for our study). The worst condition for the temperature sensor takes place when the temperature is maximum, 335 K (maximum value of measured cell temperature). The worst condition for the pyranometer take place when the irradiance is maximum, 1190W/m² (maximum value of measured irradiance). All the values presents in this section are taken from [9]

Table 3-1: Source of uncertainty associated to each measurands together with the value of the expanded uncertainty in percentage.

Measurands	Sources of uncertainty	$U_{x,worst}$ (%)
Voltage (V)	Agilent™ 34411A digital multimeter	±0.02
Current (A)	10A- 150 mV Kainos™ shunt resistor	±1.0
	CL0.5	
	Agilent™ 34411A digital multimeter	
Maximum power (W)	10A- 150 mV Kainos™ shunt resistor	±1.3
	CL0.5	
	Agilent™ 34411A digital multimeter	
Horizontal and on-plane global irradiance (W/m ²)	Kipp & Zonnen™ CMP 11 pyranometer	±0.61
PV module temperature (°C)	Agilent™ 34970A data-logger	
	Pt100 sensor	±1.16
	Agilent™ 34970A data-logger	
Wind speed (m/s)	Young™ 05305VM anemometer	±0.66
	Agilent™ 34970A data-logger	

4 Parameters Extraction

The electrical response of a photovoltaic device can be described by an equivalent electric circuit, as is mentioned in the sections 2-5 and 2-5-2. Particularly, the $I-V$ curve of a photovoltaic cell can be expressed by the equation that characterizes the circuit. There are different models that can be selected to do so and each one is defined by its analytical equation (Eq. 2-16, Eq.2-19 Eq.2-20). A model can be in more or less concordance with the experimental results depending on the operating conditions as is mentioned in the section 2-5-2. However, an accurate estimation of the parameters of the equivalent circuit allows to suitably estimate the performances of a photovoltaic device when the G and the T_c vary. For that, the extraction of the parameters is an ongoing topic which has been studied by several authors in literature. A large amount of extraction methods have been used by previous authors to determine the values of the parameters with diverse results in terms of accuracy [7].

Different classifications of the extraction methods could be done taking into account the procedure in which the parameters are computed. The classification of the optimization algorithms is also an open-ended topic for mathematicians. It is not easy to perform a general and exhaustive classification that allows to subdivide clearly all the methods into different groups. Firstly, as far as PV extraction problems is concerned, it is possible to distinguish two groups: Analytical and Numerical methods.

Analytical methods [8, 9, 10] The parameters of the equivalent circuit are calculated solving a system of analytical equations obtained after considering some approximations in order to simplify the calculation but without compromise the accuracy. Particularly, for the 5-parameter model the system of equations is obtained using Eq.(2-16), applied for different operating conditions. The Eq.(2-16) is applied in the most remarkable points of the $I-V$ curve. They are mainly, the SC, the OC and the MPP points, section 2-3. These points are known from the datasheet provided by the manufacturers or they can be evaluated from the experimental measurements. Applying the Eq.(2-16) for SC, OC, and MPP conditions, only three equations are defined. In order to solve the problems and to calculate the 5 parameters of the SDM, it is necessary to define 2 equations more. In order to determine the last two equations the Eq.2-16 can be used to verify the conditions

that occurs in the three points aforementioned ($\left.\frac{dP}{dV}\right|_{MPP} = 0, \left.\frac{dI}{dV}\right|_{SC} = -\frac{1}{R_{sh}}, \left.\frac{dI}{dV}\right|_{OC} = -\frac{1}{R_s}$). Often, to add one more equation to the system, it is possible to impose the diode ideality factor equal to a constant value included in a range between 1 and 2. For more complex models (7-parameter and 10-parameter models) is difficult to apply the analytical methods because of the high number of unknown variables and equations that define the system.

Anyway, numerical methods are techniques that allow the parameter to be evaluated solving iteratively a certain set of equations. The core of a numerical extraction method is the optimization algorithm, which is a mathematical logical procedure for solving an optimization problem. The value assumed by the objective function is able to quantifies the quality of a solution of an optimization procedure. Given a certain problem and once researched goals are fixed, the objective function is able to estimate the benefit associated to a certain set of independent variables. The optimization methods have the goal to look for the state of independent variable that optimize it (maximize or minimize). The numerical PV extraction strategy consists of researching the set of equivalent circuit parameters that minimize the error between the experimental and the estimated I - V curves, estimated using Eq.(2-16). For that, the numerical extraction of parameters problems can be considered as a part of the curve fitting analysis. In the PV curve fitting problems, the residuals are defined as a vector composed of the differences between the measured I - V curve and the I - V curve calculated from Eq.(2-16):

$$residuals = I_{measured} - I_{analytical}(V_{measured}) \quad \text{Eq.(4-1)}$$

- $I_{measured} \rightarrow$ A vector containing the experimental values of the measured current [A].
- $V_{measured} \rightarrow$ A vector containing the experimental values of the measured voltage [V].
- $I_{analytical}(V_{measured}) \rightarrow$ A vector containing the values of the current analytically calculated by Eq.(2-16) with respect the values of the measured voltage. It is related to a certain set of parameters estimated at each iteration [A].

A common technique used in the extraction of parameters is based on the Least Square Method. For that matters, the objective function often coincides with the sum of the square of the residuals (or also called the norm of the residuals) computed between the measured and the estimated (Eq.2-16) I - V curve:

$$resnorm = \sum_{U=0}^{U_{oc}} \left(I_{measured} - I_{analytical}(V_{measured}) \right)^2 \quad \text{Eq.(4-2)}$$

All in all, the purpose of the numerical optimization in the extraction of parameters is to minimize the norm of the residual Eq.(4-2) in order to reduce the differences between the two curves. The parameters are iteratively estimated and the final solution of the method consists of a set of parameters that allow the fitting of the curve to be optimized. A good fitting is characterized by a value of the resnorm lower than the requested tolerance. Different categories of numerical methods can be defined based on their characteristics.

A classification based on the “precision” of the algorithm identifies Exact methods and Heuristic methods. [11, 12, 13] The Exact methods are that techniques that always ensure the global maximum to be determined. Generally, they evaluate the objective function for each point of its domain. They require a high computational effort and sometimes the domain of the independent variables is infinite, undefined or too large. For that, it is not always possible to apply exacts method to solve an optimization problem. On the other hand, Heuristic methods (Ex. Simulated Annealing (SA), Nelder-Mead (NM)) are algorithms that produce solutions without any guarantee that the global optimal solution will be get it. These methods use “non rigorous mathematical rules” to estimate the solution at each iteration, alternatively they use logical, practical, intuitive strategy also taking inspiration from natural or artificial processes. In literature there are large amount of studies in which Heuristic methods are computed obtaining results with good accuracy especially in problems where the calculation of the solution is impossible or unfeasible with exacts methods. This gives an empirical proof of their reliability. [17], [18].

Another classification of numerical methods is between the Deterministic and the Stochastic methods. In this case, the classification is based on “how the evolution of the algorithm occurs between two successive iterations”. Stochastic (Simulated Annealing) is a method in which the flow of the algorithm evolves randomly. A random variable is used in order to calculate the objective function among two iteration. In this way the objective function becomes a random objective function. Deterministic (LM-Levenberg-Marquardt [19] [20] [21] and Nelder-Mead algorithms) methods starting from the same input value evaluating always the same output passing always from the same states of the system. Deterministic ones use mathematical function that calculate unique solution for

each point included in its domain. They are strictly related to the initial condition and can fall in local minimums.

The last classification of numerical methods is based on the calculation of the derivatives. In this sense, if the derivatives are considered there are two groups in which methods can be classified: Indirect methods (LM-Levenberg-Marquardt), search the solution making an analysis of the derivatives of the objective function and looking for the turning points. On the other hand, direct methods (Nelder-Mead and Simulated Annealing) calculates directly the values of the objective function in the points of its domain.

The main problem related to the extraction of the parameters for PV modules is connected to the solving of the transcendental equation Eq.(2-16). It is possible to find more than a single set of parameters which solve the equation and fits well the $I-V$ curve. Nevertheless, not all the combinations that give rise to a good fitting could be an acceptable solution. In this sense, parameters without real physical meaning could be achieved. This phenomenon is very common and it is called overfitting. Another fundamental aspect regarding PV curves fitting methods is related to the selection of the initial values of the parameters. A wrong evaluation of these parameters can lead to an inaccurate fitting, a divergence of the fitting operation or an excessive computational effort especially if the optimization method is deterministic. In the present work different parameters extraction methods have been used to get the variables from the single diode model:

- A combination of an analytical-numerical method and Levenberg Marquardt algorithm is implemented on Matlab by the Energetic Departement of Politecnico di Torino.
- A procedure based on the used of two heuristic methods, the Simulated Annealing Method and the Nelder-Mead algorithm is implemented on Octave from the IDEA Research Group by the University of Jaen.

4.1 Parameter extraction procedure

The complete procedure for the extraction of the 5 parameters of the SDM equivalent circuit of a PV device is not only composed by the optimization algorithm before introduced. In the whole there are more steps that must be carried out to achieve the extraction. The IV curve measurements have to be pre-treated in

order to be fitted and the fitting results have to be verified. In this section a description of the procedure applied for the extraction of the 5 parameters is applied. the complete process needed in order to extract the parameter starting from a measured IV curve will be explained in details. For a better understanding of the implemented procedure a flowchart which summarises the whole process carried out is shown in the Figure 4-1.

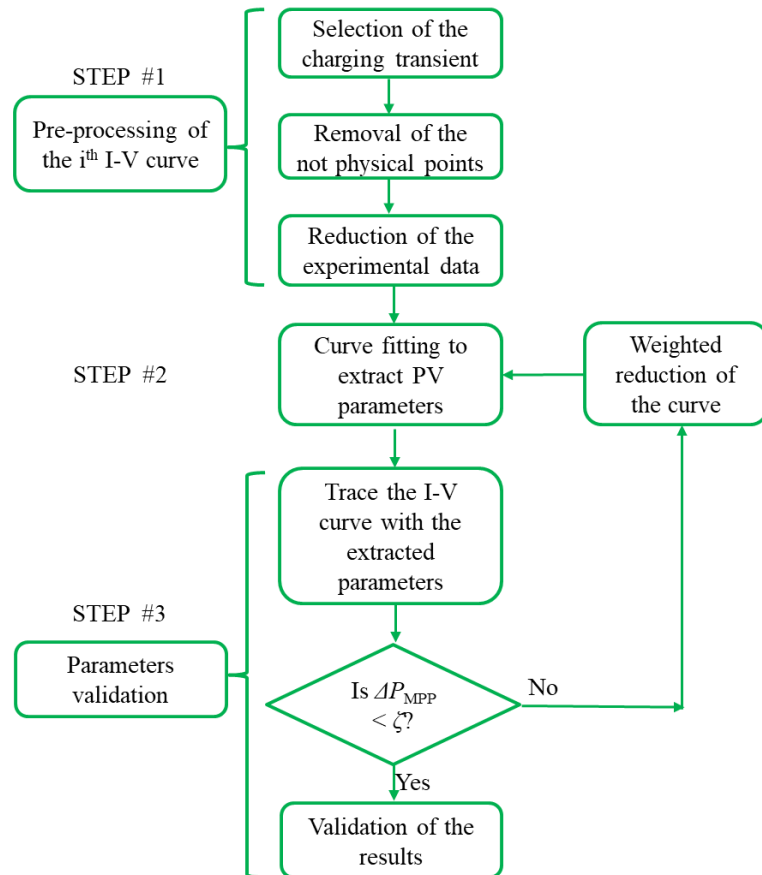


Figure 4-1: flowchart which summarises the whole process carried out to extract the SDM parameters from an experimental $I-V$ curve. This procedure is applied for each measured G and T_c conditions.

The methodology adopted can be divided into three main steps:

- Pre-processing of the IV curves, the measured $I-V$ curves have to be cleaned in order to apply the curve fitting procedure.
- Optimization algorithm, it is the step in which the curve fitting occurs. This process is the only one that is different for the two procedures. Politecnico di Torino procedure applies a numerical-

analytical method and a LM algorithm. Otherwise UJA procedure applies the Simulated Annealing and Nealder Mead Algorithm.

- Parameters validation, step in which a check on the quality of the fitting is performed with respect the resnorm and the percentage error on the maximum power. If the results from the curve fitting procedure not respects the imposed constrains the a weighted reduction of the points in the part of the curves near to the SC and OC is performed, in order to increase the quality of the fitting in the MPP. Finally the curve fitting is repeated with the new reduced *I-V* curve.

In the following sections each of one of these steps will be explained in details.

4.1.1 Pre-processing of the IV curves

4.1.1.1 Selection of the charging transient

Both extraction methods implemented in this work need from measured I-V curve to be applied. These I—V curves are experimentally recorded but they must be suitable filtered before the curve fitting procedure. The procedures applied for the two methods, Politecnico di Torino method and UJA method in order to filter the curves is slightly different. The two different pre treating procedures are reported in Table 4-1.

Table 4-1: Table of the pre-processing steps adopted by the two methods in order to filtered the $I-V$ curves before the curve fitting procedure.

Politecnico di Torino pre-treating procedure (combined numerical analytical + Levenberg Marquardt)	University of Jaen pre-treating procedure (Simulated Annealing + Nelder Mead)
<p>Selection of the initial instant of the charging transient:</p> <p>Graphically selected by the users.</p>	<p>Selection of the initial instant of the charging transient:</p> <p>Automatically implemented.</p>
<p>Selection of the final instant of the charging time:</p> <p>Calculation of the V_{OC} from the points measured before the closure of the circuit. Imposition of the end of the transient at $V=99.7 \%*V_{OC}$.</p>	<p>Selection of the final instant of the charging time:</p> <p>The end of the transient is not fixed, all the $I-V$ curve points measured near the V_{OC} are taken into account during the fitting.</p>

The measured $I-V$ curves present some noise at the beginning of the charging transient. These noise in the $I-V$ curve has to be avoided because it is extremely difficult for the program fits $I-V$ curves which present these types of irregularities. So, it is necessary to eliminate these noises from the $I-V$ curve before to apply the fitting procedure. In the code implemented by Politecnico on Matlab the selection of the initial point is manually made by the user choosing a point on the graph. In the code implemented by the University of Jaen on Octave the choice of the initial point of the charging transient is automatically implemented and the curve is filtered before the fitting processes take place. In order to reduce the computational effort the program implemented by Politecnico cancels all the points measured near to the V_{OC} imposing the end of the charging transient at 99.7% of V_{OC} . The calculation of the V_{OC} is performed before selecting the initial point of the charging transient, making the mean of the points measured before the charging of the capacitor starts of the circuit. The program implemented at the University of Jaen does not impose a final instant of the transient time and during the fitting consider all the points near to the V_{OC} measured from the multimeters. These two different approaches can lead to a different computational effort by the two programs, allowing to the method implemented by Politecnico to be faster.

4.1.1.2 Cancellation of the points without physical meaning

The measurement may have points that have no physical meaning are called outliers. These points are eliminated by the program in pre-processing operations so that they do not disturb the fitting procedures.

4.1.1.3 Reduction of the experimental point

The number of pairs of the experimental $I-V$ curve have to be reduced in order to speed up the execution of the program. The fitting program, implemented on Matlab to do the extraction of the SDM parameters, requires several iterations and a not insignificant time to go to convergence. In order to reduce the computational cost of the program the number of points have to be reduced. The program initially charges all the measured points of the $I-V$ curve in a vector, then reduces and stores them in a new reduced vector which will send to the optimization algorithm at the next step. The variable “reduction” allows the number of points which compose the $I-V$ curve to be reduced. Setting a value of “reduction” higher than one, the program applies the operations in order to cut the points. The program starting from the first point of the $I-V$ measured curve, will store one point in the new vector and will cut the “reduction” next points. Repeating this operation for all the measured points of the $I-V$ curve the new reduced vector will be generated. This procedure is repeated for the three variables experimentally recorded: time, voltage, current. Constrain is imposed with respect the minimum number of points that can be stored in an $I-V$ curve. The $I-V$ curves have a physical meaning if it is composed at least from 100 points. If one curve does not respect this limit it is necessary to repeat the procedure decreasing the value assigned to the variable "reduction".

4.1.2 Politecnico di Torino curve fitting optimization algorithm

The core of the optimization algorithm implemented by the Energy Department is the Levenberg Marquardt Optimization Algorithm. This Method is deterministic and so strictly depends on the initial values of parameters. The evaluation of the initial parameters is one of the most critical step in the parameter extraction procedure. Errors in the estimation of the parameters could lead the algorithm to diverge, to a convergence to an incorrect solution, to require a too high computational efforts in order to reach the convergence. In order to overcome this problem and make the problem more independent from the values of the initial parameters, an analytic algorithm is implemented before the Levenberg Marquardt. In the subsequent paragraphs the two methods used in the fitting procedures are explained.

4.1.2.1 Combined Analytical and Numerical Method

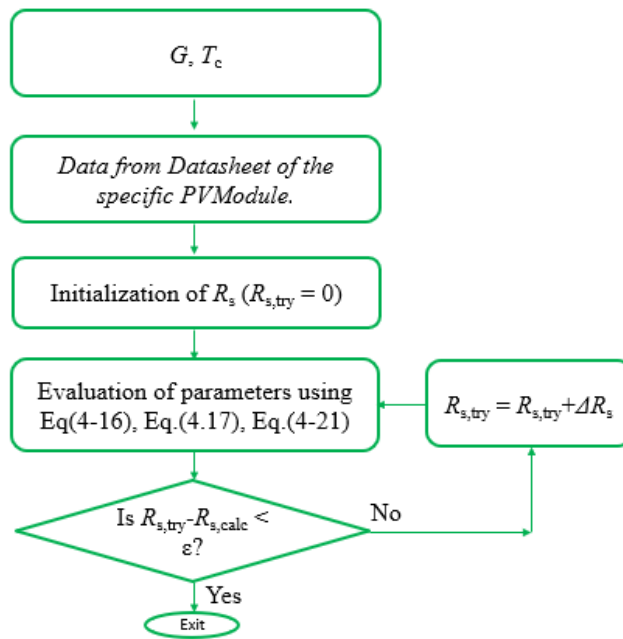


Figure 4-2: Flowchart of the Combined Analytical and Numerical Method implemented on Matlab for the extraction of the initial parameters.

The method [22] is an analytical-numerical method, based on the 5 parameters equivalent circuit. The computed equations are calculated by an analytical method. In order to not apply too many mathematical approximations, an iterative numerical algorithm is proposed to extract R_s . The application of this combined procedure is

used for the extraction of the five-parameter of the SDM equivalent circuit. Starting from the transcendental equation of the equivalent circuit, with the data provided by the manufacturers through the datasheet we can obtain the 3 equations respectively in the points:

- At Open Circuit (V_{OC} ; 0):

$$0 = I_{ph} - I_0 * \left(e^{\frac{V_{OC}}{V_{th}*n*N_s}} - 1 \right) - \frac{V_{OC}}{R_{sh}} \quad \text{Eq.(4-3)}$$

- At Short Circuit (0; I_{SC}):

$$I_{SC} = I_{ph} - I_0 * \left(e^{\frac{R_S*I_{SC}}{V_{th}*n*N_s}} - 1 \right) - \frac{I_{SC}*R_S}{R_{sh}} \quad \text{Eq.(4-4)}$$

- At maximum power point (U_{MPP} ; I_{MPP}):

$$I_{MPP} = I_{ph} - I_0 * \left(e^{\frac{V_{MPP}+R_S*I_{MPP}}{V_{th}*n*N_s}} - 1 \right) - \frac{V+I_{MPP}*R_S}{R_{sh}} \quad \text{Eq.(4-5)}$$

By Eq. (4-3) It is possible to derive the I_{ph} . Replacing it in Eq. (4-4) and Eq. (4-5) It is possible to derive the following equations:

$$I_{SC} = I_0 * \left(e^{\frac{V_{OC}}{V_{th}*n*N_s}} - e^{\frac{R_S*I_{SC}}{V_{th}*n*N_s}} \right) + \frac{V_{OC} - R_S*I_{SC}}{R_{sh}} \quad \text{Eq.(4-6)}$$

$$I_{SC} = I_0 * \left(e^{\frac{V_{OC}}{V_{th}*n*N_s}} - e^{\frac{V_{MPP}+R_S*I_{MPP}}{V_{th}*n*N_s}} \right) + \frac{V_{OC}-V_{MPP}-R_S*I_{MPP}}{R_{sh}} \quad \text{Eq.(4-7)}$$

To simplify the discussion let's define some variables:

$$X_{OC} = e^{\frac{V_{OC}}{V_{th}*n*N_s}} \quad \text{Eq.(4-8)}$$

$$X_{MPP} = e^{\frac{V_{MPP}+R_S*I_{MPP}}{V_{th}*n*N_s}} \quad \text{Eq.(4-9)}$$

$$X_S = e^{\frac{R_S*I_{SC}}{V_{th}*n*N_s}} \quad \text{Eq.(4-10)}$$

Knowing R_s and using the datasheet parameters provided by manufacturers X_s , X_m , and X_{OC} can be calculated in STC. So, the equations Eq. (4-6) and Eq. (4-7) can be rewritten:

$$I_{SC} * \left(1 + \frac{R_s}{R_{sh}}\right) = I_0(X_{OC} - X_s) + \frac{V_{OC}}{R_{sh}} \quad \text{Eq.(4-11)}$$

$$I_{MPP} * \left(1 + \frac{R_s}{R_{sh}}\right) = I_0(X_{OC} - X_{MPP}) + \frac{V_{OC}-V_{MPP}}{R_{sh}} \quad \text{Eq.(4-12)}$$

Knowing that $R_{sh} \gg R_s$ it is possible to neglect the term that multiplies the currents to the first member:

$$\left(1 + \frac{R_s}{R_{sh}}\right) \approx 1 \quad \text{Eq.(4-13)}$$

The equations become:

$$I_{SC} = I_0(X_{OC} - X_s) + \frac{V_{OC}}{R_{sh}} \quad \text{Eq.(4-14)}$$

$$I_{MPP} = I_0(X_{OC} - X_{MPP}) + \frac{V_{OC}-V_{MPP}}{R_{sh}} \quad \text{Eq.(4-15)}$$

From these equations we can derive the functions that relate I_0 , R_{sh} according to the only unknown R_s :

$$\frac{1}{R_{sh}} = \frac{I_0(X_{MPP}-X_{OC})+I_{MPP}*(X_{OC}-X_s)}{V_{OC}*(X_{MPP}-X_s)-V_{MPP}*(X_{OC}-X_s)} \quad \text{Eq.(4-16)}$$

$$I_0 = \frac{V_{OC}*(I_0-I_{MPP})-V_{MPP}*I_{SC}}{V_{OC}*(X_{MPP}-X_s)-V_{MPP}*(X_{OC}-X_s)} \quad \text{Eq.(4-17)}$$

The I_{SC} short-circuit current is easy to determine, It can be calculated from the graph. A graphical selection by the user is implemented on the Matlab program to identify the starting position of the curve with respect to which the extrapolation is processed. Then, a linear regression is performed on the points included in the range between the selected point and the point where the Voltage reaches or exceeds 20% * V_{OC} . The regression returns a vector of two parameters that corresponds respectively, to the constant term, and to the slope of the straight line obtained from the regression. The angular coefficient, can be identified as the inverse of the R_{sh} changed of sign, such that, it can be used to evaluate an indicative value of the R_{sh} . The constant term identifies the intersection between the straight line and the ordinate axis, and therefore the value of the I_{SC} . As regards the initial value assumed

by the diode ideality factor n , it is placed arbitrarily constant at a value between 1 and 2 (extremes included). Assuming as known the values of I_{SC} and n the system is composed of 2 equations and 3 unknowns, so to solve it is necessary another equation. As enounced in section 2-3 at the maximum power point:

$$\left(\frac{dI}{dV}\right)_{MPP} = -\frac{I_{MPP}}{V_{MPP}} \quad \text{Eq.(4-18)}$$

From which:

$$\frac{I_{MPP}}{V_{MPP}} = \left(1 - \frac{R_s * I_{MPP}}{V_{MPP}}\right) * \left[\frac{I_{sc}}{N_s * n * V_{th}} * X_m + \frac{1}{R_{sh}}\right] \quad \text{Eq.(4-19)}$$

$$\left(\frac{dI}{dV}\right)_{MPP} = -\frac{I_S}{n * N_s * V_{MPP}} * \left(1 - \frac{R_s * I_{MPP}}{V_{MPP}}\right) * e^{(V_m + R_s * I_{MPP}) / (n * N_s * V_{th})} - \frac{1}{R_{sh}} * \left(1 - \frac{R_s * I_{MPP}}{V_{MPP}}\right) \quad \text{Eq.(4-20)}$$

From the two equations Eq.(4-18) and Eq.(4-19) We can derive another equation that allow to calculates the parameter $R_{s_calculated}$:

$$R_{s_calculated} = \frac{V_{MPP}}{I_{MPP}} - \frac{1}{\left[\frac{I_{sc}}{N_s * n * V_{th}} * X_m + \frac{1}{R_{sh}}\right]} \quad \text{Eq.(4-21)}$$

This equation is a strongly nonlinear equation and it is possible to compute the value of $R_{s_calculated}$ through an iterative numerical process. The iterative algorithm assumes initially, $R_s=0$, increasing it gradually at each iteration. I_0 and R_{sh} are iteratively evaluated using Eq.(4-16) and Eq.(4-17). The algorithm converges when R_s and $R_{s_calculated}$ coincide. The parameters calculated at last iteration are the input initial parameters for the Levenberg Marquardt optimization algorithm. Here below is reported a graphic representation of the flowchart of the Analytical method.

4.1.2.2 Levenberg Marquardt Curve Fitting Optimization Method

The Levenberg Marquardt method is an indirect deterministic nonlinear algorithm used to solve the nonlinear least square problem. As mentioned in section 4-1, an iterative process is performed in order to reduce the sum of the square of the error between the measured points and the estimated function. At each iteration, a new set of parameters is updated. The solution are the parameters that allows to find the global minimum value of the objective function, that consists on the sum of the square of the error aforementioned. This method is the results of the application of

two minimization methods, that acts alternating itself depending on the values assumed from the objective function at each iteration. The two used methods are:

- The steepest-descent direction.
- The Gauss-Newton method

It is useful to review the formulas of the residuals and the resnorm already mentioned in section 4-1:

$$F(p) = \text{residual}(p) = \begin{bmatrix} y(t_1) - \hat{y}(t_1; p) \\ y(t_2) - \hat{y}(t_2; p) \\ \vdots \\ y(t_m) - \hat{y}(t_m; p) \end{bmatrix} \quad \text{Eq.(4-22)}$$

$$\text{resnorm}(p) = \sum_{i=1}^m (y(t_i) - \hat{y}(t_i; p))^2 = (y - \hat{y}(p))^T * (y - \hat{y}(p)) = y^T y - 2y^T \hat{y} + \hat{y}^T \hat{y} \quad \text{Eq.(4-23)}$$

Where:

- $P \rightarrow$ Set of n parameters (variables to optimize from the algorithm).
- $(t_i, y_i) \rightarrow$ i^{th} datapoint part of a set of a group of m measured points.
- $\hat{y}(t_i; p_i) \rightarrow$ fitting function value at point t_i and parameter p_i .
- $\hat{y}(p) \rightarrow$ fitting function evaluated using the set of parameters p in all the m measured points t_i .
- $y \rightarrow$ vector of m components, that contains the values of all the y measured points.

In order to minimize resnorm an iteration process is needed. At each i^{th} process a value of parameters perturbation h that allow the resnorm to be decreased is calculated. In order to understand in details how this algorithm works is needed to describe the main principles and the equations of the two algorithms listed before.

- Gradient Descent Method. The Gradient Descent Method generates a variation of the parameters in the opposite direction with respect to the gradient $\nabla \hat{y}(t_i, p)$ in order to minimize the objective function. The gradient of a curve fitting least square problem can be calculated with the subsequent formula:

$$\frac{\partial resnorm}{\partial p} = 2 * (y - \hat{y}(p))^T * \frac{\partial(y - \hat{y}(p))}{\partial p} = -2 * (y - \hat{y}(p))^T * \left[\frac{\partial \hat{y}(p)}{\partial p} \right] = -2 * (y - \hat{y}(p))^T * J(p) \quad \text{Eq.(4-24)}$$

Where $J(p)$ is the $m \times n$ Jacobian matrix that represent the matrix of the partial derivative of the fitting function with respect the parameters p for each value of the measured voltages.

$$J(p) = \begin{bmatrix} \frac{\partial \hat{y}(p, t_1)}{\partial p_1} & \dots & \frac{\partial \hat{y}(p, t_1)}{\partial p_n} \\ \vdots & \ddots & \vdots \\ \frac{\partial \hat{y}(p, t_m)}{\partial p_1} & \dots & \frac{\partial \hat{y}(p, t_m)}{\partial p_n} \end{bmatrix} \quad \text{Eq.(4-25)}$$

So, it is possible to identify a vector h_{gd} that represents the variations of the parameters in order to obtain a minimization of the objective function. As mentioned before the direction of the movement has to be opposite to that of the gradient.

$$h_{gd} = \alpha * J(p)^T (y - \hat{y}(p, t)) = \alpha * J(p)^T * F(p) \quad \text{Eq.(4-26)}$$

where :

- $\alpha \rightarrow$ the size of the movement in the “downhill direction”.
- Gauss-Newton Method. A Taylor series expansion is used to approximates the function after a perturbation of the parameters from $p \rightarrow p + h$:

$$\hat{y}(p + h) \approx \hat{y}(p) + \left[\frac{\partial \hat{y}(p)}{\partial p} \right] * h = \hat{y} + J(p)h \quad \text{Eq.(4-27)}$$

It is possible now to determine the formula used to estimate the $resnorm$ in the perturbed state in which parameters assume values equal to $p+h$ substituting the values of $\hat{y}(h+p)$ of Eq.(4-27) in the Eq.(4-23).

$$resnorm(p + h) = y^T y + \hat{y}(p)^T \hat{y}(p) - 2y^T \hat{y}(p) - 2(y - \hat{y}(p))^T J(p)h + h^T J(p)^T J(p)h \quad \text{Eq.(4-28)}$$

In order to calculate the perturbation h that allow to minimize $resnorm(p+h)$ it is needed to calculate the value of h that solve the equation $\frac{\partial(resnorm(p+h))}{\partial h} = 0$:

$$\frac{\partial \text{resnorm}(p+h)}{\partial h} \approx -2(y - \hat{y}(p))^T * J(p) + 2h^T J(p)^T J \quad \text{Eq.(4-29)}$$

At the end the Gauss-Newton equation can be writes as:

$$[J(p)^T J(p)] h_{gn} = J^T (y - \hat{y}(p)) \quad \text{Eq.(4-30)}$$

The Levenberg-Marquardt behaves more as the steepest-descent method if the parameters are distant from the global minimum, instead behaves more as the Gauss-Newton method if the parameters are close to the global minimum. The characteristic equation of the Levenberg Marquardt method is the subsequent:

$$[J(p)^T J(p) + \lambda I] h_{lm} = J(p)^T * (y - \hat{y}(p)) \quad \text{Eq.(4-31)}$$

The value of λ allow the algorithm to be manage:

- For small values of λ the algorithm approaches the Gaus Newton Method.
- For high values of λ the algorithm approaches the Gradient Search Method.

The variation of λ allow to vary the behaves of the algorithm at each iteration. A large starting value of λ is imposed at the beginning of the process in order to obtain small variation of the parameters in the steepest-descent direction. λ is increased if the variation results in a worse approximation. ($\text{resnorm}(p + h_{lm}) > \text{resnorm}(p)$). Otherwise, λ is decreased when the solution improves so, the Levenberg-Marquardt method acts more like the Gauss-Newton method.

4.1.2.3 Implementation of Levenberg Marquardt algorithm in Politecnico di Torino proposed procedure for the extraction of parameters

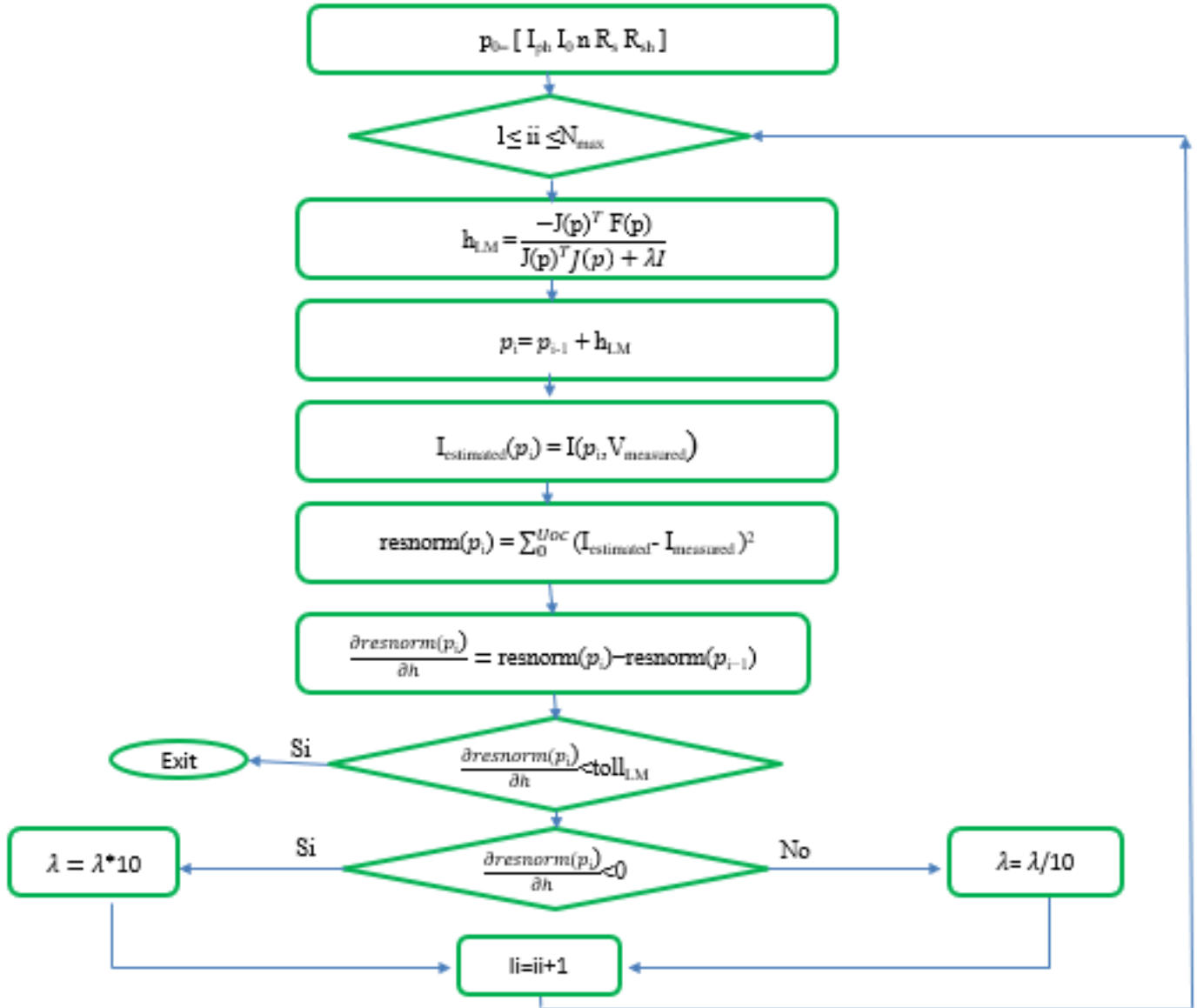


Figure 4-3: Flowchart of the Levenberg Marquardt Method computed in Matlab for the extraction of Parameter.

In this paragraph is explained in details the application of the Levenberg Marquardt algorithm computed on Matlab by the Politecnico di Torino. At the beginning an evaluation of an initial set of parameters is performed in order to give a first input argument to the algorithm. At each iteration the Levenberg Marquardt

Equation Eq.(4-31) is applied to calculate perturbation of parameter expressed by the vector h_{LM} . In the first iteration the values of λ are imposed as default values and equal to 0.01 because it is needed to calculate h_{LM} . After that the new set of parameters is calculated. The current and the resnorm (objective function) are estimated through the Eq.(2-16) and Eq.(4-2). The variation of the resnorm between the current and the previous steps is evaluated. The `lsqcurvefit` function implemented on Matlab has a proper tolerance that is fixed equal to 10^{-4} times the `tolfun` imposed in the `optimset` structure. In our case `tolfun` = 10^{-30} and so is equal to `tolLM` = 10^{-34} . If the algorithm calculates a tolerance lower than this value it stops the iteration and terminates the execution of the program. At the end a new value of λ is calculated in order to manage the application of the Levenberg Marquardt. If the variation of the resnorm is in the right direction, so the resnorm decreases, λ is decreased and divided by 10 in order to approach the Gauss Method and the solution typically accelerates to the local minimum. Else if resnorm increases, λ is multiplied by 10 and Levenberg Marquardt moves towards the Gradient Descent method.

4.1.3 University of Jaen curve fitting optimization algorithm

In order to find the parameters that minimize Eq.(4-2) firstly a stochastic global minimization known as Metropolis Algorithm Simulated Annealing method is employed following its implementation in octave. Secondly, a Nelder-Mead algorithm is used in order to refine the result obtained by the stochastic minimization avoiding the differentiation of the objective function.

4.1.3.1 Simulated Annealing Methods

The first method used to extract the parameters and find the range in which the global maximum is included is called Metropolis Algorithm. It is included in a group of methods named Simulated Annealing methods. Simulated Annealing methods are heuristic probabilistic direct techniques based on the analogy between the physical process of hardening solids and solving optimization problems. Hardening is a physical process in which a metal immersed in a hot bath is progressively heated by increasing the bath temperature to the melting point. In this state the system's particles are distributed randomly. The second part of the process consist in a slow cooling by a slowly lowering of the bath temperature. In this way, a state of thermal equilibrium with a minimum internal energy value is achieved and crystallization occurs. The optimization method simulates the phases of the physical process while the solid cools and anneals into a configuration of minimum energy. For each Temperature, the system is able to reach the thermal equilibrium. The Gibbs or Boltzmann distribution express the probability that the particles assume a configuration i with energy E_i :

$$P(E_i) = \frac{\exp\left(-\frac{E_i}{k*T}\right)}{\sum_{j \in S} \exp\left(-\frac{E_j}{k*T}\right)} \quad \text{Eq.(4-32)}$$

Where :

- $T \rightarrow$ Temperature [K].
- $i \rightarrow$ The current state at temperature T.
- $j \rightarrow$ Generic state that can be assumed from the system.
- $E_i \rightarrow$ Energy associated to the i -state of the system [J].
- $E_j \rightarrow$ Energy associated to the j -state of the system[J].
- $k \rightarrow$ Boltzman costant [J/K].
- $S \rightarrow$ number of all possible states.

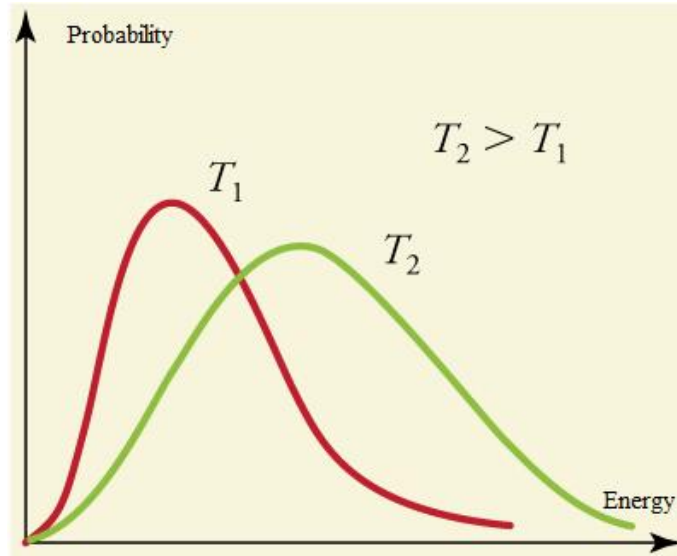


Figure 4-4: Boltzman (or Gibbs) pdf.

From this equation it is possible to understand that the lower is the temperature the more likely is that the system assumes the minimum energy configuration. If a rapid cooling is performed (quenching) the system solidifies in glass that correspond to a local minimum of E . Otherwise, if a slow cooling is performed (annealing) the system solidifies forming a crystal at a value of E closely to the global minimum. These methods are computed using numerical software like Matlab or Octave simulating the physical annealing processes in order to estimate the global minimum energy state. The optimal solution is searched starting from an high T value and moving to a low T value. The simulated Annealing Methods can be defined as a heuristic method that apply an approximation of the Boltzman distribution to estimate the probability to accept or discard a randomly generated population. The energy to be minimized represents the objective function to optimize in the simulated algorithm. Each configuration of particles corresponds to a certain set of the independent variables and the goal is to determine the set of variables that minimize the objective function. The formulation of the probability function, approximates the Temperature its normalized to avoid the Boltzman constant, so the equation of the probability becomes as follow:

$$P(m) = \frac{\exp\left(-\frac{E(m_i)}{T}\right)}{\sum_{j \in S} \exp\left(-\frac{E(m_j)}{T}\right)} \quad \text{Eq.(4-33)}$$

Where :

- $E(m) \rightarrow$ It is the error function associated to the state m . The error function represents the difference between two successive values of the objective function and substitute the Energy in the equation.
- $m \rightarrow$ Set of variables associated to a certain state.

The role of T is to boost or attenuate the effects of the objective function variation on the probability calculation. The limit of the probability function when the temperature tends to zero or to infinite must be commented:

- $\lim_{T \rightarrow \infty} P(m) = 1 \forall m$. At high T the probability is more uniform and it is not so affected from the values assumed by the variation of the objective function through different iterations. If $T \rightarrow \infty$, all the solutions are accepted and the value of the objective function is far from the optimum.
- $\lim_{T \rightarrow 0} P(m) = E(m)$. At low T the probability is strongly dependent from the variation of the objective function. Only the set of variables that improve the solution moving toward the optimal value are accepted.

In the curve fitting for PV devices the measured and estimated $I-V$ curves. On the other ends, the set of independent variables m coincide with the values of the parameters at each iteration. There are different Simulated Annealing Method that vary with respect the approximation of the Boltzman pdf adopted for the evaluation of the probability. The most common is the Metropolis algorithm, which is the one used in the proposed work, implemented with the use of Octave.

4.1.3.2 *Metropolis Algorithm*

Metropolis et al. [1953] proposed a method that allows the process of a solid in a heat bath to thermal equilibrium to be simulated. This method is the first to be implemented in the field of Simulated Annealing method. In Fig 4-5 is shown a schematic representation of the algorithm.

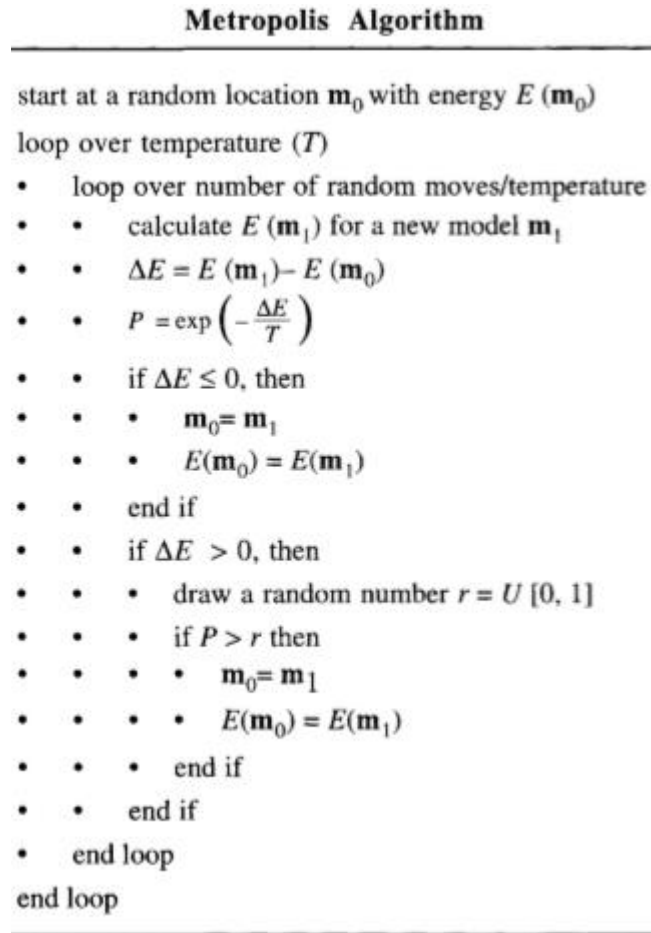


Figure 4-5: Schematic representation of Metropolis Algorithm.

Assuming a set of independent variables m_i of energy $E(m_i)$. Then, a mutation is performed to obtain the new population of variables m_j with Energy $E(m_j)$:

$$m_j = m_i + \Delta m \quad \text{Eq.(4-34)}$$

$\Delta E_{i,j}$ is defined as the variation in the energy between the two states:

$$\Delta E_{i,j} = E(m_j) - E(m_i) \quad \text{Eq.(4-35)}$$

The selection between the two population is based on the value $\Delta E_{i,j}$. If $\Delta E_{i,j} < 0$, the new population is accepted. Otherwise, if $\Delta E_{i,j} > 0$, the new population could be accepted or not, depending on the probability P , derived from the analogy with the Boltzman pdf:

$$P = \exp\left(-\frac{\Delta E_{i,j}}{T}\right) \quad \text{Eq.(4-36)}$$

This rule to estimate the probability is called Metropolis criterion. If the aforementioned chained process of mutation and selection is repeated for a sufficiently large number of iterations, the thermal equilibrium can be reached at each temperature. If the decrease of the T occurs slowly, following a cooling schedule, and continuously, until that the T values approaches zero, the global minimum energy state can be reached. In a local search method, or indirect search method, a new population survives at each successively iteration only if $\Delta E_{i,j} < 0$. The algorithm always searches the solution only in the downhill direction. This not happens in the Metropolis Algorithm where every population has a finite probability of acceptance even though $\Delta E_{i,j} > 0$. So, also the set of variables that lead to a local pejorative effect could be selected. This allows “to jump” the local optimal values avoiding to pitfall in them, for this reason the Metropolis algorithm can be used to determinate a global optimal value. However, when the temperature decrease near the zero (as we have seen in the section 4.1.3.1) only the mutation that move the solution towards the optimal solution have an high probability to be accepted for the next iteration. When T it is closed to 0, the algorithm reduces to a direct search algorithm. In these cases, the algorithm converges only if the energy remains constant for several iterations.

4.1.3.3 Implementation of Metropolis Simulated Annealing algorithm in University of Jaen proposed procedure for the extraction of parameters

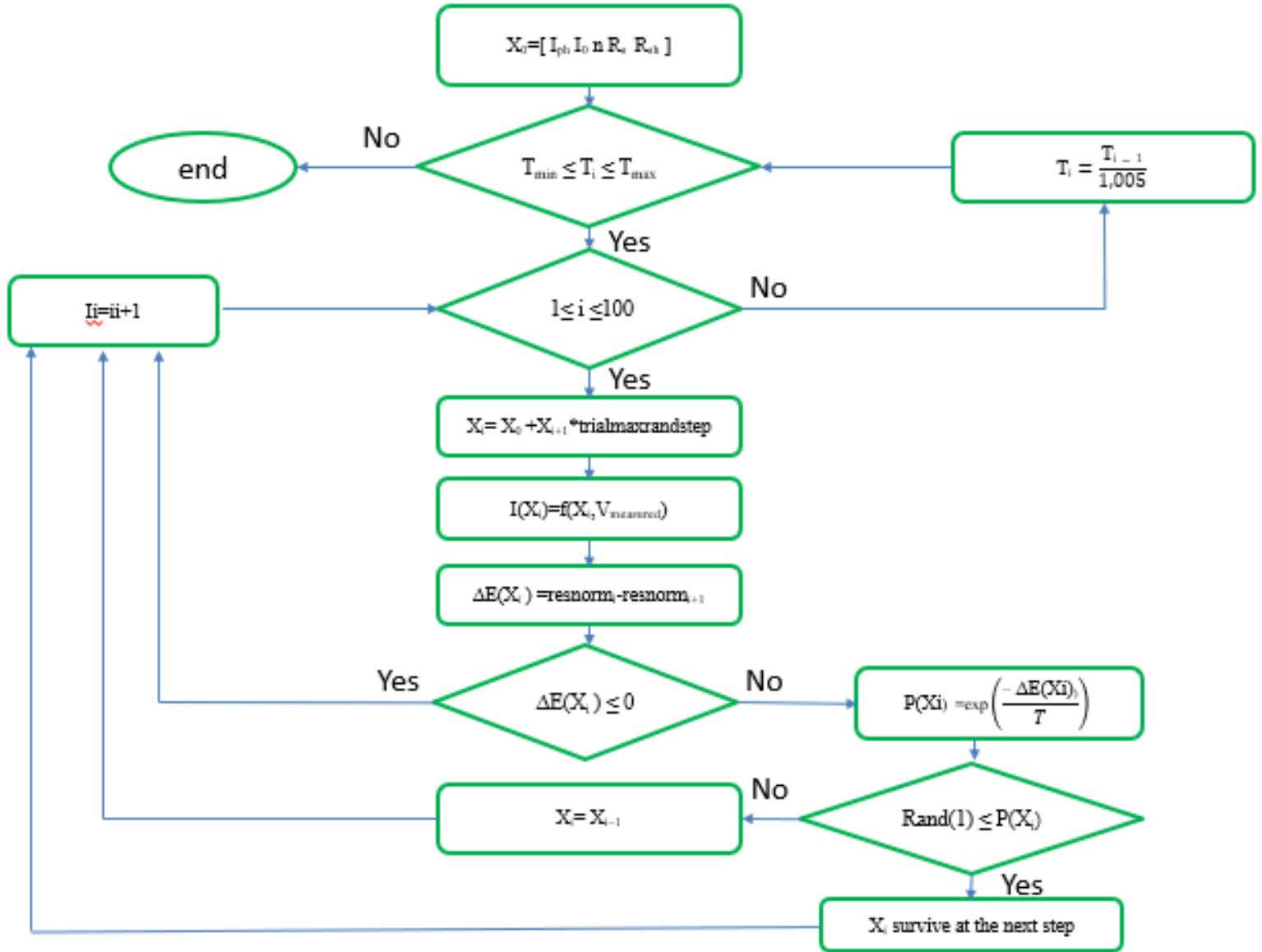


Figure 4-6: Flowchart of the Metropolis Simulated Annealing algorithm implemented in University of Jaen procedure for the extraction of the SDM parameters.

In this paragraph is explained in details how the Metropolis Simulated Annealing algorithm is implemented by the University of Jaen. At the beginning an evaluation of an initial set of parameters is performed in order to give a first input argument to the algorithm to start the iteration. As it was explained in the previous

section, 4.1.3.1, the finding of the global minimum requires a slowly decrease of T from the maximum value to the minimum. Besides, different iterations for the same value of T have to be carried out. In order to accurately simulate the Annealing physical process two loop cycles are used:

- The T vary from T_{\max} to T_{\min} decreasing at each iteration of a factor of 1.005. As values of T_{\max} and T_{\min} are setted $T_{\min}=10^{-5}$ and $T_{\max}=0.01$.
- A for loop of 100 iterations is imposed for each value of T .

The first procedure applied inside the loop cycle is the mutation. In University of Jaen procedure, Simulated Annealing algorithm with constrains is applied to extract the SDM parameters. So, the independent variables can vary at each iteration between the imposed constrains. The vector of variables “Trialmaxrandstep” fixes the maximum variation that each parameter can assume at each iteration. So, the parameters can vary randomly in limited range of values. The new set of parameters is defined. After the mutation, the selection procedure is performed. In order to do that the current is calculated using the Eq.2-16 with the new set of parameters calculated after the mutation. The resnorm associated to the new set of parameters is evaluated, it is the objective function that has to be minimized. The error function of this algorithm is calculated as the difference between the resnorm of the i^{th} iteration and of the $i^{\text{th}}-1$ iteration. As was commented in section, 4.1.3.1, if the error function decreases the set of parameters overcomes to the next iteration. If it not decreases, probability distribution of Boltzman is applied. A condition is defined in order to establish what set of parameters will overcome at the next iteration. A random number included between 0 and 1 is calculated. if the calculated number is lower or equal to the probability, the new set of parameters, estimated in the current iteration is kept constant at the next iteration. Otherwise, the new set of parameters is discarded and the old set of parameters, calculated in the previous iteration, is taken into account for the next iteration.

4.1.3.4 Nelder-Mead Algorithm

The Nelder-Mead method is a deterministic heuristic direct search method, that allow a multivariable objective function to be optimized. The algorithm uses the idea of simplex in order to optimize the objective function. To define the simplex, it is necessary to clarify the concept of polytope. Polytope is a generic geometric unit with "flat" sides connected each other to form a closed line. In mathematics, the n -dimensional simplex is the n -dimensional polytope with the least number of

vertices. For example, the 0-d simplex is a single point, the 2-d simplex is a triangle and the 3-d simplex a tetrahedron. The n-d simplex has n+1 vertices. Each vertex of the simplex coincides with a set of independent variables in which the values of the objective function are evaluated directly (direct method). Then the simplex is modified in order to find the optimal set of variables that solve the problem.

A new point of the simplex is generated at each iteration to replace the point for which the objective function assumes the worst value among the vertices of the simplex.

The new point is generated starting from the centroid of the best n vertices of the simplex. The new point of the simplex is generated moving the parameters through a specific direction. if that variation lead to an improving of the solution the method tries to stretch the research of the solution exponentially out along this line. Otherwise, the variation leads to a negative effect on the solution the method tries to extend the research through points situated in the opposite direction. The Nelder-Mead method can converge to a not stationary point. Here below is reported a general procedure applied from the algorithm in a simple optimization problem with 2 variables. The simplex presents in this study is more complex than the ones presented in the following explanation, however the used algorithm is based on the same principle. For the sake of simplicity, a problem with only two variables is analysed in this section in order to easily explain the steps that take place during the Nelder Med algorithm.

Assuming an optimization problem in which the objective function $f(x)$ has to be minimize, where x is a vector composed of $n=2$ independent variables. A simplex composed by the $2+1$ set of independent variables x_W, x_B, x_G can be defined . The first step of the process consists on the calculation of the objective function in all the points of the simplex. Supposing that the point of the simplex are arranged in decreasing order of objective function in this way:

$$f(x_B) \leq f(x_G) \leq f(x_W) \quad \text{Eq.(4-37)}$$

In this configuration if the goal is to minimize the objective function, x_B is the best point x_G is the intermediate point and x_W is the worst point. The second step is the calculation of the centroid of the $n=2$ best points of the simplex that can be obtained making the mean of them:

$$x_M = \sum_{i=1}^n \frac{x_i}{n} = \frac{(x_B+x_G)}{2} \quad \text{Eq.(4-38)}$$

Then, a step called reflection is performed. In this step is generated a new point reflecting the worst point of the system with respect the centroid with the subsequent formula:

$$x_R = x_M + \alpha(x_M - x_W) \quad \text{Eq.(4-39)}$$

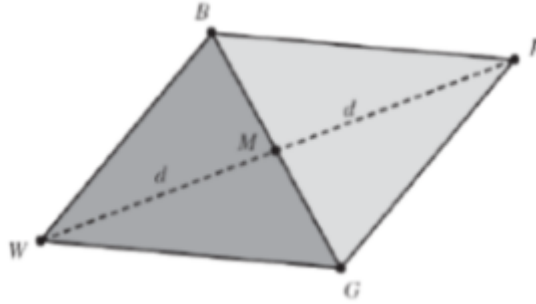


Figure 4-7: reflection of a three points simplex.

At this point there are more than one possibilities depending on the value assumed by x_R :

- If $f(x_B) \leq f(x_R) \leq f(x_G)$ if the new point has the value of the objective included between the best and the intermediate point the worst point of the simplex is replaced by the reflected point. In this way the simplex is the triangle in light grey in Fig 4-7.
- If $f(x_R) \leq f(x_B)$ the new point has the value of the objective lower than the best point. It means that the variation has led to an improvement of the system. For that we try to extend that variation generating a new point through an expansion. It consist to generate a new point in the same direction but with higher distance length (generally a double distance). The coordinate of the new point can be calculated through :

$$x_E = x_M + \gamma(x_M - x_W) \quad \text{Eq.(4-40)}$$

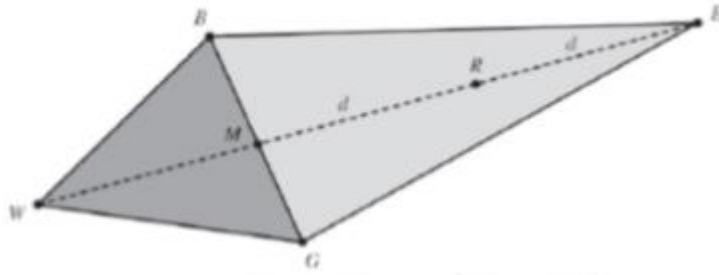


Figure 4-8: expansion of a three points simplex.

At this point the point generated from the expansion can be :

- If $f(x_E) \leq f(x_R)$ this means that the solution is improved and so the point x_E replace the worst point x_W . In this way the simplex is the triangle in light grey in Fig 4-8.
- Else means that the solution is worsened and the point x_R replace the worsened point x_W . In this way the simplex is the triangle in light grey in Fig 4-8.
- If $f(x_W) \leq f(x_R)$ the reflected point is worse than the worst point of the simplex . This means that the direction chosen is wrong, for that a variation in the opposite direction is performed. This procedure is called contraction and allow to generate a point in the opposite direction with respect the reflection. The coordinate of the new point can be calculated through:

$$x_C = x_M + \beta(x_M - x_W) \quad \text{Eq.(4-41)}$$

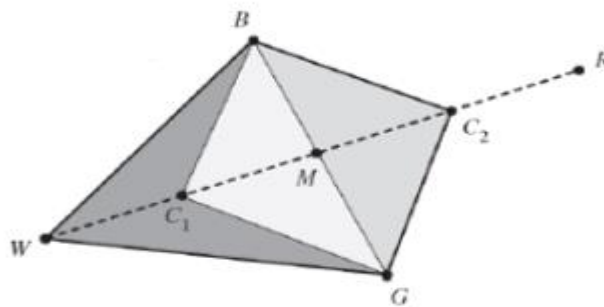


Figure 4-9: contraction of a three points simplex.

At this point :

- If $f(x_C) \leq f(x_W)$ the worst point x_W is replaced from the point generated through the contraction x_C .
- Else if no one of the previous procedures have been improved the simplex, a new simplex is generated through a shrink process. The point are generated with respect the subsequent formula:

$$x_S = x_B + \delta(x_W - x_B) \quad \text{Eq.(4-42)}$$

$$x_M = x_B + \delta(x_G - x_B) \quad \text{Eq.(4-43)}$$

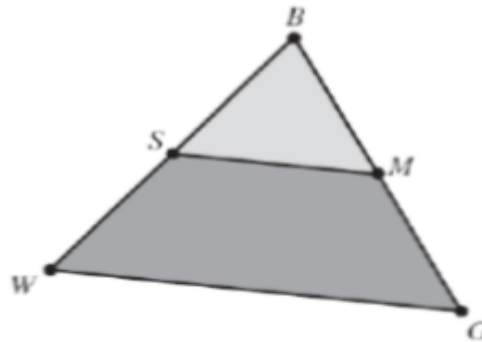


Figure 4-10: Shrink of a three points simplex.

Iteratively changing the points of the simplex, it is possible to explore a great part of the domain of the independent variables in order to find the optimal solution of the problem.

4.1.3.5 Implementation of Nelder Med algorithm in University of Jaen proposed procedure for the extraction of parameters

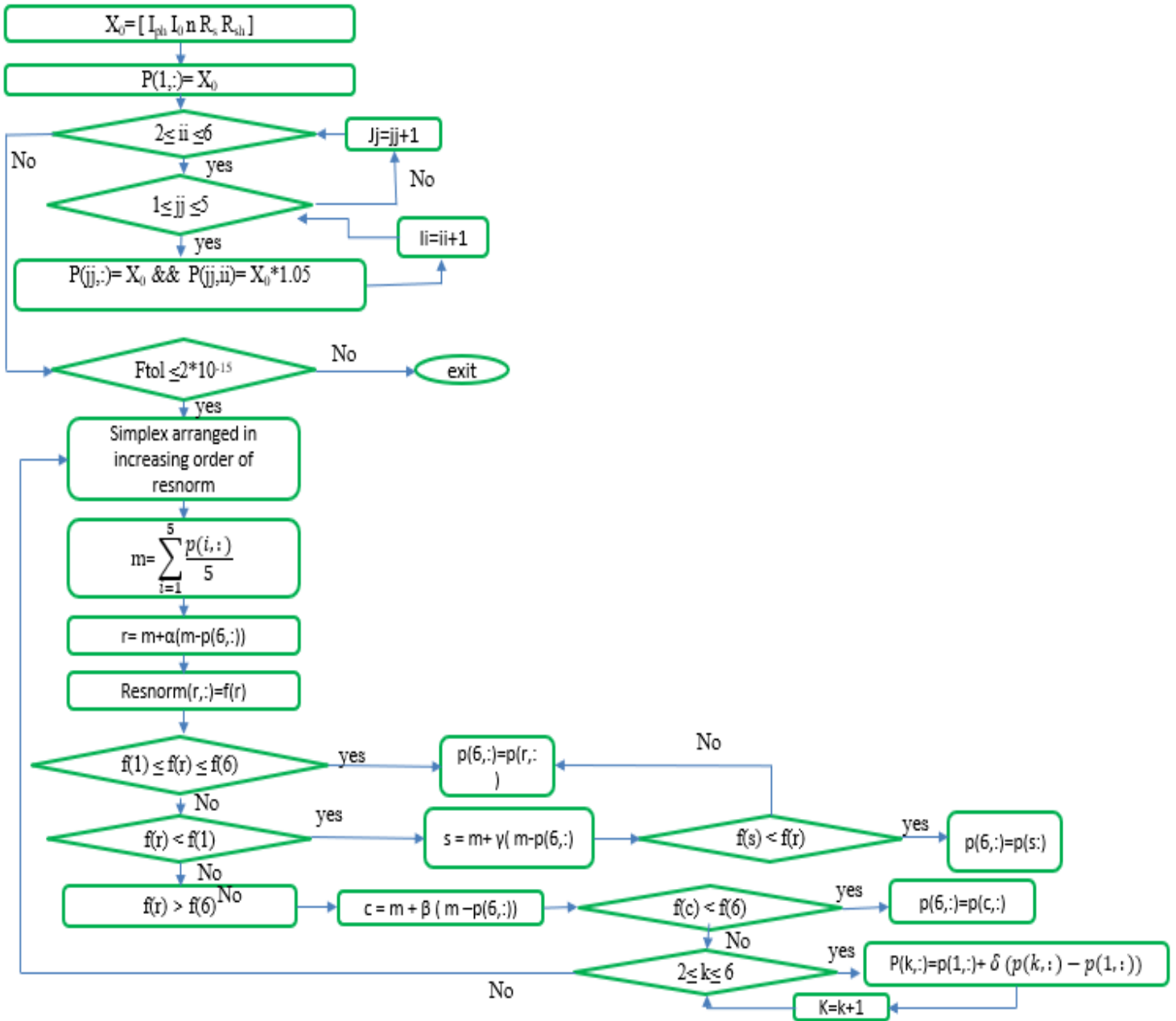


Figure 4-11: Flowchart of the Nelder-Mead Method computed in Octave for the extraction of the Parameters.

In this paragraph is explained in details the application of the Nelder-Mead algorithm computed on Octave by the University of Jaen in order to extract the

parameters of the SDM equivalent circuit. The vector X_0 represented in the first step of the flowchart of Figure 4-11 is composed by the set of parameters resulted by the previous application of the Simulated Annealing method explained in section 4.1.3.3. The Nelder Med is applied in order to refine the solution obtained by Metropolis Simulated Annealing algorithm and calculate the real global maximum value. The goal of the optimization algorithm is to find the minimum value of resnorm between the measured current and the current calculated by the equation. The function builds the initial simplex of $n+1=6$ points, where n consist of the number of independent variables that has to be optimized. The simplex is built using the parameters of the aforementioned vector X_0 obtained as result of the previous extraction algorithm. To create the simplex, 5 vectors are generated. Each of these vectors has 4 parameters equal to X_0 and 1 parameter that is increased 5% with respect the initial value. All the extraction procedure is performed through a while loop, that stops the iterations when the imposed tolerance is reached. The imposed tolerance is computed as the relative difference between the resnorm calculated in the worst and the best vertices of the simplex divided into the resnorm calculated with respects the best vertex. The limit value of the tolerance for which the iterations are stopped is set equal to $2 \cdot 10^{-15}$. When the program exits from the while loop the extraction is finished. As first step of the while loop the simplex is orderly arranged in an increasing order of resnorm value. Then, the centroid is calculated according with Eq.(4.38). The procedure applied in the subsequent steps is the same described in the previous section. The only difference in this case, is the number vertices of the simplex, which are 6 and not 3 (because $n=5$ and not $n=2$). For these reasons, it is avoided to explain a second time the passages related to the Reflection, Expansion, Contraction and Shrink processes. At the end of each iteration a new simplex matrix is generated. At the beginning of the next iteration the matrix is rearranged and the vectors are swift according to the value of the resnorm. it is worth mentioning regarding the values of the coefficient associated to the Reflection (α), to the Expansion (γ), to the Contraction (β) and to the Shrink (δ). The values of these coefficients, used into the equation explained in the previous paragraph are reported in Table 4-2.

Table 4-2: Coefficient of simplex algorithm applied in the extraction procedure for the SDM parameters by the University of Jaen. Applied in the Eq.(4-38), Eq.(4-39), Eq.(4-40), Eq.(4-41), Eq.(4-42) and Eq.(4-43) explained in the previous section.

Reflection coefficient (α)	1
-------------------------------------	---

Expansion coefficient (γ)	2
Contraction coefficient (β)	-1/2
Shrink coefficient (δ).	$\frac{1}{2}$

4.1.4 Parameter Validation

4.1.4.1 Control of the fitting quality depending on error of the power produced at MPP

The resnorm is the parameter that is directly optimized during the fitting procedure. If a simulation converges, generally, the value of the resnorm at the end of the fitting procedure achieve values inside an acceptable tolerance. However, to consider a simulation valid, there is a second indicator that must reach a proper tolerance. That indicator is the percentage error with respect to the power produced at the maximum power point. The final purpose of the present study consists of to determining correlations that allow the performance of the module in different conditions of irradiance and cell temperature to be estimated. Although the error on the maximum power is not a common indicator for the quality of a fitting, in this work, the accuracy on the estimation of the maximum power must be accurately estimated. So, this error becomes the most important indicator that allows the quality of the fitting to be estimated. The tolerance is set at 2%. Moreover a check of the final value of the resnorm parameter is performed. For that reason the limit of the resnorm is imposed at 0.03. The user checks if this limit is verified at the end of each simulation. If a test complies with the set limit with respect to the maximum power and with respect to the resnorm, the parameters extracted are validated. If the values got after the iteration are beyond the set limits, a weighted reduction of the points far from the MPP is applied. After that the extraction procedure is repeated with respect the new reduced $I-V$ curve.

4.1.5 Weighted reduction of the I-V curve points

The main purpose of the weighted reduction is to reduce the points in the areas with low interest. The area of maximum power point has a great interest in this study, while the point of short circuit and open circuit are less interesting. For that reason, the number of points closer to the short circuit and open circuit can be

reduced. In this way it is possible to obtain an $I-V$ curve with an higher concentration of points in the area near to the maximum power point and a lower concentration of the points in the remaining areas. To reduce the number of points in the open circuit area both the programs implemented in Octave and Matlab provides the possibility to select the part of the curve in which the reduction is applied. It is possible to select the maximum and the minimum current values that define the interval in which the reduction will take place. To quantify how severe the reduction, the variable 'reduction_point_open_circuit' has to be set. If a value higher than 1 for this variable is set, a reduction in the selected current interval can be obtained. To make a reduction of points in the closest area to the short circuit, it is possible to modify the variable 'reduction_point_short_circuit' by assigning it a value higher than 1. The zone in which this reduction is perform is graphically selected from the user. After that, the maximum power error is reduced and the extraction parameters can be validated.

5 Analysis of the obtained results

5.1 Experimental campaigns

The experimental campaign necessary to obtain the experimental data of the measurements for the study about the parameters extraction and the energy production can be divided into 2 parts:

- The experimental campaign performed at Politecnico di Torino.
- The experimental campaign conducted at University of Jaen.

The PV module selected in order to carry out this study belong to the silicon cell technology, in particular two monocrystalline and 1 polycrystalline panel are studied. Monocrystalline and polycrystalline technologies are wide-spread on the market so, it is relevant to focus on this kind of technology. In future, this study could be extended also towards different PV cell technologies.

5.1.1 Politecnico di Torino experimental campaign

For the experimental measurements carried out at Politecnico di Torino the PV modules under test are the two listed below:

- the model TSM-DD05A.08 by Trina Solar, this is a monocrystalline module and has a nominal power of 300W.
- the model JAP60S01 by JA-Solar, this is a polycrystalline module and has a nominal power of 280W.

The main characteristics of these modules are present in the datasheet provided by manufacturers included in Appendix. The conditions of the modules under tests are previously checked. A check on the maximum power at STC is performed correcting the $I-V$ curve to STC conditions. In order to carry out the corrections of the measured $I-V$ curves, the application of the norm of reference is the IEC EN 60891 standard, [23] ("Procedures for temperature and radiation corrections to the measured $I-V$ characteristics of photovoltaic devices"). Experimental campaign performed at Politecnico di Torino is carried out in a clear sky day with very low wind. The two days are 12th September 2018 and 15th February 2019. The

advantage to perform measurements in winter and in summer is the possibility to collect data in two different conditions: low cell temperatures (close to STC) and high irradiance during the winter clear sky day, and high cell temperatures and high irradiance during the summer clear sky day. The ranges of the temperatures and irradiance collected in the campaigns are shown in table5-1 and table5-2.

Table 5-1: Cell temperature and irradiance ranges of the TRINA solar monocrystalline experimental campaign performed at Turin Polytechnique.

Trina Solar Monocrystalline TSM-DD05A.08 (300 W).		
irradiance G [W/m ²]	min	max
	144	876
Tc [K]	min	max
	304	328

The experimental measurements take place in 2 days, 12th September 2018 and 15th February 2019. Over the global amount of measurements carried out in these days, only 8 measurements respect the requirements in order to be collected.

Table 5-2: Cell temperature and irradiance ranges of the JA solar polycrystalline experimental campaign performed at Politecnico di Torino.

JA-Solar Polycrystalline JAP60S01 (280 W)		
irradiance G [W/m ²]	min	max
	155	937
Tc [K]	min	max
	294	317

The experimental measurements take place only in 1 day, the 15th February 2019. Over the global amount of measurements carried out in this day, only 7 measurements respect the requirements in order to be collected.

5.1.2 UJA experimental campaign

For the experimental campaign carried out at University of Jaen the PV module under test is the model LX-100M by Luxor. this is a monocrystalline module and has a nominal power of 100W. The main characteristics of this module are present in the datasheet provided by manufacturers included in Appendix. Before starting the measurements, the PV module was calibrated by an independent certificated laboratory in Madrid (research centre for energy environmental

and technology, CIEMAT). The results of the calibration are reported in the Appendix. The electrical response is in coherent with manufacturers datasheet data. The experimental campaign is performed in a period of time of 20 days that goes from 10th of April 2019 to 30th of April 2019. The parameters collected during the experimental campaign are the wind speed, the cell temperature and the irradiance. The range of measurements (maximum and minimum) of these parameters are reported in table 5-3.

Table 5-3: Range of measurements of cell temperature, irradiance, and wind speed for the Luxor monocrystalline experimental campaign performed at University of Jaen.

Luxor Monocrystalline LX-100M (100W)		
irradiance G [W/m ²]	min	max
	195	1190
Tc [K]	min	max
	283	335
Wind speed [m/s]	min	max
	0,02	5

During these 20 days of experimental campaigns, a large amount of measurements is collected. Only 2967 measurements respect the requirements in order to be collected.

5.2 Parameter extraction results and estimation of the correlations

As it was introduced in section 4-1 procedures for parameter extraction are applied using the measured I - V curve in order to obtain the SDM equivalent circuit parameters. At Politecnico di Torino, a combined analytical-numerical method and a Levenberg Marquardt Algorithm (LM) are used to extract the parameters, (section 4-1-2). At University of Jaen, a comparison between the aforementioned procedure and an optimization method based on Metropolis Simulated Annealing algorithm and Nelder Mead algorithm (SA-NM) is performed in order to establish a comparison with the Politecnico di Torino extraction procedure (wider commented in section section 4-1-3). The goal of the proposed study is to estimate the correlations that describe the variations of the 5 parameters with irradiance and cell temperature. Once at this point, and before explaining in details the correlations, it worth mentioning again what are the parameters which their dependency with cell temperature and irradiance will be defined below: I_{ph} , I_0 , n , R_s , R_{sh} . The used correlations are taken from the literature [24]and depend on some coefficients. A nonlinear regression based on a curve fitting procedure that use Levenberg Marquardt Algorithm, is applied to calculate the values of these coefficients. The proposed equations are the subsequent ones:

- For photogenerated current a correlation, proportional with the irradiance and linear with temperature (α angular coefficient), defined by Eq.(5-1) is proposed.

$$I_{Ph} = I_{ph_{STC}} * \left\{ 1 + \frac{G}{G_{STC}} * \left[\frac{\alpha}{100} * (T_c - T_{STC}) \right] \right\} \quad \text{Eq.(5-1)}$$

Where:

- $\alpha \rightarrow$ Temperature coefficient provided by the manufacturer datasheet, $\left[\frac{\%I_{SC}}{^{\circ}C} \right]$. (section 2-14).
- $(G_{STC}, T_{STC}) \rightarrow$ STC operating condition (section 2-12), $G_{STC} \left[\frac{W}{m^2} \right]$ and $T_{STC} [^{\circ}C]$.
- $I_{ph_{STC}} \rightarrow$ It is the photogenerated current in STC condition, it is the coefficient that will be optimized in the nonlinear regression [A].

- For saturation current a cubic correlation with cell temperature, defined by Eq.(5-2) is proposed.

$$I_0 = I_{0_{STC}} * \left(\frac{T_c}{T_{STC}}\right)^3 * \exp\left(\left(\frac{E_{g_{STC}}}{T_{STC}} - \frac{E_g(T_c)}{T_c}\right) * \frac{1}{k}\right) \quad \text{Eq.(5-2)}$$

Where:

- $I_{0_{STC}}$ → saturation current at STC condition, it is the coefficient that will be optimized in the nonlinear regression. [A].
- k → Boltzman constant, equal to $1.381 \frac{J}{K}$.
- $E_{g_{STC}}$ → Energy Gap between the valence band and the conduction band at STC condition (section 1-1) [eV]. It is defined by Eq.(5-3)

$$E_{g_{STC}} = 1.121 * q \quad \text{Eq.(5-3)}$$

Where :

- q → Charge of electron, $1.602e-19$ C
- $E_g(T_c)$ → Energy Gap between the valence band and the conduction band at T_c condition [eV]. It is defined by Eq.(5-4)

$$E_g(T) = E_{g_{STC}} * (1 - 0.0002677 * (T_c - T_{STC})) \quad \text{Eq.(5-4)}$$

- For the cadimensional diode non-ideality factor a constant correlation defined by Eq.(5-5), is proposed.

$$n = const. \quad \text{Eq.(5-5)}$$

- For serie resistance a correlation, proportional with the cell temperature and logarithmical with irradiance, defined by Eq.(5-6) is proposed.

$$R_s = R_{s_{STC}} * \frac{T_c}{T_{STC}} * \left(1 - \lambda * \log\left(\frac{G}{G_{STC}}\right)\right) \quad \text{Eq.(5-6)}$$

Where:

- R_{sSTC} → series resistance in STC, it is one of the two coefficients that is optimized by the nonlinear regression [Ω].
- λ → Adimensional empirical coefficient, proportional to the logarithmic variation of the irradiance, it is the other coefficient that is optimized by the nonlinear regression.
- For shunt resistance a correlation, inversely proportional with the irradiance, defined by Eq.(5-7) is proposed.

$$R_{sh} = R_{shSTC} * \frac{G_{STC}}{G} \quad \text{Eq.(5-7)}$$

Where:

- R_{shSTC} → Shunt resistance evaluated at STC, it is the coefficient that will be optimized from the nonlinear regression [Ω].

The coefficients I_{phSTC} , I_{0STC} , R_{shSTC} , R_{sSTC} , and λ are optimized at each iteration in order to minimize the norm of the residual (Eq.4-2) among the extracted points and the points evaluated through the correlation. The Percentage Relative Standard Deviation (PRSD) of the extracted parameters is evaluated in order to evaluate the quality of the estimated correlations using the subsequent formula (here reported as application to the saturation current):

$$PRSD = 100 * \frac{N_{params}}{\mu} \sqrt{\frac{1}{N_{params}} * \sum_{i=1}^{N_{params}} (I_{0CORRELATION} - I_{0EXTRACTED})^2} \quad \text{Eq.(5-8)}$$

Where:

- $I_{0CORRELATION}$ → Parameter value calculated from correlation (in this case an example with saturation current is done).
- $I_{0EXTRACTED}$ → Extracted parameters with respect the PRSD is calculated (in this case an example with saturation current is done).
- N_{params} → Number of extracted parameters with respect to perform the nonlinear regression.
- μ → Mean value of the extracted parameters (in this case an example with saturation current is done). evaluated with:

$$\mu = \frac{\sum_{i=1}^{N_{params}} I_{0EXTRACTED}}{N_{params}} \quad \text{Eq.(5-9)}$$

These fitting operations are separately carried out for each parameter. They are implemented by the use of the application Curve Fitting App and the available

structured functions provided by Matlab. In the next chapters the results of these nonlinear regression procedure are going to be described.

5.2.1 Politecnico di Torino Nonlinear Regression Results

5.2.1.1.1 Results regarding monocrystalline PV module TSM-DD05A.08 by Trina Solar

The results from the parameters extraction for the SDM circuit using Politecnico extraction procedure, irradiance, cell temperature, and percentage error on maximum power are reported in table 5-4:

Table 5-4: SDM parameters extracted for monocrystalline PV module TSM-DD05A.08 by Trina Solar using the Politecnico extraction procedure, irradiance, cell temperature, and percentage error on the maximum power.

G [W/m ²]	T _c [K]	I _{ph} [A]	I ₀ [A]	n [-]	R _s [Ω]	R _{sh} [Ω]	E _{MPP} [%]
876	316	8,4	8,88E-10	1,01	0,361	136	-0,08%
875	328	8,5	3,84E-09	0,97	0,388	211	0,15%
694	315	6,8	8,07E-10	1,04	0,459	1279	0,43%
553	309	5,2	4,10E-10	0,98	0,450	962	0,05%
460	320	4,4	1,44E-09	1,00	0,435	784	0,11%
394	304	3,6	2,17E-10	0,99	0,483	1695	-0,71%
359	317	3,4	1,06E-09	1,02	0,452	918	0,06%
144	305	1,4	4,40E-10	1,03	0,560	1599	-0,05%

The Table 5-4 shows that all the fitting simulation results are largely inside the constrains imposed on the maximum power percentage error ($E_{MPP} < 2\%$). This represent an index on the high quality of the fitting results.

All the values assumed from the parameters present a monotonic trend excepting R_{sh} . The photovoltaic current dependence with the irradiance is monotonic increasing. Moreover, the saturation current dependence with the cell temperature is monotonic increasing. Finally, monotonic decreasing of the series resistance with the irradiance are clearly shown in the Table 5-4.

The values of the extracted parameters presented in table 5-4 are used in order to estimate the correlations. The nonlinear regression is performed with respect the correlations purposed in [24]. This choice is based on the tendencies showed from the Table 5-4 and above mentioned. The results of the correlations evaluated through the method described in section 5-1-3 is reported in the graphs attached below.

Photogenerated current:

The graphs, which show the dependence of the correlation and the extracted points of the photogenerated current with respect irradiance and temperature are respectively shown in Figure 5-1 and in Figure 5-2

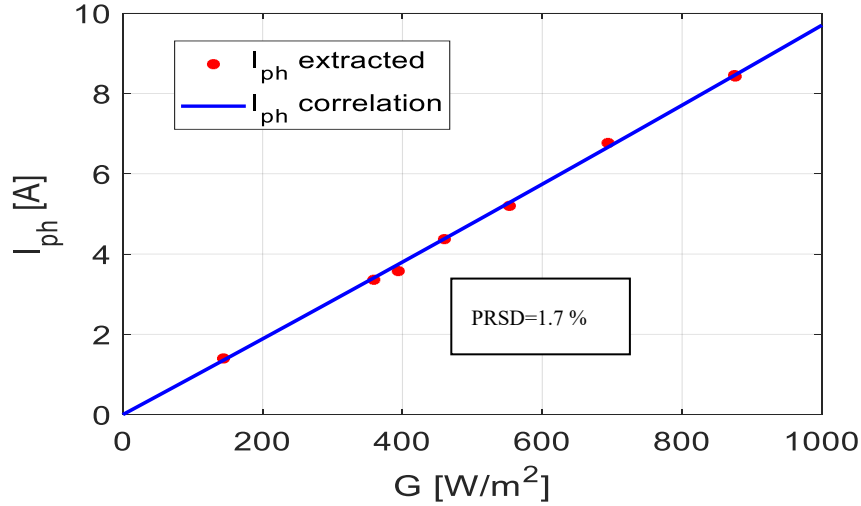


Figure 5-1: nonlinear regression results for I_{ph} monocrystalline by Trina Solar. The blue line is the estimated correlation function for I_{ph} . The red dots represent the extracted points.

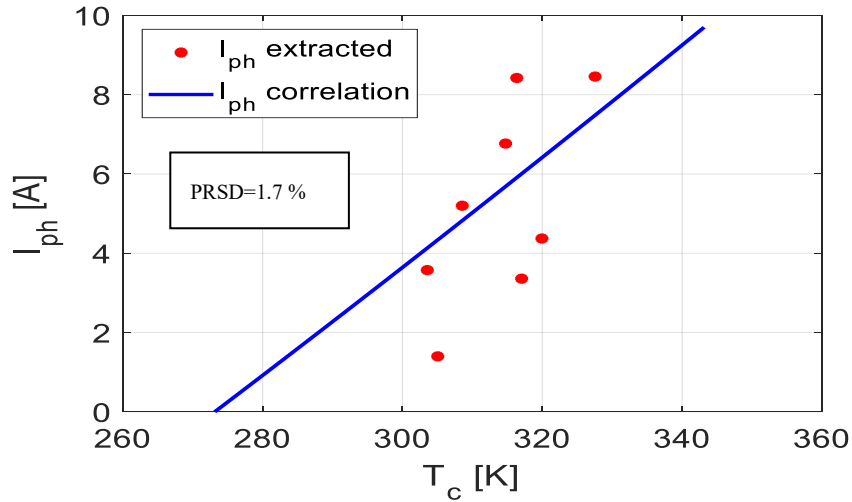


Figure 5-2: nonlinear regression results for I_{ph} for monocrystalline by Trina Solar. The blue line is the estimated correlation function for I_{ph} . The red dots represent the extracted points.

$$I_{ph} = 9.49 * \left\{ 1 + \frac{G}{G_{STC}} * \left[\frac{\alpha}{100} * (T_c - T_{STC}) \right] \right\} \quad \text{Eq.(5-10)}$$

The best value of $I_{Ph_{STC}}$ in order to optimize the fitting is 9.49 A. As it shows from Figure 5-1, the value of PRSD is 1.7% this means that the correlation accurately fits the points. The I_{Ph} strongly depends on the irradiance and weakly on the T_c because of that the tendency of I_{Ph} variation with T_c is shown in Figure 5-2 but it never will be not reported in future.

Saturation current:

The graphs, which show the dependence of the correlation and of the extracted points of the saturation current with respect temperature are shown in Figure 5-3.

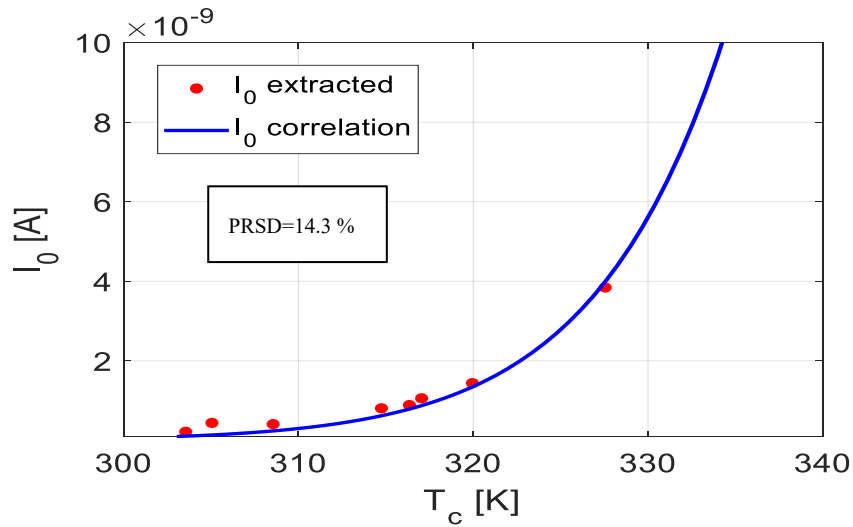


Figure 5-3: monocrystalline by Trina Solar nonlinear regression results for I_0 . The blue line is the estimated correlation function for I_0 . The red dots represent the extracted points.

$$I_0 = 4.4 * 10^{-11} * \left(\frac{T_c}{T_{STC}}\right)^3 * \exp\left(\left(\frac{E_{g_{STC}}}{T_{STC}} - \frac{E_g(T_c)}{T_c}\right) * \frac{1}{k}\right) \quad \text{Eq.(5-11)}$$

$$E_{g_{STC}} = 1.121 * q \quad \text{Eq.(5-12)}$$

$$E_g(T) = E_{g_{STC}} * (1 - 0.0002677 * (T_c - T_{STC})) \quad \text{Eq.(5-13)}$$

The optimum value of $I_{0_{STC}}$ in order to perform the best fitting is $4.4 * 10^{-11}$ A. As it shows from Figure 5-3, the value of PRSD is 14.3% which represents a non-negligible error between the correlation function and the extracted points. Although the error is high, to verify the reliability of our correlations, a further validation must be computed. This validation of the estimated correlation will consist of a

comparison between the values of the maximum power estimated by the use of the correlations and the experimental ones. The agreement on the evaluation of the maximum power with respect the experimental results will establish the accuracy of our correlation functions. The I_0 exclusively depends on the T_c as it was reported in the literature, for that only the cell temperature dependence is reported in Figure 5-3.

Diode’s ideality factor:

The graph, which shows the dependence of the correlation and of the extracted points of the diode ideality factor with respect irradiance are shown in Figure 5-4.

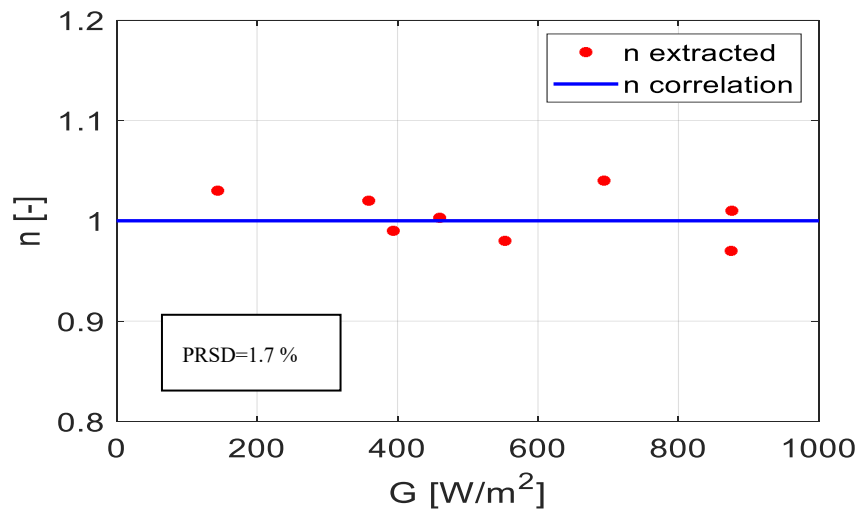


Figure 5-4: nonlinear regression results for n for monocrystalline by Trina Solar. The blue line is the estimated correlation function for n . The red dots represent the extracted points

$$n = 1 \tag{Eq.(5-14)}$$

The extracted points are very close to one and because of that, the values of n are set constant and equal to 1 as proposed in many studies from literature. The low PRSD=1.7% shows the accuracy of the estimation. The dependency of n with respect T_c is not reported because the curve and the points are exactly the same.

Series resistance:

The graphs, which show the dependence of the correlation and of the extracted points of the saturation current with respect irradiance and temperature are respectively shown in Figure 5-5 and in Figure 5-6

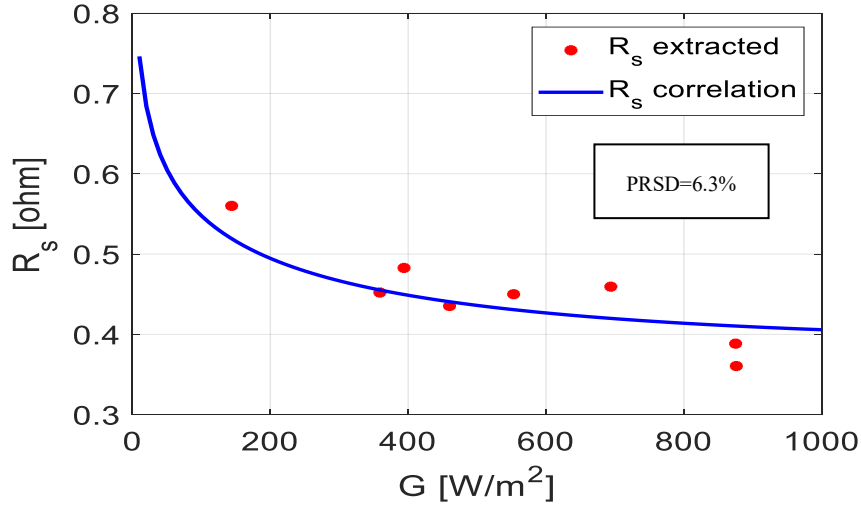


Figure 5-5: nonlinear regression results for R_s for monocrystalline by Trina Solar. The blue line is the estimated correlation function for R_s . The red dots represent the extracted points.

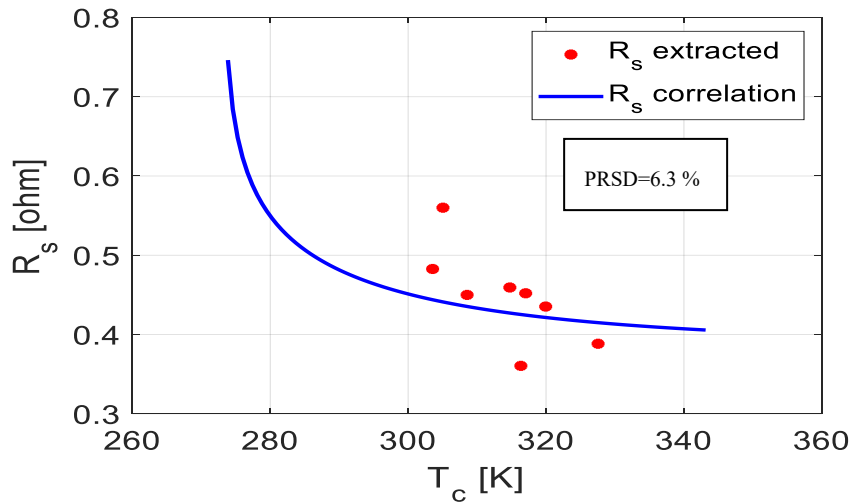


Figure 5-6: nonlinear regression results for R_s for monocrystalline by Trina Solar. The blue line is the estimated correlation function for R_s . The red dots represent the extracted points.

$$R_s = 0.353 * \frac{T_c}{T_{STC}} * \left(1 - 0.384 * \log \left(\frac{G}{G_{STC}} \right) \right) \quad \text{Eq.(5-15)}$$

In this case the coefficients extracted in order to optimize the fitting are two, R_{STC} , that is equal 0.353Ω and λ , that is equal to 0.384 . The empirical coefficient λ is iteratively calculated from the Levenberg Marquardt in order to optimize the fitting. The choice to not impose a fixed value of λ equal to the ones proposed by [24] is done in order to increase the quality of the fitting. As it shows from Figure 5-6, the value of PRSD is 6.3% , that is an acceptable value.

The nonlinear regression is performed with respect the two variables irradiance and cell temperature. So, the curves plotted on the graphs are simultaneously affected by the variation of both variables. In Figure 5-5 and Figure 5-6 are represented the aforementioned variation, from them it is possible to realise that the estimated correlation function accurately follows the irradiance variation but not the temperature ones. This means that the variation of the series resistance depends more on the irradiance than on the cell temperature.

Shunt resistance:

The graph, which shows the dependence of the correlation and of the extracted points of the diode ideality factor with respect irradiance are shown in Figure 5-7.

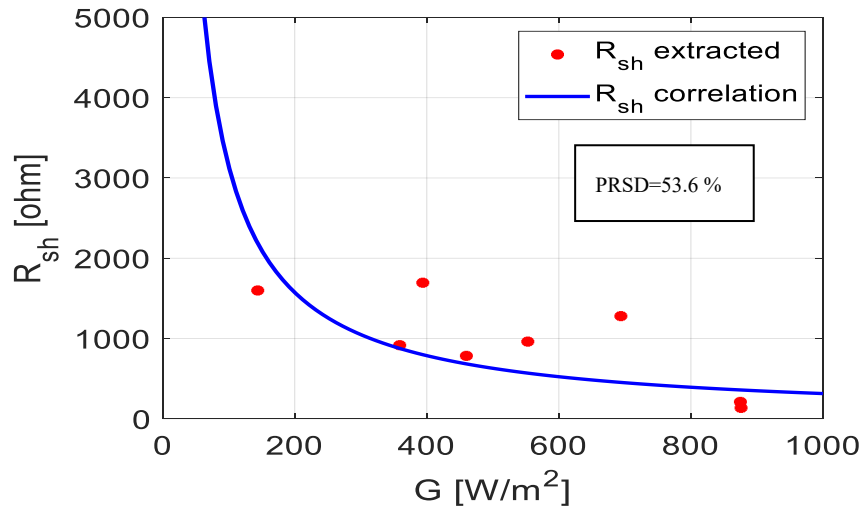


Figure 5-7: nonlinear regression results for R_{sh} for monocrystalline by Trina Solar. The blue line is the estimated correlation function for R_{sh} . The red dots represent the extracted points

$$R_{sh} = 315 * \frac{G_{STC}}{G} \quad \text{Eq.(5-16)}$$

The optimum value of $R_{sh_{STC}}$ in order to perform the best fitting is 315 Ω . The value of PRSD with respect this fitting is 53.6 %. Clearly there is an high error between the correlations and the extracted points. The low accuracy in the estimation of the shunt resistance can be explained analysing the Eq.2-16. The shunt resistance determines the slope of the curve at the short circuit point, where the $I-V$ curve can be approximated to a straight line. The higher is the shunt resistance lower is the slope of the $I-V$ curve in the short circuit point. Generally, the value of shunt resistance for a commercial PV module is higher than 250 Ω at STC. The purposed algorithm evaluates R_{sh} in a range between 136 and 1599 Ω without a clear monotonic trend with cell temperature or irradiance. Although this is a wide range of values, it is possible to verify that, when R_{sh} assumes a value higher than 250 Ohm, a further increase of R_{sh} have a negligible effect on the values of the estimated current. In fact, the Eq.(2-16). shows that for a higher value of R_{sh} the last term of the equation becomes negligible, then the curve is horizontal and the slope variation of the curve is imperceptible. For that reason, Levenberg Marquardt algorithm is not able to accurately estimate the value of R_{sh} . However, for the same reason the accuracy of the estimation of the shunt resistance is not binding for our purposes.

The estimated coefficients are reported together in Table 5-5.

Table 5-5: Coefficients of the proposed correlations for TSM-DD05A.08 PV module by Trina Solar evaluated performing the nonlinear regression.

NONLINEAR REGRESSION COEFFICIENTS				
$I_{ph_{STC}}$ [A]	$I_{0_{STC}}$ [A]	$R_{s_{STC}}$ [Ω]	λ [-]	$R_{sh_{STC}}$ [Ω]
9,49	4,40E-11	0,353	0,284	315

The percentage relative standard deviation calculated among the extracted values and the values calculated with the correlations presented in section 5-4 are reported for each value in Table 5-6.

Table 5-6: Percentage Relative Standard Deviation calculated between extracted points and correlation points for monocrystalline by Trina Solar.

CORRELATION PRSD [%]				
I_{ph} [A]	I_0 [A]	n [-]	R_s [Ω]	R_{sh} [Ω]
1,43%	11,52%	1,08%	5,48%	26,7%

As a result of the analysis, it is possible to observe that the I_{ph} , n , R_s are correctly estimated by the correlation. The correlation proposed from [24] , are wide spread

used on the literature to describe dependency of SDM parameters with respect irradiance and cell temperature. So, the good fitting between the proposed correlation and the extracted points confirms the reliability of the values of the parameters extracted from the measured $I-V$ curve. About the values of the shunt resistance and the saturation current, it is difficult so far claim if these estimations are suitable ones. In order to validate these results, the application of this model for the estimation of the power have been analysed. Thus the level of concordance between the estimated values and the measured ones for the maximum power will establish the accuracy for the shunt resistance and the saturation current correlations.

5.2.1.1.2 Results regarding polycrystalline PV module JAP60S01 by JA-Solar

The results from the parameters extraction using Politecnico procedure, irradiance, cell temperature, and percentage error on maximum power are reported in table 5-7 for polycrystalline PV module JAP60S01 by JA-Solar.

Table 5-7: SDM parameters extracted for polycrystalline by JA-Solar using the Politecnico extraction procedure, irradiance, cell temperature, and percentage error on the maximum power.

G [W/m ²]	T _c [K]	I _{ph} [A]	I ₀ [A]	n [-]	R _s [Ω]	R _{sh} [Ω]	E _{MPP} [%]
937	317	8,6	2,3E-09	1,01	0,320	566	0,15%
738	310	6,8	8,6E-10	1,01	0,313	336	0,16%
592	305	5,4	4,7E-10	1,00	0,308	315	-0,08%
458	302	4,1	3,3E-10	1,00	0,334	330	-0,06%
433	301	3,8	2,7E-10	1,00	0,389	541	0,06%
244	297	2,3	1,7E-10	1,00	0,376	696	-0,35%
155	294	1,4	1,1E-10	1,04	0,413	1514	-0,05%

The values of the parameters from the SDM using the Politecnico extraction procedure, confirms the monotonic tendency previously commented for the monocrystalline PV module TSM-DD05A.08 PV module by Trina Solar. The correlations proposed by [24] are used to carry out the nonlinear regression. The results of the correlations are reported in the subsequent graphs.

Photogenerated current:

The graph, which show the dependence of the correlation and the extracted points of the photogenerated current with respect irradiance shown in Figure 5-8.

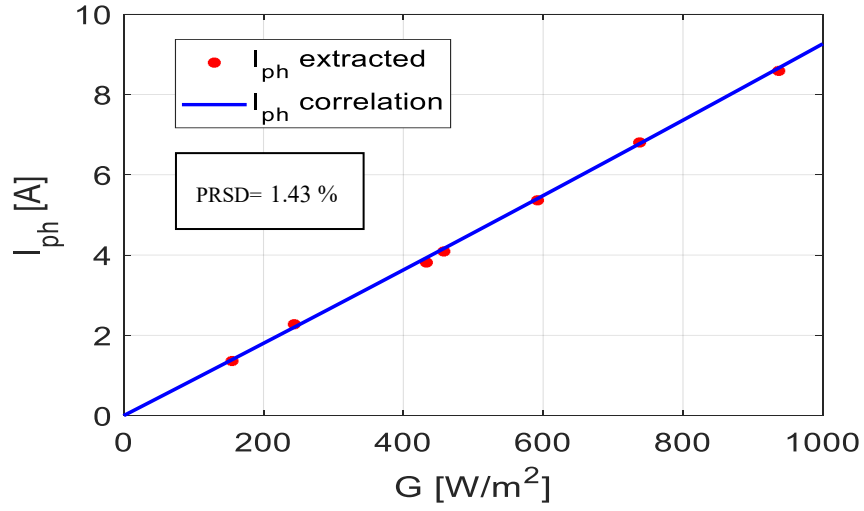


Figure 5-8: nonlinear regression results for I_{ph} for polycrystalline by JA-Solar. The blue line is the estimated correlation function for I_{ph} . The red dots represent the extracted points.

$$I_{Ph} = 9.06 * \left\{ 1 + \frac{G}{G_{STC}} * \left[\frac{\alpha}{100} * (T_c - T_{STC}) \right] \right\} \quad \text{Eq.(5-17)}$$

The best value of $I_{ph_{STC}}$ in order to optimize the fitting is 9.06 A. As it shows from Figure 5-8, the value of PRSD is 1.43% this means that the correlation accurately fits the points.

Saturation current:

The graph, which show the dependence of the correlation and the extracted points of the saturation current with respect cell temperature shown in Figure 5-9.

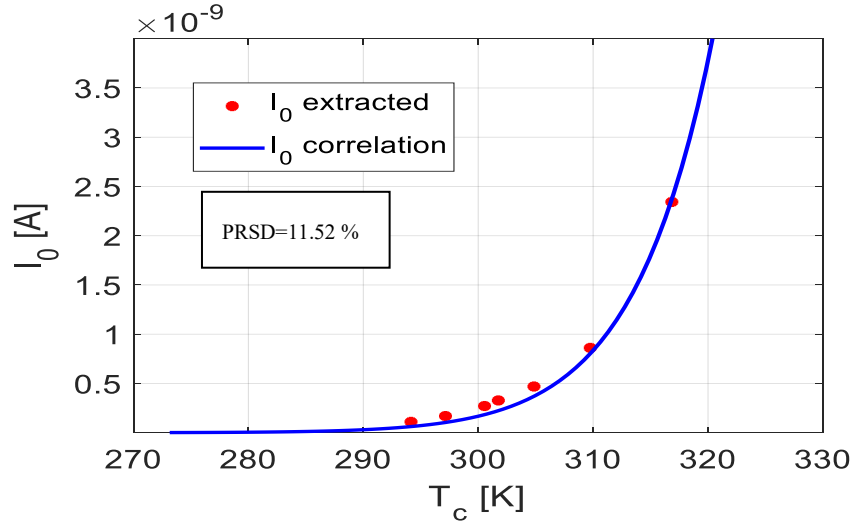


Figure 5-9: nonlinear regression results for I_0 for polycrystalline by JA-Solar. The Blue line is the estimated correlation function for I_0 . The red dots represent the extracted points.

$$I_0 = 1.23 * 10^{-10} * \left(\frac{T_c}{T_{STC}}\right)^3 * \exp\left(\left(\frac{Eg_{STC}}{T_{STC}} - \frac{Eg(T_c)}{T_c}\right) * \frac{1}{k}\right) \quad \text{Eq.(5-18)}$$

$$Eg_{STC} = 1.121 * q \quad \text{Eq.(5-19)}$$

$$Eg(T) = Eg_{STC} * (1 - 0.0002677 * (T_c - T_{STC})) \quad \text{Eq.(5-20)}$$

The optimum value of $I_{0_{STC}}$ in order to perform the best fitting is $1.23 * 10^{-11}$ A. As it shows from Figure 5-9, the value of PRSD is 11.52% which represents a non-negligible error between the correlation function and the extracted points. The aforementioned comparison with respect the correlation and experimental maximum power estimation has to be performed in order to confirm the accuracy of this correlation. The values of I_0 are higher for this polycrystalline PV module JAP60S01 by JA-Solar than for monocrystalline PV module TSM-DD05A.08 by Trina Solar. It can be expected because the polycrystalline technology is the one with worse performance than the monocrystalline technology.

Diode’s ideality factor:

The graph, which show the dependence of the correlation and the extracted points of the diode’s ideality factor with respect cell temperature shown in Figure 5-10.

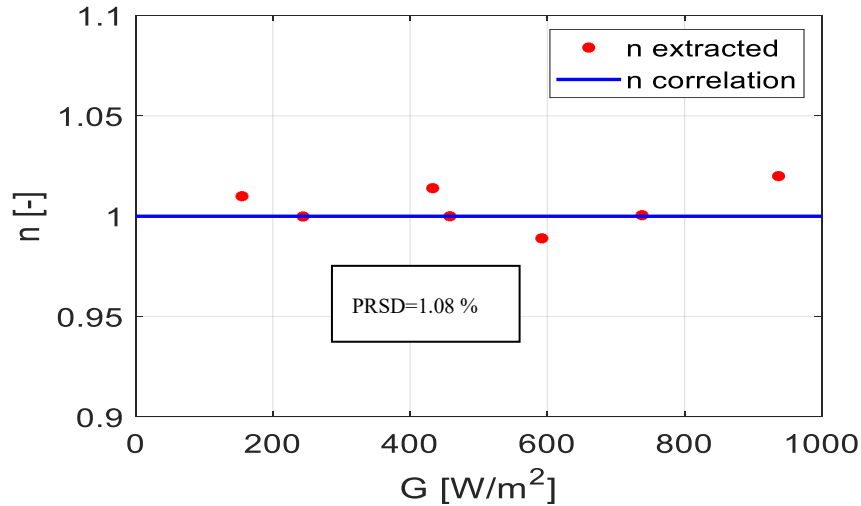


Figure 5-10: nonlinear regression results for n for polycrystalline by JA Solar. The blue line is the estimated correlation function for n . The red dots represent the extracted points

$$n = 1 \quad \text{Eq.(5-21)}$$

Even in this case, as for the monocrystalline technology, the extracted points assume values near to 1, for that reason a constant correlation $n=1$ is set. This correlation is very accurate because PRSD is equal to 1.08%.

Series resistance:

The graphs, which show the dependence of the correlation and of the extracted points of the saturation current with respect irradiance and temperature are respectively shown in Figure 5-11 and in Figure 5-12

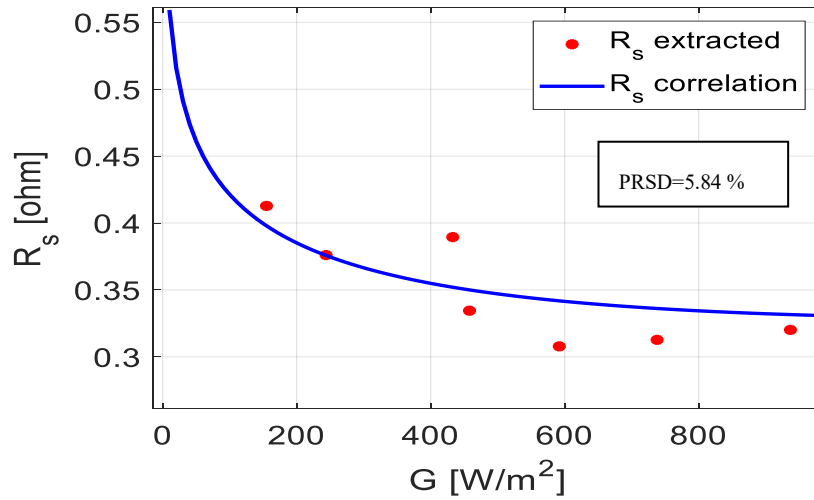


Figure 5-11: nonlinear regression results for R_s for polycrystalline by JA Solar The blue line is the estimated correlation function for R_s . The red dots represent the extracted points.

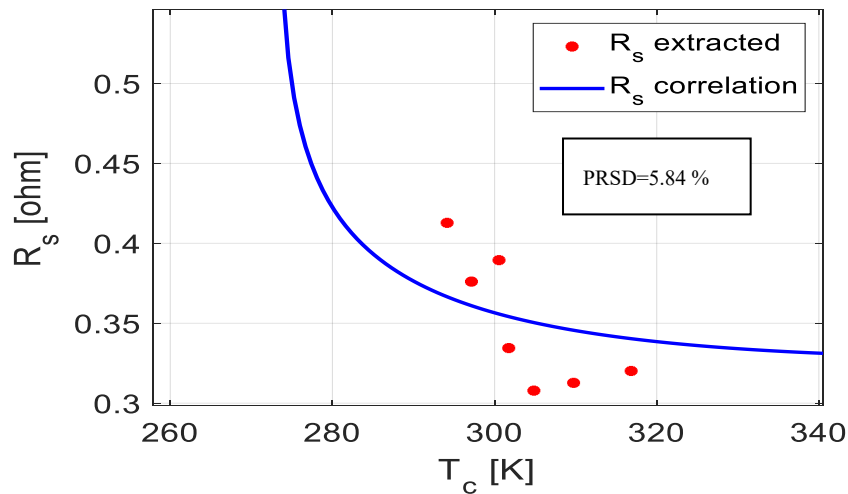


Figure 5-12: nonlinear regression results for R_s for polycrystalline by JA Solar The blue line is the estimated correlation function for R . The red dots represent the extracted points.

$$R_s = 0.287 * \frac{T_c}{T_{STC}} * \left(1 - 0.244 * \log \left(\frac{G}{G_{STC}} \right) \right) \quad \text{Eq.(5-22)}$$

In this case the coefficients extracted are two, $R_{s_{STC}}$, that is equal 0.287Ω and λ that is equal to 0.244. The low PRSD=5.84 % shows the accuracy of our estimation. Comparing these series resistance's values with the values previously extracted for monocrystalline technology, the series resistance for the

monocrystalline technology is larger than the series resistance for the polycrystalline technology. This is an unexpected result because polycrystalline technology has a lower efficiency than monocrystalline technology and so the R_s was expected higher.

Shunt resistance:

The graph, which shows the dependence of the correlation and of the extracted points of the diode ideality factor with respect irradiance are shown in Figure 5-13.

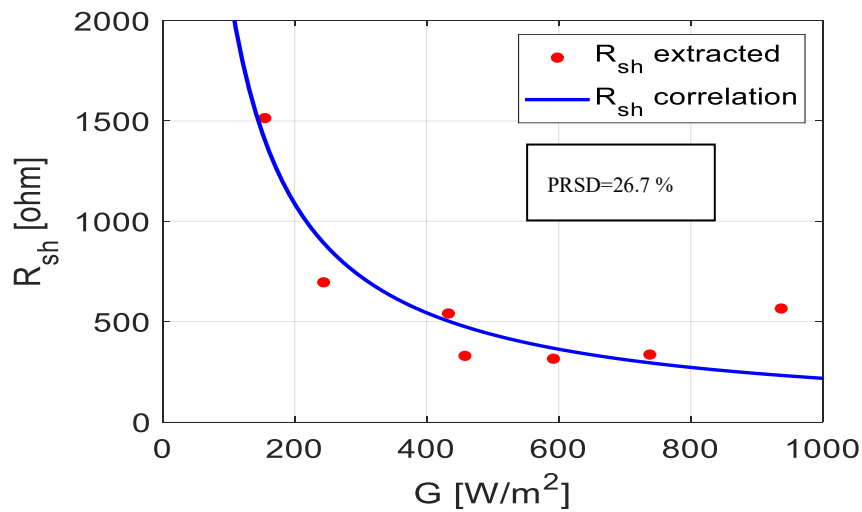


Figure 5-13: nonlinear regression results for R_{sh} for polycrystalline by JA Solar. The blue line is the estimated correlation function for R_{sh} . The red dots represent the extracted points

The optimum value of $R_{sh_{STC}}$ in order to perform the best fitting is 218 Ω . The value of PRSD with respect this fitting is 26.7 %

The optimum value of $R_{sh_{STC}}$ in order to perform the best fitting is 218 Ω . The value of PRSD with respect this fitting is 26.7 %. The error with respect this value is very high, the reason and the explanation of why this error is accepted are explained in section 5-2-1-1-1, in the part where the nonlinear regression of shunt resistance is analysed. The values of the shunt resistance are higher for monocrystalline than for polycrystalline this can be expected because monocrystalline technology is better electrically insulated. The values of the parameters extracted from the nonlinear regression are reported in the table 5-8

Table 5-8: Coefficients of the proposed correlations evaluated performing the nonlinear regression for polycrystalline by JA-Solar.

NONLINEAR REGRESSION COEFFICIENTS				
I_{ph_STC} [A]	I_{0_STC} [A]	R_{s_STC} [Ω]	λ [-]	R_{sh_STC} [Ω]
9,06	1,23E-10	0,287	0,244	218

The values of the percentage relative standard deviation error between the correlation functions and the extracted points are reported in Table 5-9

Table 5-9: Percentage Relative Standard Deviation between extracted points and correlation points of Polycrystalline JA-Solar.

CORRELATION PRSD [%]				
I_{ph} [A]	I_0 [A]	n [-]	R_s [Ω]	R_{sh} [Ω]
1,43%	11,52%	1,08%	5,48%	26,7%

All the errors for the polycrystalline are lower than for the monocrystalline technology. For polycrystalline all the I - V curves are measured at the same day 15th of February 2019. For that, only low cell temperatures could be measured and the recorded I - V curves have a low dispersion in terms of temperature. For that reason, the range of temperatures is smaller and the measured temperatures are close to each other, so the fitting is more accurate than in the case of monocrystalline nonlinear regression.

5.2.2 University of Jaen Nonlinear Regression Results

At the University of Jaen a monocrystalline PV module LX-100M by Luxor with nominal power of 100W is analysed applying two extraction procedures based on two different fittings algorithms. The procedure implemented by Politecnico di Torino section 4-1-2 is based on a combined analytical-numerical algorithm and a Levenberg Marquardt algorithm. The procedure implemented by University of Jaen section 4-1-3 is based on Metropolis Simulated Annealing algorithm and Nelder Med algorithm. In this section the results of the two procedures are compared. A representative collection of 14 $I-V$ curves that covered a wide range of cell temperature and irradiance values are selected among all the measurements in order to perform the extraction procedure. The results of the parameters extractions using Politecnico and University of Jaen procedures are reported in table 5-14 and Table 5-15:

Table 5-10: SDM parameters extracted for monocrystalline by Luxor using the Politecnico di Torino (LM) extraction procedure, irradiance, cell temperature, and percentage error on the maximum power.

G [W/m ²]	Tc [K]	I _{ph} [A]	I ₀ [A]	n [-]	R _s [Ω]	R _{sh} [Ω]	E _{MPP} [%]
1031	324	6,0	4,4E-08	1,11	0,326	399	-0,09%
897	328	5,2	4,7E-08	1,09	0,345	240	-0,70%
841	304	4,9	2,3E-10	1,01	0,331	250	-0,33%
833	297	4,8	7,7E-11	1,01	0,325	200	-0,42%
778	320	4,5	1,3E-08	1,08	0,327	270	-0,36%
708	318	4,1	1,2E-08	1,08	0,327	762	-0,36%
634	314	3,7	5,1E-09	1,07	0,344	300	-0,42%
541	316	3,1	9,7E-09	1,09	0,353	400	-0,58%
483	304	2,8	8,1E-10	1,04	0,344	600	-0,66%
398	310	2,3	3,7E-09	1,08	0,365	515	-0,57%
350	301	2,0	1,1E-09	1,08	0,345	750	-0,24%
313	299	1,8	7,3E-10	1,07	0,349	900	-0,25%
240	299	1,4	1,7E-10	1,00	0,400	660	-0,13%
168	312	1,0	7,5E-09	1,08	0,396	1375	0,12%

Table 5-11: SDM parameters extracted for monocrystalline by Luxor using the University of Jaen (SA-NM) extraction procedure, irradiance, cell temperature, and percentage error on the maximum power.

G [W/m ²]	T _c [K]	I _{ph} [A]	I ₀ [A]	n [-]	R _s [Ω]	R _{sh} [Ω]	E _{MPP} [%]
1031	324	6,0	4,2E-08	1,11	0,326	386	-0,17%
897	328	5,2	4,7E-08	1,09	0,345	470	-0,12%
841	304	4,8	4,5E-10	1,02	0,319	331	-0,31%
833	297	4,8	2,1E-10	1,04	0,311	387	-0,33%
778	320	4,5	1,4E-08	1,08	0,323	470	-0,27%
708	318	4,1	8,0E-09	1,06	0,329	423	-0,38%
634	314	3,7	3,6E-09	1,05	0,354	469	-0,09%
541	316	3,1	7,6E-09	1,06	0,342	522	-0,15%
483	304	2,8	3,8E-10	1,01	0,365	868	-0,32%
398	310	2,3	3,0E-09	1,07	0,354	846	-0,16%
350	301	2,0	8,3E-10	1,07	0,348	797	-0,24%
313	299	1,8	6,9E-10	1,07	0,344	844	-0,10%
240	299	1,4	9,4E-10	1,09	0,346	1031	-0,20%
168	312	1,0	6,9E-09	1,07	0,373	1031	0,16%

The results obtained applying both methods show the monotonic tendency described in section 4-1-3-1-1. The values for the extracted parameters are similar in both cases. The fact that two different methods converge approximatively to the same points confirm the validity of the extracted parameters results.

A nonlinear regression between the points extracted and the correlation functions proposed by [24] is performed and the best coefficients to optimize the fitting are calculated. These correlations estimate how the SDM parameters vary with respect irradiance and cell temperature. The results of that correlations are graphically represented for both methods in the figures below for each single parameter.

Photogenerated current:

The graphs, which show the dependence of the correlation and the extracted points of the photogenerated current with respect the irradiance for the parameters extracted with the two methods Politecnico di Torino (LM) and University of Jaen (SA-NM) are respectively shown in Figure 5-14 and in Figure 5-15.

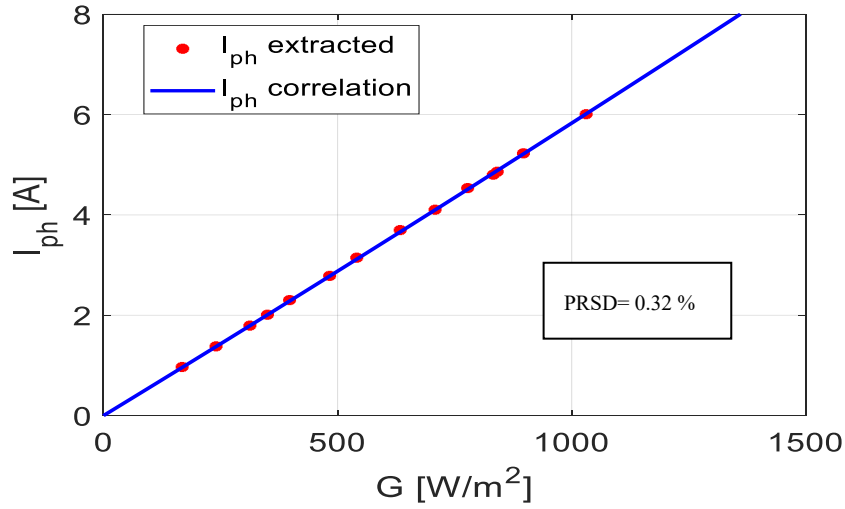


Figure 5-14: nonlinear regression results for I_{ph} for polycrystalline by Luxor. Blue line is the correlation function for I_{ph} . The red dots are the I_{ph} . Extracted using Politecnico di Torino procedure (LM).

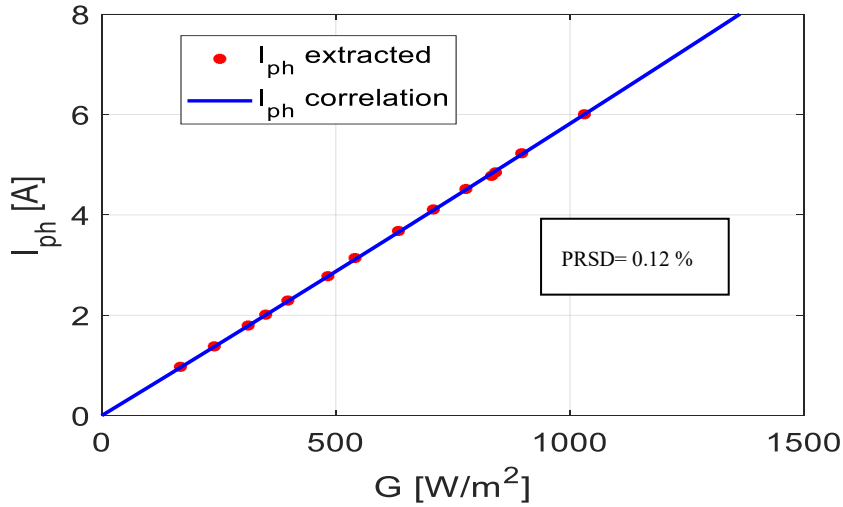


Figure 5-15: nonlinear regression results for I_{ph} for polycrystalline by Luxor. Blue line is the correlation function for I_{ph} . The red dots are the I_{ph} . Extracted using University of Jaen procedure (SA-NM).

$$I_{Ph} = I_{ph_{STC}} * \left\{ 1 + \frac{G}{G_{STC}} * \left[\frac{\alpha}{100} * (T_c - T_{STC}) \right] \right\} \quad \text{Eq.(5-23)}$$

The best value of I_{phSTC} in order to optimize the fitting and the percentage relative standard deviations assume approximatively the same values when the points are extracted by both methods:

- $I_{phSTC}=5.747$ A and PRSD= 0.32 % for the parameters extracted by Politecnico di Torino method.
- $I_{phSTC}=5.750$ A and PRSD= 0.12 % for the parameters extracted by the University of Jaen method.

Saturation current:

The graphs, which show the dependence of the correlation and the extracted points of the saturation current with respect the cell temperature for the parameters extracted with the two methods Politecnico di Torino (LM) and University of Jaen (SA-NM) are respectively shown in Figure 5-16 and in Figure 5-17.

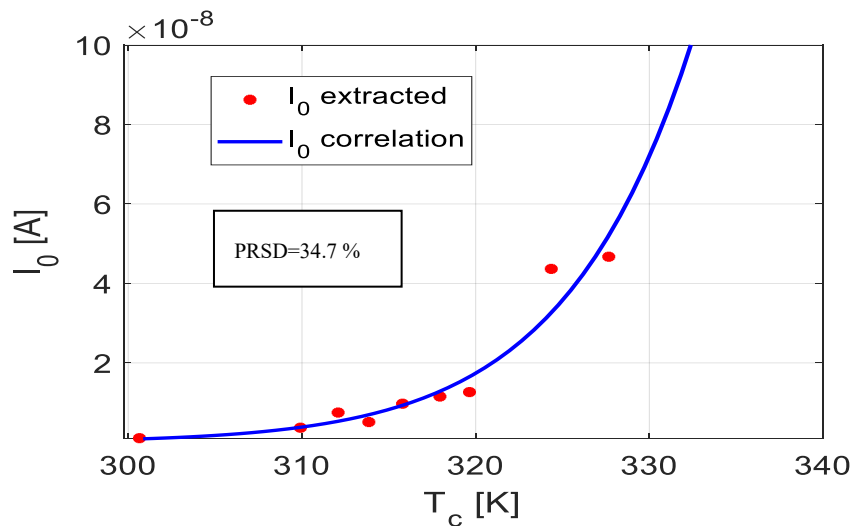


Figure 5-16: nonlinear regression results for I_0 for polycrystalline by Luxor. Blue line is the correlation function for I_0 . The red dots are the I_0 . extracted using Politecnico di Torino procedure (LM).

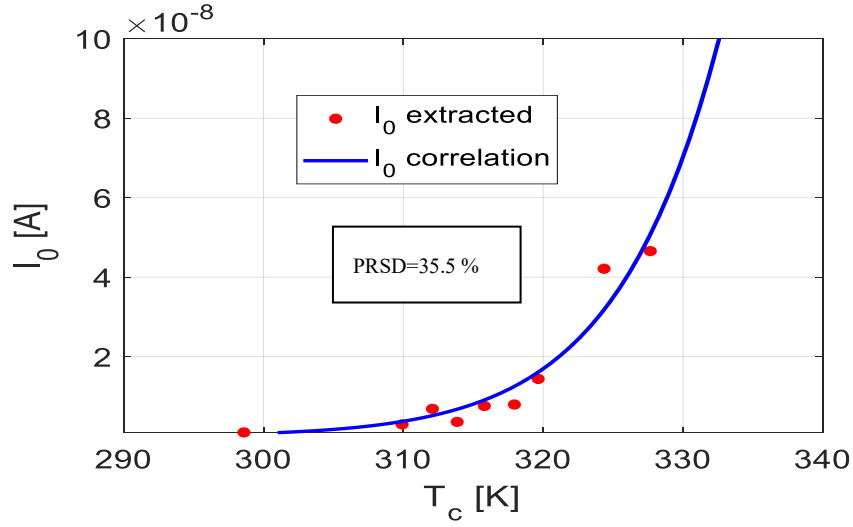


Figure 5-17: nonlinear regression results for I_0 for polycrystalline by Luxor. Blue line is the correlation function for I_0 . The red dots are the I_0 . extracted using University of Jaen procedure (SA-NM).

$$I_0 = I_{0_{STC}} * \left(\frac{T_c}{T_{STC}}\right)^3 * \exp\left(\left(\frac{E_{g_{STC}}}{T_{STC}} - \frac{E_g(T_c)}{T_c}\right) * \frac{1}{k}\right) \quad \text{Eq.(5-24)}$$

$$E_{g_{STC}} = 1.121 * q \quad \text{Eq.(5-25)}$$

$$E_g(T) = E_{g_{STC}} * (1 - 0.0002677 * (T_c - T_{STC})) \quad \text{Eq.(5-26)}$$

The best value of $I_{0_{STC}}$ in order to optimize the fitting and the percentage relative standard deviations assume approximatively the same values when the points are extracted by both methods:

- $I_{0_{STC}}=5.65\text{e-}10$ A and PRSD=34.7% for the parameters extracted by Politecnico di Torino method.
- $I_{0_{STC}}=5.51\text{e-}10$ A and PRSD=35.5 % for the parameters extracted by the University of Jaen method.

Diode's ideality factor:

The graphs, which show the dependence of the correlation and the extracted points of the diode ideality factor with respect the irradiance for the parameters extracted with the two methods Politecnico di Torino (LM) and University of Jaen (SA-NM) are respectively shown in Figure 5-18 and in Figure 5-19.

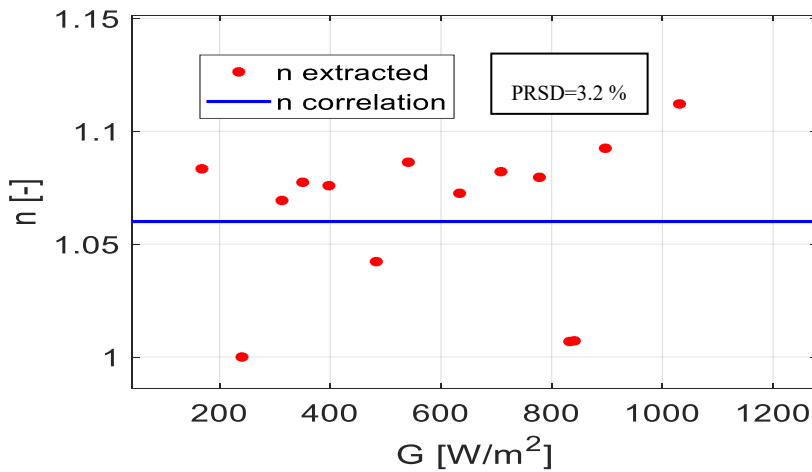


Figure 5-18: nonlinear regression results for n for polycrystalline by Luxor. Blue line is the correlation function for n . The red dots are the n extracted using Politecnico di Torino procedure (LM)

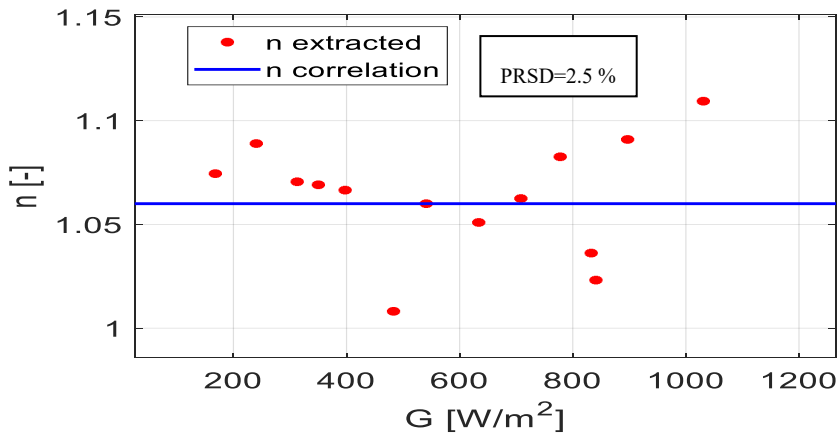


Figure 5-19: nonlinear regression results for n for polycrystalline by Luxor. Blue line is the correlation function for n . The red dots are the n extracted using University of Jaen procedure (SA-NM).

Differently from the previous correlations, the n extracted values are dispersed in a range of values close to one. However, in this case the points are larger scattered than the previous studies. For that reason, an optimization process is applied in order to calculate the constant value assigned to n . A constant correlation fixed to a constant value equal to 1,06 is applied for both methods. The errors with respect the correlation and the extracted points are respectively:

- PRSD= 3.2 % for the parameters extracted by Politecnico di Torino method.
- PRSD=2.5 % for the parameters extracted for by University of Jaen method.

Series resistance:

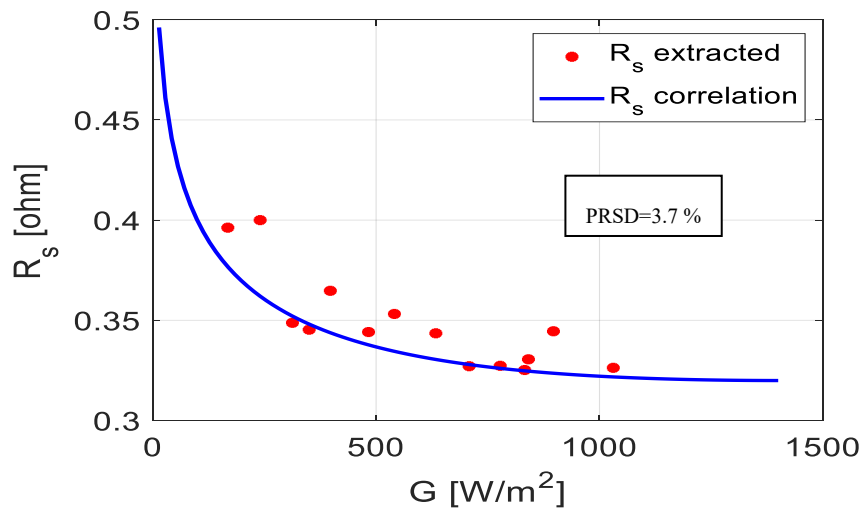


Figure 5-20: nonlinear regression results for R_s for polycrystalline by Luxor. Blue line is the correlation function for R_s . The red dots are the R_s extracted using Politecnico di Torino procedure (LM)

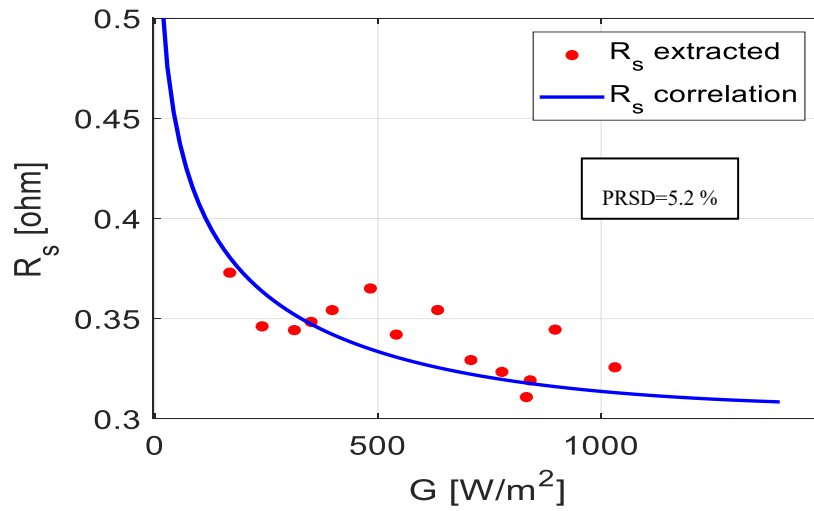


Figure 5-21: nonlinear regression results for R_s for polycrystalline by Luxor. Blue line is the correlation function for R_s . The red dots are the R_s extracted using University of Jaen procedure (SA-NM).

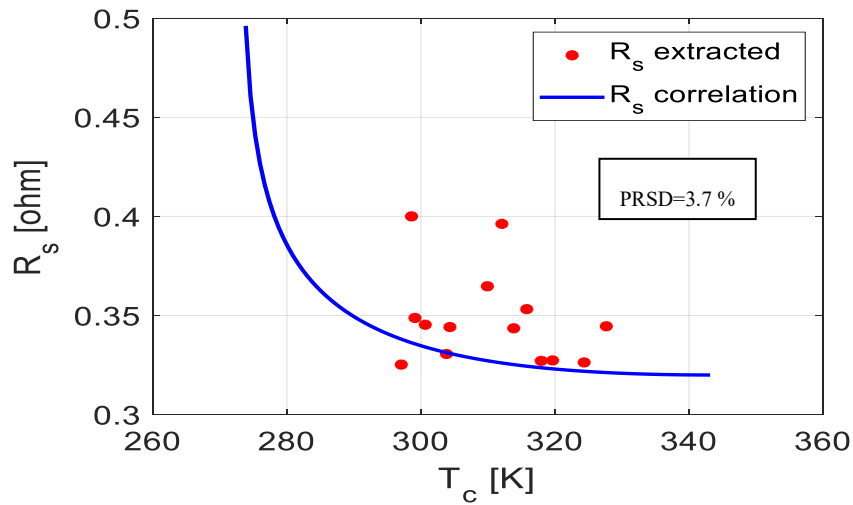


Figure 5-22: nonlinear regression results for R_s for polycrystalline by Luxor. Blue line is the correlation function for R_s . The red dots are the R_s extracted using Politecnico di Torino procedure (LM)

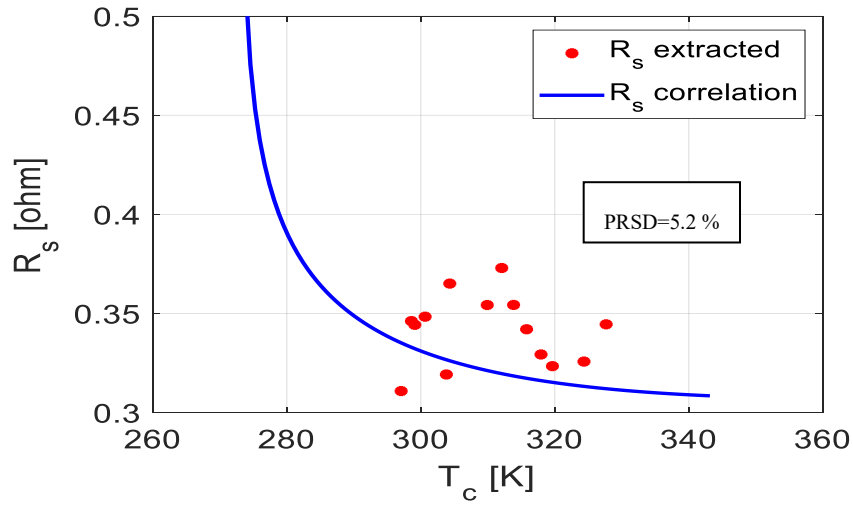


Figure 5-23: nonlinear regression results for R_s for polycrystalline by Luxor. Blue line is the correlation function for R_s . The red dots are the R_s extracted using University of Jaen procedure (SA-NM).

$$R_s = R_{s_{STC}} * \frac{T_c}{T_{STC}} * \left(1 - 0.244 * \log \left(\frac{G}{G_{STC}} \right) \right) \quad \text{Eq.(5-23)}$$

The best value of $R_{s_{STC}}$ in order to optimize the fitting and the percentage relative standard deviations assume approximately the same values when the points are extracted by both methods:

- $R_{s_{STC}}=0.297$ A and PRSD=3.7% for the parameters extracted with Politecnico di Torino method.
- $R_{s_{STC}}=0.293$ A and PRSD=5.2 % for the parameters extracted for the University of Jaen method.

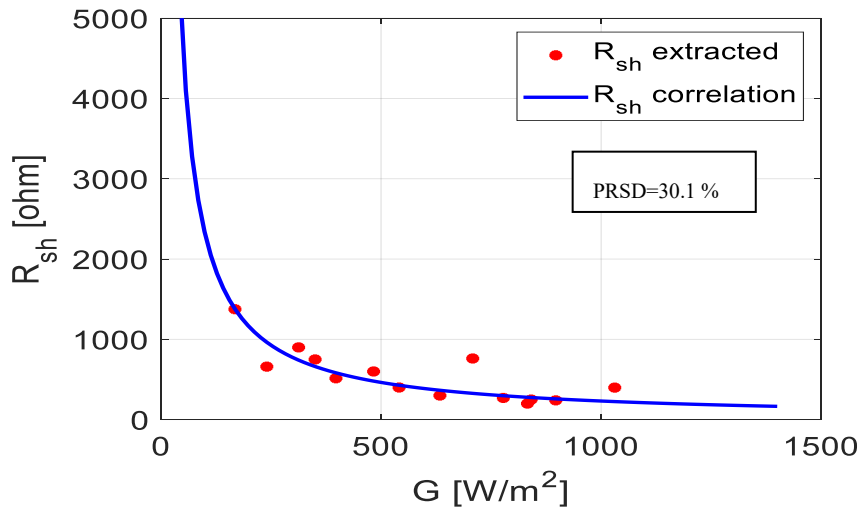


Figure 5-24: nonlinear regression results for R_{sh} for polycrystalline by Luxor. Blue line is the correlation function for R_{sh} . The red dots are the R_{sh} extracted using Politecnico di Torino procedure (LM).

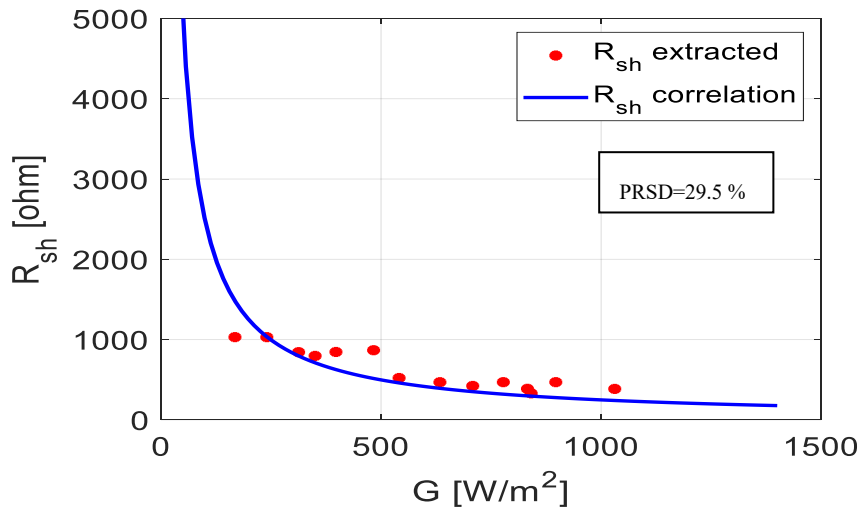


Figure 5-25: nonlinear regression results for R_{sh} for polycrystalline by Luxor. Blue line is the correlation function for R_{sh} . The red dots are the R_{sh} extracted using University of Jaen procedure (SA-NM).

The best value of $R_{sh_{STC}}$ in order to optimize the fitting and the percentage relative standard deviations assume approximatively the same values when the points are extracted by both methods:

- $R_{sh_{STC}}=232$ A and PRSD=30.1% for the parameters extracted with Politecnico di Torino method.
- $R_{sh_{STC}}=249$ A and PRSD=29.5% for the parameters extracted for the University of Jaen method.

The table 5-12 summarises the results regarding correlation coefficients obtained applying the nonlinear regression from parameter extracted by the two methods , Politecnico di Torino method and University of Jaen methods.

Table 5-12: Coefficients of monocrystalline by Luxor (100W), evaluated from the nonlinear regression for the Politecnico di Torino and University of Jaen extracted parameters.

NONLINEAR REGRESSION COEFFICIENTS						
OPTIMIZATION ALGORITHM	I_{ph_STC} [A]	I_{0_STC} [A]	R_{s_STC} [Ω]	λ [-]	R_{sh_STC} [Ω]	R_{sh_STC} [Ω]
POLITECNICO	5,75	5,65E-10	1,06	0,297	0,192	232
UJA	5,75	5,51E-10	1,06	0,293	0,197	249

On the other hands in table 5-13 is shown the values for PRSD obtained considering both extraction methods.

Table 5-13: PRSD for the nonlinear regression for the two methods for monocrystalline by Luxor (100W)

CORRELATION PRSD [%]					
OPTIMIZATION ALGORITHM	I_{ph} [A]	I_0 [A]	n [-]	R_s [Ω]	R_{sh} [Ω]
POLITECNICO	0,28%	34,7%	3,2%	3,7%	30,1%
UJA	0,12%	35,5%	2,5%	5,2%	29,5%

A comparison between the two methods is done taking into consideration several factors: the mean value of the resnorm, the mean value of the percentage error on the maximum power at different irradiance ranges (irradiance > 500 W/m² and irradiance < 500 W/m²) and the mean value of the time needed to compute the algorithm. The results are presented in Table 5-14

Table 5-14: Comparison of the mean values of the convergence time, of the error on the maximum power at different irradiance ranges, and of the of the resnorm resulted from the application of the two algorithms.

Algorithm	mean Empp (G<600 W/m ²) [%]	mean Empp (G>600 W/m ²) [%]	resnorm [-]	time convergence [s]
POLITECNICO	0,37%	0,38%	0,014	70
UJA	0,24%	0,19%	0,006	363

The fitting algorithm implemented by the University of Jaen algorithm provides lower values of resnorm and of maximum power error for each fitting than the algorithm of the University of Jaen. This means that the quality of the fitting provided by University of Jaen procedure is a little bit better than the fitting provided by the Politecnico di Torino. However, the values of the mean maximum power error and of the mean value the resnorm show that errors are of the same order. Moreover, as far as accuracy and scope of this master thesis is concerned, with respect to the purposes of this study, the results provided by both fitting algorithms exhibit a high level of accuracy. If both algorithms are compared, it must be said that the one from University of Jaen is more accurate than the one implemented by Politecnico di Torino. Nevertheless, there is a key point related to the time required for the convergence of the algorithm. The results of the mean time value Table.5-14 shows that the procedure implemented by the Politecnico di Torino is faster than the procedure implemented by University of Jaen. This is extremely relevant for an eventually application of the model in a real time system, in order to carry out an analysis of the performance of the PV module.

5.3 Estimation of the maximum power at different cell temperatures and irradiances

A PV device equipped with a maximum power point tracker is always able to work at maximum power point in different irradiance and cell temperature. The correlations estimated in section 5-2 can be used in order to estimate the power produced at maximum power point for different values of irradiance and cell temperature. So, this model allows the performance of a real PV module, equipped with maximum power point tracker, in completely irradiated cells conditions, to be predicted. For a given values of G and T_c , the parameters can be estimated by the correlations functions. Using the values of the estimated parameters of SDM into the transcendental equation Eq.(2-16), it is possible to trace the I - V curve with a good accuracy, especially with respect to the maximum power point. Once the I - V curves have been obtained, it is easy to find the position of the maximum power point and to evaluate the maximum power. In this section a comparison among the proposed model, the Osterwald Model (OM) commonly used and the experimental measurements is performed. The goal is to evaluate the closeness of agreement between the aforementioned models and the experimental results with respect to the evaluation of the maximum power. verify how much accurate are that models in the prediction of the maximum power. An agreement between the experimental results and our model also could validate; the values of the single diode module parameters extracted by the applied extraction procedures, and the tendency with G and T_c proposed by the correlations. Thus, the procedure based on the computing the I - V curve according to the values of I_{ph} , I_0 , n , R_s and R_{sh} obtained from the correlations previously computed and then, the comparison of the maximum power for that estimated curve with the measured one is carried out at University of Jaen and Politecnico di Torino. A first check of the estimation of the maximum power, using the method described before, is performed at Politecnico di Torino for JA-Solar Polycrystalline JAP60S01 and Trina Solar Monocrystalline TSM-DD05A.08. However, thanks to the automatic measurements system available at University of Jaen, described in section 3-1 a large number of curves were collected. The large amount of measured data allows the experimental validation of the present model to be achieved. So, the correlations estimated by the two extraction procedures (LM and SA-NM) described in section 4-1-2 and 4-1-3 will be compared between them and also with the OM. The experimental data for the maximum power will be compared with the maximum power estimated by the aforementioned methods to know what method is the most accurate on the prediction of the maximum power.

5.3.1 Politecnico di Torino estimation of maximum power results

5.3.1.1 Monocrystalline PV module TSM-DD05A.08 by Trina Solar (300W)

The correlations estimated in section 5-2-1-1, are used to evaluate the parameters, for the values of irradiance and cell temperature measured at Politecnico di Torino reported in Table 5-4 for monocrystalline by Trina Solar (300 W). The analysed $I-V$ curves are the same as those ones used to make the extraction using the curve fitting procedure based on LM proposed by Politecnico di Torino. Then, the calculated parameters are used in Eq.2-16 to trace the $I-V$ curves for the aforementioned operating conditions. The $I-V$ curves obtained with this method are graphically compared with the measured ones in order to establish the quality of the approximation. For the purpose of this work, the most important point to be exactly estimated is the maximum power point, for that reason, this point will be highlighted in the following graph Figure 5-26. For a graphical reason in Figure 5-26 only 6 curves over 8 are reported in order to avoid to overlap the results.

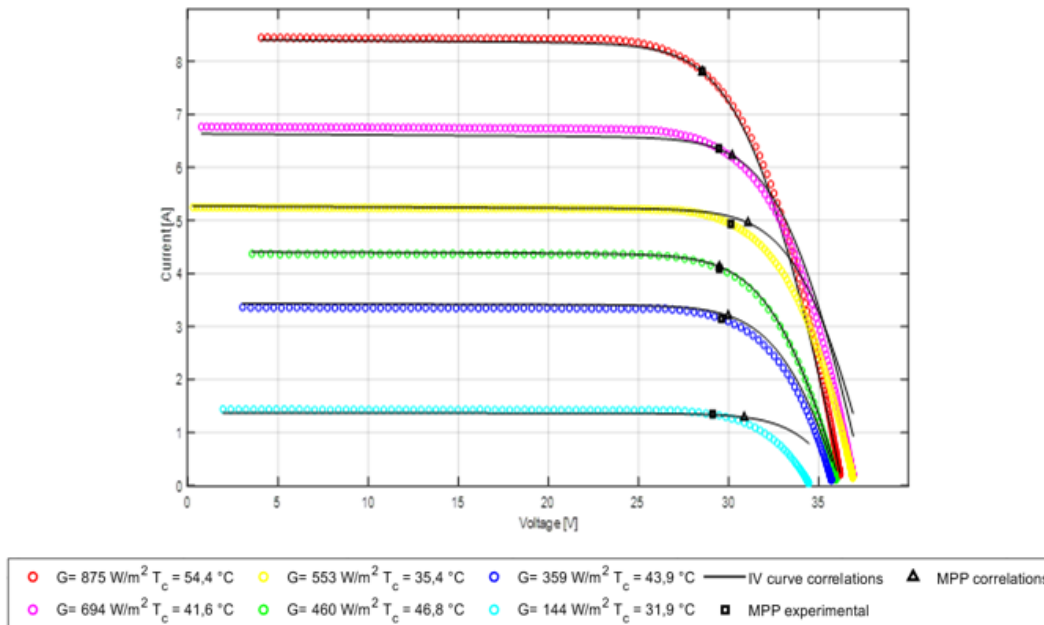


Figure 5-26: $I-V$ curves experimentally measured and $I-V$ curves estimated with the correlations for Trina Solar Monocrystalline TSM-DD05A.08 (300W).

In order to understand which method better estimates the PV module under study performance, a comparison among the maximum power evaluated by the correlation, evaluated by the OM and the experimental one shown in Table 5-15. Moreover the relative percentage errors and absolute errors on the maximum power,

with respect the experimental data are reported in Table 5-15. The I-V curves analysed are the same mentioned before for the tracing of the I-V curves.

Table 5-15: Comparison between Maximum power and errors (absolute and %) on maximum power with respect the experimental data. Respectively estimated using correlations and OM for monocrystalline by Trina Solar (300 W), reported together with G, T_c and experimental maximum power values.

G [W/m ²]	T _c [K]	P _{EXP.} [W]	P _{corr.} [W]	P _{OM} [W]	ΔP _{corr} [W]	ΔP _{OM} [W]	%ΔP _{corr} [%]	%ΔP _{OM} [%]
876	43,20	232	235	244	2,74	12,16	1,18	5,24
875	54,40	223	223	232	-0,26	9,48	-0,11	4,25
694	41,60	187	188	195	0,66	7,47	0,35	3,99
553	35,40	149	154	159	5,36	10,55	3,61	7,10
460	46,80	121	122	126	1,10	5,60	0,91	4,64
394	30,40	104	112	116	7,85	11,70	7,55	11,24
359	43,90	93	96	100	2,89	6,62	3,11	7,11
144	31,90	39	40	42	0,59	2,87	1,50	7,34

The results presented in table 5-15 show that the method based on correlation functions proposed by Politecnico di Torino is more accurate than the OM. The PRSD is calculated with respect the experimental maximum power for both methods using Eq.5.8: PRSD for OM is 6.16 % and PRSD for correlations model is 2.56 %. It is possible to observe that, lower is the irradiance higher is the percentage error on the estimation of maximum power. In other words, both models estimate more accurate the power at high irradiance than at low irradiance. Nevertheless, although the errors are higher in terms of percentage, at low irradiance the power produced is very low, so, the absolute errors in terms of watts is also low. Especially for an estimation of the productivity over a long time period, these errors at low irradiance are negligible.

Although the peak of power is more accurately estimated by the correlations model, the approximation done by the OM is good. The reliability of the OM to estimate the maximum power is largely verified in literature [14, 15]. So, a first check of the accuracy of the proposed model is carried out comparing the average hourly maximum power calculated, with the one estimated by OM over a period of one year. A set of average hourly irradiances and cell temperatures data previously measured over a one year in Turin is used to perform the comparison. In Figure 5-27 is shown the evaluation of the average hourly maximum power with respect the irradiance computed by the two methods before commented over the measurements performed during one year.

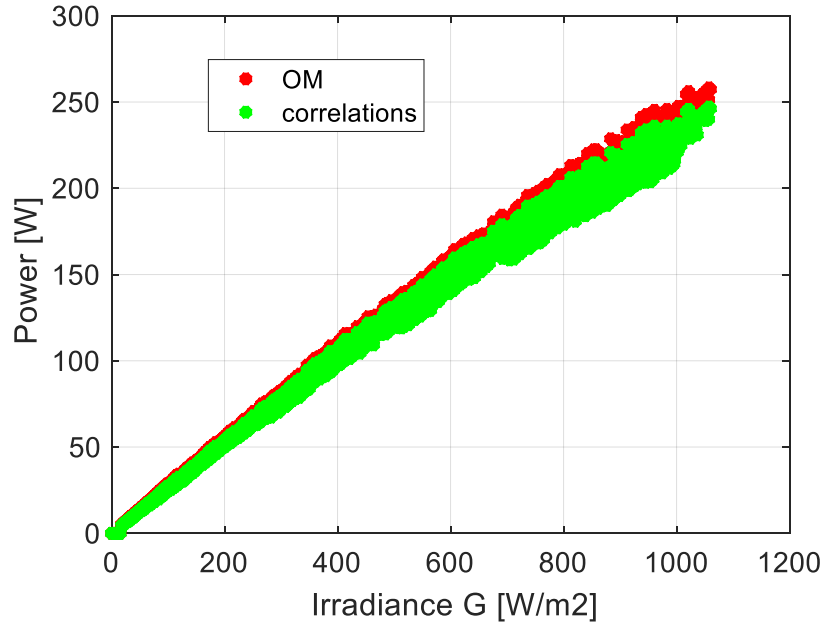


Figure 5-27: comparison of maximum power estimated by correlations and by OM for a wide range of irradiances (0 1200 W), for the monocrystalline by Trina Solar (300 W).

The Figure 5-27 shows that the model proposed by Politecnico di Torino based on correlations functions underestimates the maximum power for the whole range of irradiance when is compared with OM. It is relevant to say that, the maximum power values estimated with the two models are almost overlapped at low irradiances values. When the irradiance increases, the estimated maximum power starts to diverge and the correlations model starts to heavily underestimate the power. The obtained results in Table 5-15 for the short amount of available data show that, OM always overestimates the power with respect to the experimental data. This means that, it is likely that the underestimation of power performed by the proposed model with respect to OM, leads to a close estimation with respect to experimental data. However, there are not enough available data regarding this PV module, in order to support the conclusion before commented. To thoughtfully confirm these preliminary conclusions a larger amount of experimental data it is necessary.

5.3.1.2 Polycrystalline PV module by JA-Solar Polycrystalline JAP60S01 (280W)

The correlations estimated in section 5-2-1-2, are used to evaluate the parameters for the values of irradiance and cell temperature measured at Politecnico

di Torino reported in Table 5-4 for polycrystalline by JA-Solar (280 W). The analysed $I-V$ curves are the same as those ones used to make the extraction using the curve fitting procedure based on LM proposed by Politecnico di Torino. Then, the calculated parameters are used in Eq.2-16 to trace the $I-V$ curves for the aforementioned operating conditions. The $I-V$ curves obtained with this method are graphically compared with the measured ones in order to establish the quality of the approximation. For the purpose of this work, the most important point to be exactly estimated is the maximum power point, for that reason, this point will be highlighted in the following graph in Figure 5-28. For a graphical reason only 6 curves over 7 are reported in order to avoid to overlap the results in Figure 5-28.

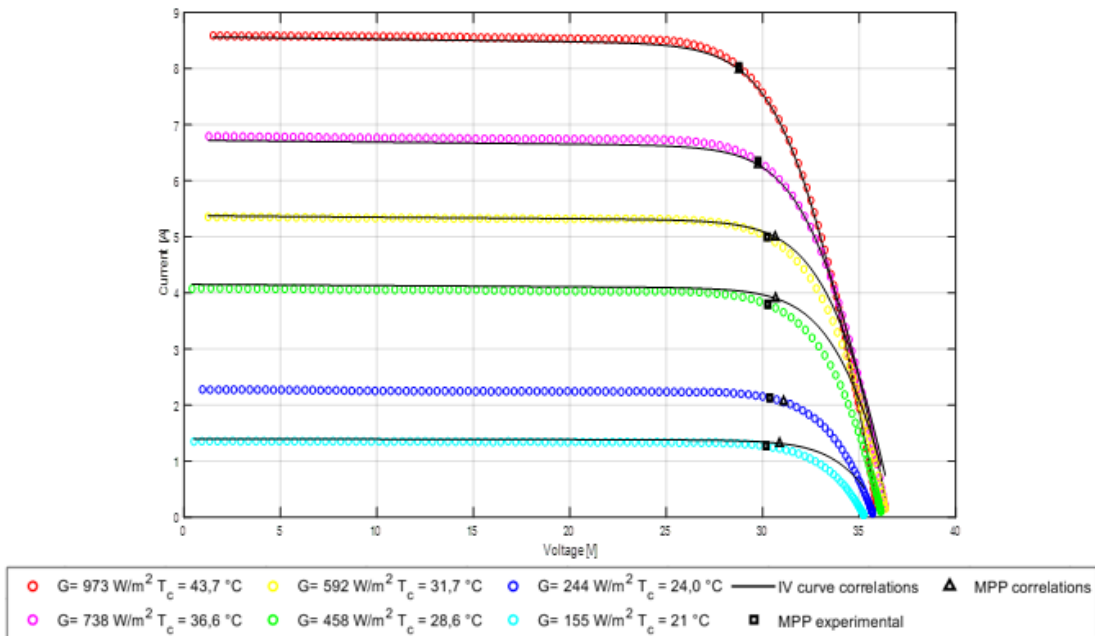


Figure 5-28: $I-V$ curves experimentally measured and $I-V$ curves estimated with the correlations for JA-Solar Polycrystalline JAP60S01 (280W).

In Table 5-16 are shown the results regarding the maximum power for the module under test. The values of maximum power calculated by Politecnico di Torino proposed correlations is shown together with the experimental ones and the ones calculated with OM.

Moreover, the relative percentage errors and the absolute errors on the maximum power with respect the experimental data are shown in Table 5-16. The $I-V$ curves analysed are the same mentioned before for the tracing of the $I-V$ curves.

Table 5-16: Maximum power and errors (absolute and %) on maximum power with respect the experimental data estimated using correlations and OM for polycrystalline by JA Solar (280 W), reported together with G, T_c and experimental maximum power values.

G [W/m ²]	T _c [K]	P _{EXP.} [W]	P _{corr.} [W]	P _{OM} [W]	ΔP _{corr} [W]	ΔP _{OM} [W]	%ΔP _{corr} [%]	%ΔP _{OM} [%]
937	317	231	230	243	-1,47	11,50	-0,64	4,97
738	310	189	187	197	-1,88	8,05	-0,99	4,26
592	305	151	153	161	2,09	10,19	1,38	6,74
458	302	115	120	126	4,84	11,45	4,21	9,96
433	301	108	114	120	5,95	12,27	5,52	11,39
244	297	65	64	69	-0,47	3,91	-0,73	6,04
155	294	39	41	44	2,24	5,59	5,81	14,51

Even for the polycrystalline technology Table 5-16 shows that the method based on correlation functions proposed by Politecnico di Torino is more accurate than the OM. The PRSD is calculated with respect the experimental maximum power for both methods using Eq.5.8: PRSD for OM is 7.40 % and PRSD for correlations model is 2.54 %. The errors are of the same order of the errors calculated for monocrystalline technology described in the previous section 5-3-1-1.

Although the peak of power is more accurately estimated by the correlations model, the approximation done by the OM is good. The reliability of the OM to estimate the maximum power is largely verified in literature [14, 15]. So, even in this case, a first check of the accuracy of the proposed model is carried out comparing the average hourly maximum power calculated, with the one estimated by OM over a period of one year. The same set, of average hourly irradiances and cell temperatures data before commented, is used to perform the comparison. In Figure 5-29 is shown the evaluation of the average hourly maximum power with respect the irradiance computed by the two methods before commented over the measurements performed during one year.

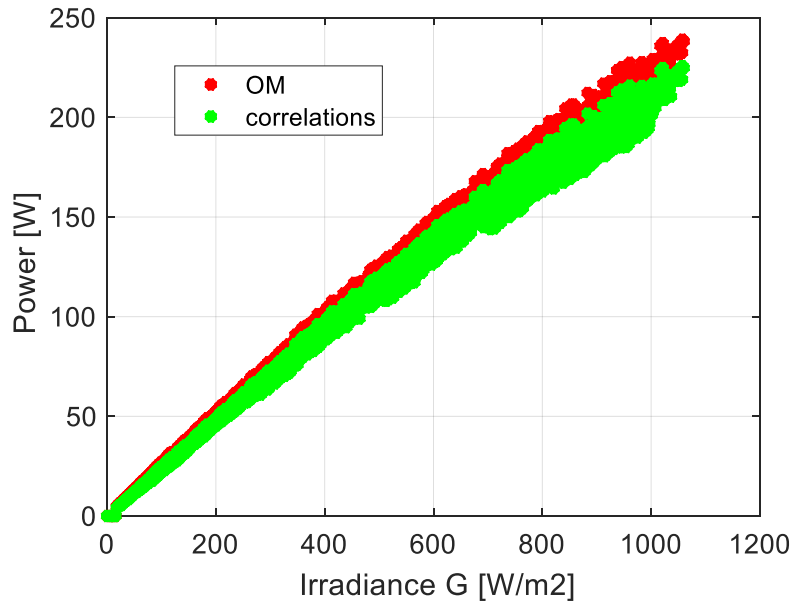


Figure 5-29: comparison of maximum power estimated by correlations and by OM for a wide range of irradiances (0 1200 W), for polycrystalline by JA Solar (280 W).

Even for polycrystalline technology, Figure 5-29 shows that the model proposed based on correlations underestimates the maximum power for the whole range of irradiance when is compared with OM. The obtained results in Table 5-16 for the short amount of available data show that, OM always overestimates the power with respect to the experimental data. This means that, it is likely that the underestimation of power performed by the proposed model with respect to OM, leads to a close estimation with respect to experimental data. However, there are not enough available data regarding this PV module, in order to support the conclusion before commented. To thoughtfully confirm these preliminary conclusions a larger amount of experimental data it is necessary.

5.3.2 University of Jaen estimation of power peak results

At University of Jaen a huge amount of $I-V$ curves were experimentally measured under a wide range of irradiances and cell temperatures. In this research the PV module under test is monocrystalline PV panel LX-100M by Luxor with a nominal power of 100 W. The measurements of these amount of data were possible thanks the automatic measurement systems designed by IDEA Solar Energy Research Group described in section 3-1. This large Volume of data allows the accuracy of the two theoretical models under tests regarding the estimation of the maximum power (model based on correlation Politecnico di Torino and OM) to be estimated.

The two set of correlations estimated in section 5-2-2 by the two methods, LM implemented by Politecnico di Torino and SA-NM implemented by University of Jaen, are used to calculate the SDM parameters for several cell temperature and irradiance conditions. The analysed $I-V$ curves are the same as those ones used to make the two extraction fitting procedures (LM and SA-NM) for monocrystalline PV panel LX-100M by Luxor presented in Table 5-10 and Table 5-11. Then, the calculated parameters are used in Eq.2-16 to trace the $I-V$ curves. The $I-V$ curves obtained with both these methods are graphically compared with the measured ones in order to establish the quality of these models approximations. For the purpose of this work, the most important point to be exactly estimated is the maximum power point, for that reason, this point will be highlighted in the following graph in Figure 5-30. For a graphical reason only 3 curves over 14 are reported in order to avoid to overlap the results in Figure 5-30.

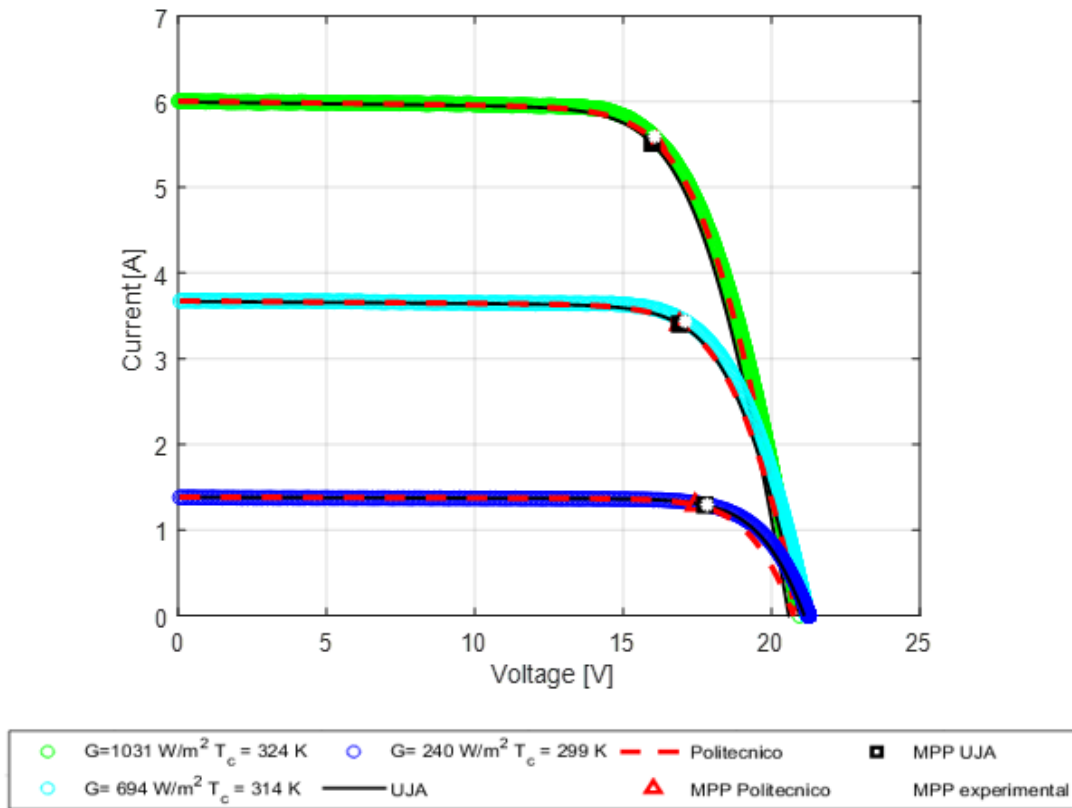


Figure 5-30: I - V curves experimentally measured, estimated with the Politecnico di Torino model and with the University of Jaen model for Luxor monocrystalline (280W).

In order to understand which is the more accurate method between the one proposed by Politecnico di Torino and the one proposed by University of Jaen, a comparison is performed. The maximum power together with the percentage error and the absolute error with respect the maximum power are evaluated with the two before commented methods (Politecnico di Torino and University of Jaen). The results are shown in the Table 5-17. In this table are omitted the values of the maximum power, the absolute and percentage error, on the maximum power calculated by OM. These results are not presented because is more interesting to emphasize the comparison between the two proposed methods than with respect OM. The I - V curves with respect this comparison is performed analysed are the same mentioned before regarding the tracing of the I - V curves.

Table 5-17: Comparison between Maximum power and errors (absolute and %) on maximum power with respect the experimental data, respectively estimated using Politecnico di Torino model and University of Jaen model for monocrystalline by Luxor (100 W), reported together with G, T_c and experimental maximum power values.

G [W/m ²]	T _c [°C]	P _{EXP} [W]	P _{polit. (LM)} [W]	P _{UJA (SA-NM)} [W]	ΔP _{polit. (LM)} [W]	ΔP _{UJA (SA-NM)} [W]	%ΔP _{polit. (LM)} [W]	%ΔP _{UJA (SA-NM)} [W]
834	296	83	79	77	-4,10	-6,0	-4,92%	-7,22%
843	300	82	79	78	-2,73	-4,22	-3,33%	-5,16%
170	291	15	16	16	1,58	1,15	10,63%	7,72%
1036	314	90	92	92	1,96	1,8	2,19%	2,01%
782	309	70	72	71	1,56	1,04	2,22%	1,48%
712	307	65	66	65	1,39	0,8	2,15%	1,20%
902	315	77	80	80	3,31	3,3	4,30%	4,27%
485	295	47	47	46	0,10	-0,95	0,22%	-2,04%
637	304	59	60	59	1,11	0,32	1,89%	0,54%
545	303	49	51	51	1,91	1,2	3,86%	2,51%
400	297	37	39	38	1,47	0,70	3,96%	1,88%
315	288	30	31	30	0,75	-0,2	2,46%	-0,64%
351	290	34	34	34	0,58	-0,4	1,70%	-1,16%
242	286	23	24	23	0,88	0,09	3,81%	0,38%

The results obtained are graphically presented in two charts for a better understanding. In this sense, in Figure 5-31 is shown the comparison between the values of the maximum power calculated by: the method proposed by Politecnico di Torino, the OM and the experimental one. In the other hand, in Figure 5-32 is shown the comparison between the values of the maximum power calculated by: the method proposed by Politecnico di Torino, the one proposed by University of Jaen, and the experimental one. Moreover, the value of the RMSE calculated with respect the experimental data is also reported in the charts. result is also reported in the graph. So, Politecnico di Torino and University of Jaen models can be compared and their goodness regarding the evaluation of the maximum power of the PV module under test can be estimated.

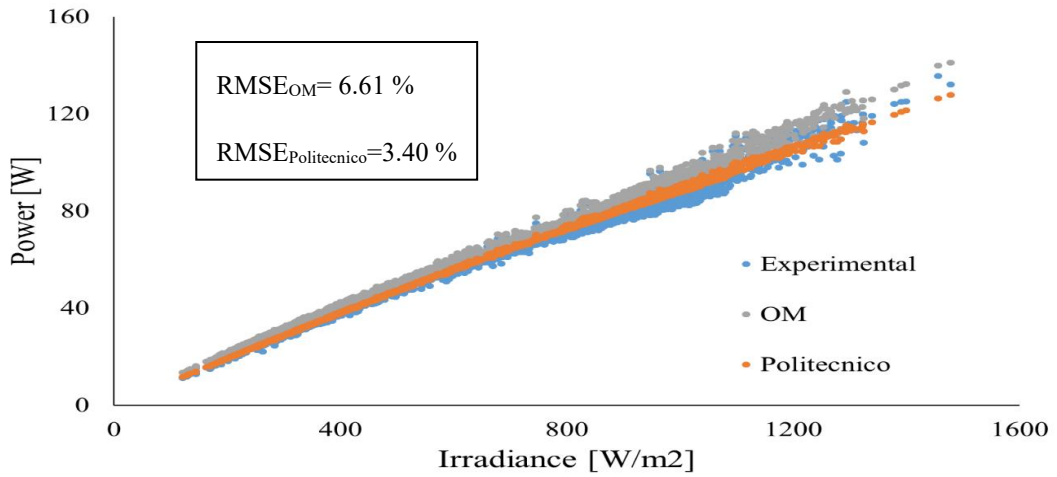


Figure 5-31: comparison among the maximum power estimated: by Politecnico di Torino model, by OM and experimental one for monocrystalline by Luxor (100 W).

The Figure 5-31 clearly shows that the maximum power estimated by the Politecnico di Torino model approximate with higher accuracy than the OM the experimental results. Indeed, value of the RMSE for the Politecnico di Torino model are lower than the value of RMSE for OM.

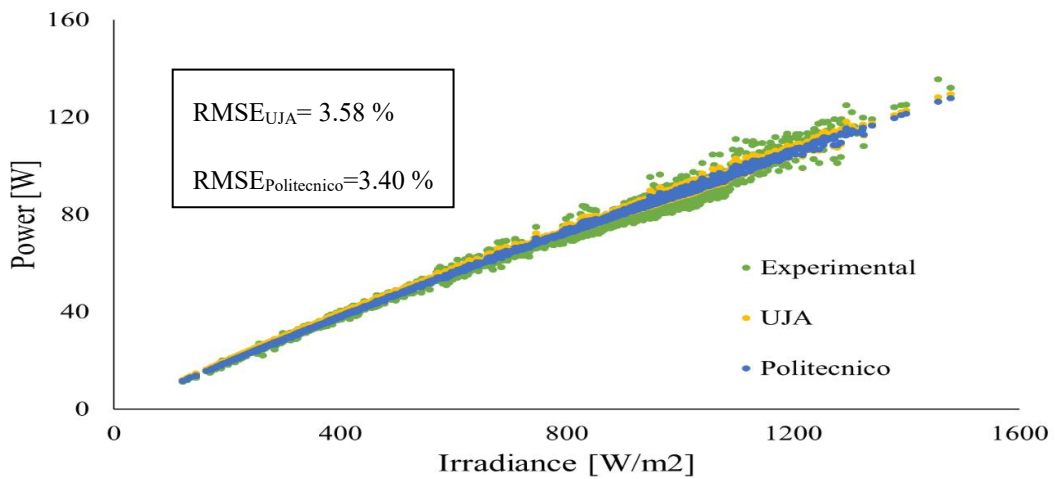


Figure 5-32: comparison among the maximum power estimated: by Politecnico di Torino model, by University of Jaen model and experimental one for monocrystalline Luxor (100W).

The comparison between the maximum power calculated by the two extraction methods and the experimental data is reported in Fig.5-32. The chart shows that the two models estimate with similar accuracy the experimental data, the curves are overlapped for a wide range of irradiance. This can be observed also from the values of the RMSE that only present a 0.2 % of variation between the two methods. It is possible to realise that the University of Jaen model slightly overestimate the power with respect to the Politecnico model. However, the values of the RMSE reported in Fig. 5-31 and Fig.5-32 show that also the method proposed by University of Jaen is largely more accurate than the OM in the estimation of the maximum power.

5.3.3 University of Jaen estimation of energy results

As it is mentioned before the experimental campaign performed at the University of Jaen allowed a large number of I - V curves to be collected. In order to evaluate the amount of energy produced during the 20 days of measurements by the monocrystalline PV module by Luxor (100 W), a numerical integration of the maximum power is done. To perform this integration some assumptions are necessary. Thus, the experimental campaign is performed recording the I - V curves every 5 minutes (300s). Assuming constant the cell temperature and the irradiance during this period, it is possible to consider constant the instantaneous power produced during this period. Moreover, assuming that the PV module is equipped with a Maximum power point tracker, it is also possible to consider that the system always works at maximum power point condition. Making this assumption is possible to estimate the energy with the subsequent formula:

$$E_{tot} = \int_0^{t_2} P(t)dt = \Delta t * \sum_{i=1}^{N_{tot}} P_{MPP_i} \quad \text{Eq.(5-27)}$$

Where:

- P_{MPP_i} → Power at maximum power point during the i^{th} measurement interval. [W]
- Δt → time between two measurements, equal to 300 s (5 min.).
- N_{tot} → total number of collected measurements in the period between 10 April and 20 of April.
- t_2 → period of time (expressed in seconds) during which the I - V curves were continuously recorded every 5 minutes.

The Table 5-18 shows the results regarding the energy produced by the PV module under test. The experimental result is compared with three theoretical estimations. In Table 5-18 the results on the energy estimation are represented together with the percentage and the absolute errors with respect the experimental energy. These values are calculated using the integration method respectively for the LM correlations, SA-NM correlations and the OM. In somehow the method to compute the energy produced by the PV module try to reproduce the response of the device under test in case it was connected to an inverter which will fix the maximum power point at every moment. So for each recorded I - V curve the maximum power is computed and considered constant for 5 minutes between measurements.

Table 5-18: Energy produced during the experimental campaign of 20 days: estimated by Politecnico di Torino correlations, estimated by University of Jaen correlations, estimated by OM and experimentally measured.

Model	Energy [KWh]	ΔE [KWh]	$\Delta E_{\%}$ [%]
Experimental	16,4	[-]	[-]
Politecnico	16,6	0,25	1,55%
UJA	16,7	0,37	2,23%
OM	17,4	1,08	6,61%

The error is evaluated comparing the energy estimated by each method and the experimental energy. The estimation of the energy during the 20 days of measurements, performed from 10 of April to 20 of April, shows that the procedure implemented by Politecnico di Torino is the most accurate. As we expected from the results on the maximum power analysis, where the UJA model overestimate the power in a wide range of irradiance, the energy estimated by UJA is 0.68 % larger than the energy estimated by Politecnico model. However, the estimation of the energy performed by both the correlations models is more accurate than the estimation by the OM.

6 Conclusion

A PV generator in normal operation works in a wide range of irradiance and cell temperature values and its electrical performance can be different with respect to nominal data. Nevertheless, in the datasheet provided by the manufacturer only the electrical data at Standard Test Conditions (STC) are defined, with coefficients taking into account the effects of cell temperature on PV performance. Several models are present in literature to estimate the electrical response of a PV generator without shadings. Actually, the Osterwald Model (OM) is commonly used for the evaluation of the maximum power in several irradiance and cell temperature conditions. However, more accurate models permit to evaluate the electrical performance of a PV generator with an electrical equivalent circuit. In this work, the Single Diode Model (SDM) is adopted and it consists of five parameters: the photovoltaic current I_{ph} , the saturation current I_0 , the non ideality factor n , the series resistance R_s , and the shunt resistance R_{sh} .

This thesis aims to propose an innovative technique to extract the parameters of the SDM from experimental I-V curves. Moreover, correlations are defined to estimate the electrical response in terms of maximum power and productivity of a PV generator in real operation by describing the dependence of the SDM parameters with respect to irradiance and cell temperature.

The first part of this study is carried out at Politecnico di Torino and it consists of the definition of an innovative technique to extract the parameters of the SDM for two PV modules. In particular, the modules under tests are a monocrystalline by Trina Solar (300 W) and a polycrystalline by JA-Solar (280W). First, a procedure for the extraction of the SDM parameters from the experimental I-V curves is implemented on Matlab code. It is based on the application of a combined analytical-numerical method, based on the Levenberg Marquardt (LM) algorithm. The SDM parameters resulting from the extraction are used in a nonlinear regression to identify the semi-empirical coefficients of equations describing the dependence of SDM parameters with respect to environmental conditions. Then, the correlations are used in order to estimate the maximum power of the two PV modules in the measurement conditions. These results are compared with the results obtained with OM and the experimental data in order to check the accuracy of the

correlations. For monocrystalline PV module by Trina Solar, the Percentage Root Mean Square Error (PRMSE) with respect the experimental data is 2.56 % and 6.16 %, respectively, using the innovative technique and the OM. For polycrystalline PV module by JA-Solar, the PRMSE calculated using the proposed technique is 2.54 %, while the error using the OM increases up to 7.40 %.

The second part of this work is performed at University of Jaen, where the above described technique is applied on a monocrystalline PV module by Luxor (100 W). Moreover, a comparison between the extraction procedure developed at Politecnico di Torino and another extraction procedure performed at the University of Jaen is carried out. In particular, the latter is based on two Heuristics algorithms: the Simulated Annealing the and Nelder Med (SA-NM) algorithms. Regarding the mean computational time of the algorithms, the LM procedure is faster than SA-NM. In particular, it is equal to 70 s and 363 s, respectively, for LM and SA-NM. This could be extremely relevant for a possible application of the model in a real time monitoring system, in order to check the performance of a large-scale PV system, up to several hundreds of kW installed. Finally, the two models (LM and SA-NM) and OM are used to calculate the maximum power and the energy produced during the 20 days of experimental campaign. By comparing these results with the experimental measurements, both the analysed models (LM and SA-NM) estimate the maximum power and the generated energy with higher accuracy with respect to OM. In the first case, the root mean square error is equal to 3.40 %, 3.58 %, and 6.14 %, respectively for, LM, SA-NM e OM. Regarding the energy, the obtained errors are equal to 1.55 %, 2.23 %, and 6.61 % for, respectively, LM, SA-NM e OM. In conclusion, the proposed extraction procedure in Politecnico di Torino (LM) is the most accurate.

7 References

- [1] M. Sampietro, «INTRODUZIONE AI DISPOSITIVI ELETTRONICI, Appunti delle prime lezioni del coorso di elettronica 1,» 2001;2002;.
- [2] G. Pozo, B.Romero e B.Arredondo, «Extraction of circuital parameters of organic solar cells using the exact solution based on Lambert W-function,» *SPIEDigitalLibrary.org/conference-proceedings-of-spie*, 2012.
- [3] A. O. Conde, F. J.Garcia-Sanchez, J. Muci e A. Sucre-Gonzalez, «A Review of diode and solar cell equivalent circuit model lumped parameter extraction procedures,» *Electronics and Energetics*, vol. 27, 2014.
- [4] C. R. OSTERWALD, «TRANSLATION OF DEVICE PERFORMANCE MEASUREMENTS TO REFERENCE CONDITIONS*,» *Solar Cells*, 18 (1986) 269-279 , 1985.
- [5] F. Spertino, J. Ahmad, A. Ciocia, P. D. Leo, A. F.Murtaza e M. Chiaberge, «Capacitor Charging method for I-V curve tracer and MPPT in photovoltaic systems,» *Solar Energy*, vol. 119, 2015.
- [6] F. Spertino, A. Ciocia, P. D. Leo, S. Fichera, G. Malgaroli e A. Ratclif, «Towards the Complete Self-Sufficiency of a nZEBs microgrid by Photovoltaic Generators and Heat Pumps: Methods and Applications,» *IEEE Transactions on Industry Applications*, 2019.

- [7] C. Coskun, U. Toygar, O. Sarpdag e Z. Oktay, «Sensitivity analysis of implicit correlations for photovoltaic module temperature: A review.,» *Journal of Cleaner Production*, 2017.
- [8] JCGM, Guide to the expression of uncertainty in measurement., Geneve,Switzerland, 1995.
- [9] S. Gulkowski, J. V. M. Diez, J. A. Tejero e G. Nofuentes, «Computational modeling and experimental analysis of heterojunction with intrinsic thin-layer photovoltaic module under different environmental conditions,» *Energy*, 2019.
- [10] A. Gastli, L. Benbrahim e M. Rhouma, «ANN-Based Extraction Approach of PV Cell Equivalent Circuit Parameters,» 2015.
- [11] R. Majdoul, E. Abdelmounim, M. Aboulfatah, A. Wahed Touati, A. Moutabir e A. Abouloifa, «Combined analytical and numerical approach to determine the four parameters of the photovoltaic cells models,» *1st International Conference on Electrical and Information Technologies ICEIT'2015*, 2015.
- [12] H. Ibrahim e N. Anani, «Evaluation of Analytical Methods for Parameter Extraction of PV modules,» *Energy Procedia*, 2017.
- [13] A. m. f. e. o. t. s. d. m. p. f. p. p. f. d. data, «Efstratios I. Batzelis ,» *IEEE Transactions on Sustainable Energy* .
- [14] A. V. Esmoris, «TRABAJO FIN DE MASTER. ALGORITMOS HEURISTICOS EN OPTIMIZACION,» 2013.
- [15] D. Fébba, R. Rubinger, A. Oliveira e E. C. Bortoni, «Impactsof temperature and irradiance on polycrystalline silicon solar cells parameters,» *Solar Energy*, 2018.

- [16] G. Xiong, J. Zhang, D. Shi e Y. He, «Parameter extraction of solar photovoltaic models using an improved whale optimization algorithm,» *Energy Conversion and Management*, 2018.
- [17] S. Gómez, D. Patiño e C. Vélez, «Variante del método de Nelder & Mead para optimización de funciones multivariadas,» *Cuaderno ACTIVA, ISSN 2027-8101*, 2012.
- [18] K. Kamatani, «Random walk Metropolis algorithm in high dimension with non-Gaussian target distributions,» *Stochastic Procedure and their Applications*, 2019.
- [19] D. W. Marquardt, «An Algorithm for Least-Squares Estimation of Nonlinear Parameters,» *Journal of the Society for Industrial and Applied Mathematics*, vol. 2, 1963.
- [20] K. LEVENBERG, «A METHOD FOR THE SOLUTION OF CERTAIN NON-LINEAR PROBLEMS IN LEAST SQUARES».
- [21] A. I. Chrysochos, T. fi. A. Papadopoulos e G. K. Papagiannis, «Robust Calculation of Frequency-Dependent Transmission-Line Transformation Matrices Using the Levenberg–Marquardt Method,» *IEEE TRANSACTIONSONPOWERDELIVERY*, vol. 29, n. 4, 2014.
- [22] A. K.Tossa, Y. Soro, Y. Azoumah e D. Yamegueu, «A new approach to estimate the performance and energy productivity of photovoltaic modules in real operating conditions,» *Solar Energy*, vol. 110, 2014.
- [23] «IEC EN 60891 standard – Procedures for temperature and irradiance corrections to measured I-V characteristics,» 2009.
- [24] A. K. Tossa, Y.M.Soro, Y. Azoumah e D.Yamagueu, «A new approach to estimate the performance and energy productivity of a

photovoltaic modules in real operating conditions,» *Solar Energy*, vol. 110, 2014.

[25] J. V. Munoz, G. Nofuentes, M.Fuentes, J. I. Casa e J.Aguilera, «DC energy yield prediction in large monocrystalline and polycrystalline PV plants: Time-domain integration of Osterwald's model,» *Energy*, 2016.

[26] M.Torres-Ramirez, G.Nofuentes, J.P.Silva, S.Silvestre e J.V.Munoz., «Study of analytical modelling approaches to the performance of thin film PV modules in sunny inland climates.,» *Energy*, 2014.

8 Appendix

8.1 Monocrystalline Trina SolarTSM-DD05A.08-P300

8.1.1 Electrical data at STC

Table 8-1: Main features for Trina SolarTSM-DD05A.08-P300

P_N	300 W
Power tolerance	0/+5 W
I_{SC}	9.77 A
V_{OC}	39.8 V
V_{MPP}	32.6 V
I_{MPP}	9.19 A
η	18.3 %

8.1.2 Cell temperature coefficients α , β , γ and NOCT

Table 8-2: NOCT and cell temperature coefficients for Monocrystalline Trina SolarTSM-DD05A.08-P300.

NOCT	44+/-2 °C
Power thermal coefficient γ_{PN}	-0.39 %/°C
Voltage thermal coefficient β_{Uoc}	-0.29 %/°C
Current thermal coefficient α_{Isc}	+0.05 %/°C

8.1.3 Specifications

Table 8-3: Main specifications for Trina SolarTSM-DD05A.08-P300

Dimensions	1650 mm x 992 mm x 35 mm
Weight	18.6 Kg
Type of cell	mono
Number of cells	60

The transversal and frontal sections of the PV module are shown.

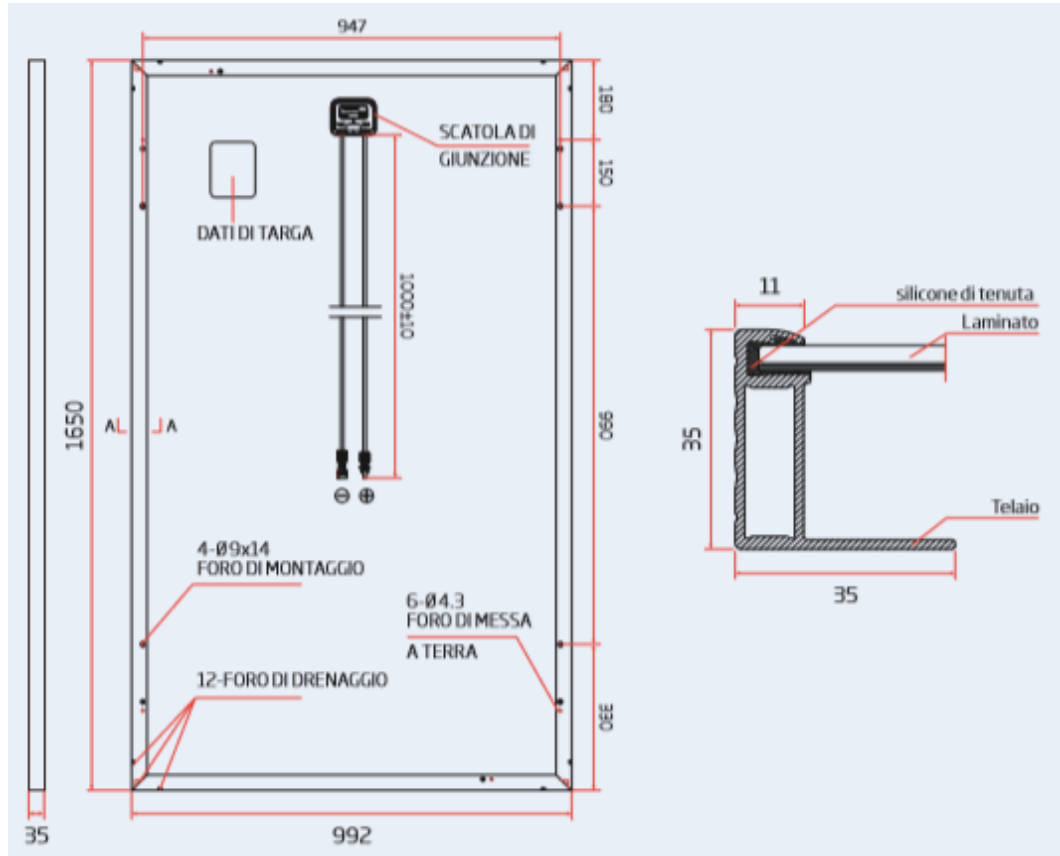


Figure 8-1: Transversal and frontal views for Trina Solar TSM-DD05A.08-P300

8.1.4 I - V curves provided by manufacturers

Here are reported the I - V curves provided by the manufacturers at different irradiance conditions. In the datasheet only the I - V curves related to the PV module of nominal power 305W are reported. (the module used in this study has a nominal power of 300 W)

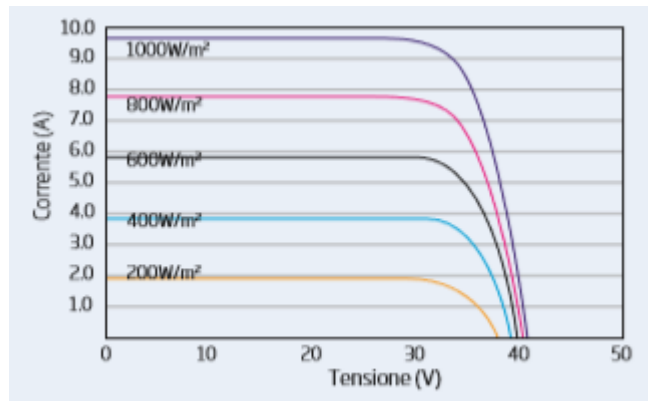


Figure 8-2: I - V curves at different irradiance values for Trina Solar TSM-DD05A.08-P305

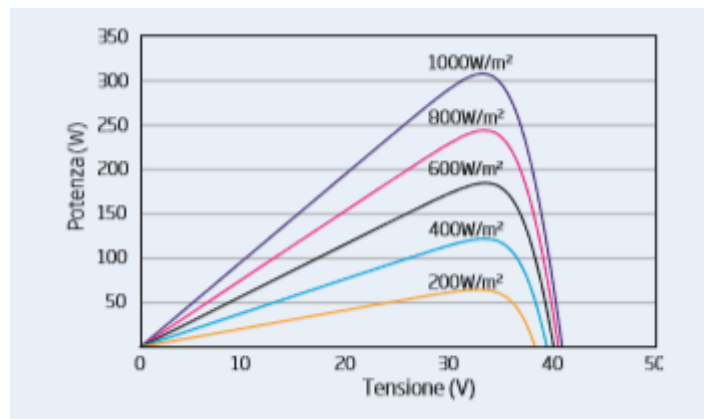


Figure 8-3: P-V curves dependence on irradiance for Trina Solar TSM-DD05A.08-P305

8.2 Polycrystalline JA-Solar JAP60S01 -P280

8.2.1 Electrical data at STC

Table 8-4: Main features for Polycrystalline JA-Solar JAP60S01 -P280

P_N	280 W
Power tolerance	0/+5 W
I_{SC}	9.37 A
V_{OC}	38.65 V
V_{MPP}	31.61 V
I_{MPP}	8.86 A
η	17.1 %

8.2.2 Cell temperature coefficients α , β , γ and NOCT

Table 8-5: NOCT and cell temperature coefficients for Polycrystalline JA-Solar JAP60S01 -P280

NOCT	45+/-2 °C
Power thermal coefficient γ_{PN}	-0.40 %/°C
Voltage thermal coefficient β_{Uoc}	-0.33 %/°C
Current thermal coefficient α_{Isc}	+0.058 %/°C

8.2.3 Specifications

Table 8-6: Main specifications for Trina SolarTSM-DD05A.08-P300

Dimensions	1650mm×991mm×35mm
Weight	18.2kg ±3%
Type of cell	poly
Number of cells	60

In **Errore. L'origine riferimento non è stata trovata.**4, The transversal and frontal sections of the PV module are shown

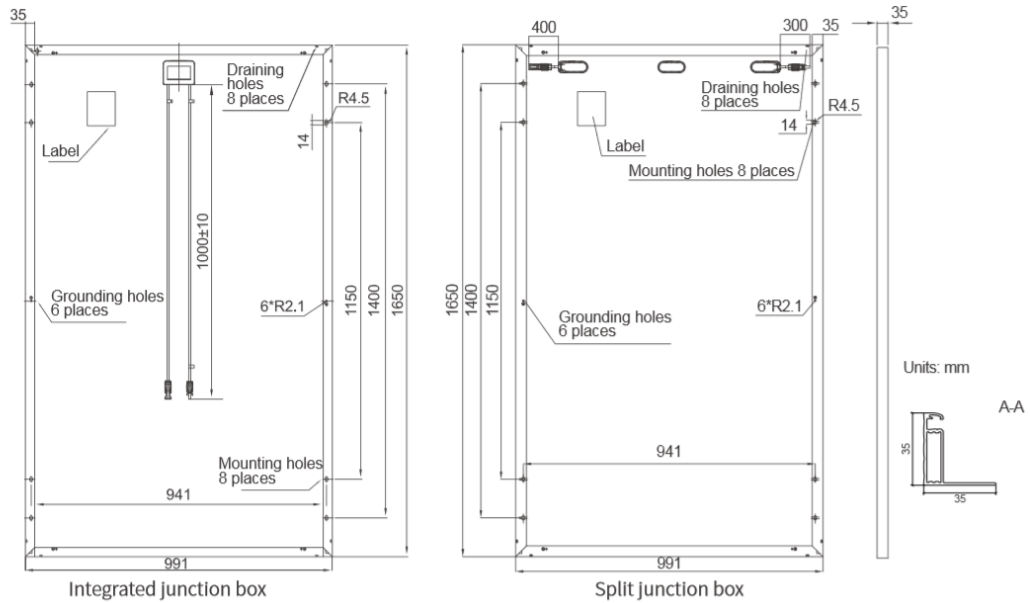


Figure 8-4: transversal and frontal for the two sides (front and back) views for Polycrystalline JA-Solar JAP60S01 -P280

8.2.4 $I-V$ curves provided by manufacturers

Here are reported the $I-V$ curves provided by the manufacturers at different irradiance and cell temperature conditions. In the datasheet only the $I-V$ curves related to the PV module of nominal power 270W are reported. (the module used in this study has a nominal power of 280 W)

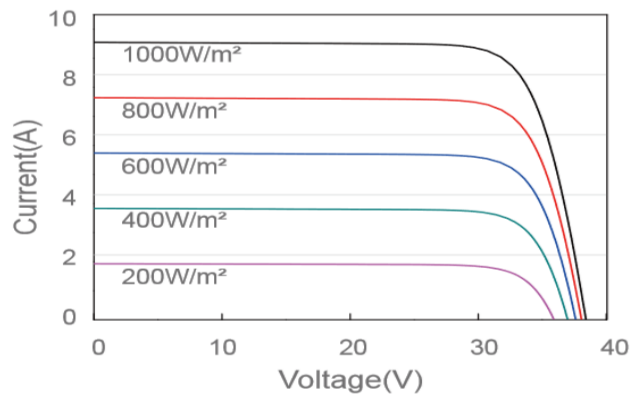


Figure 8-5: $I-V$ curves at different irradiance values for JA-Solar JAP60S01 -P270

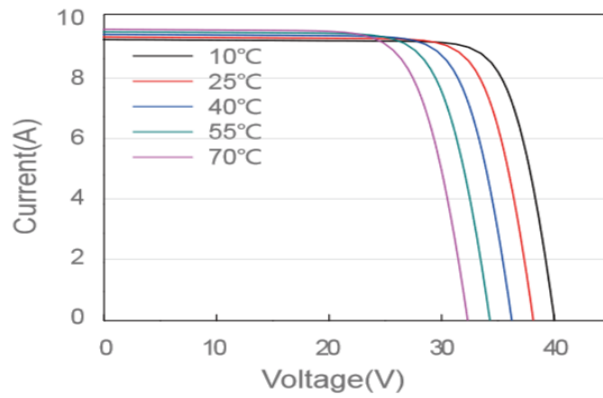


Figure 8-6: *I-V* curves at different cell temperature values for JA-Solar JAP60S01 -P270

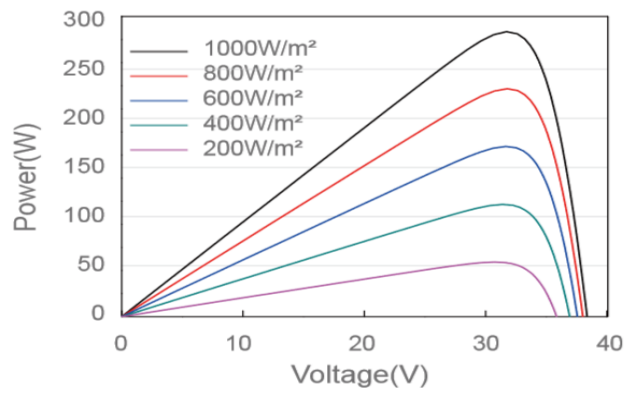


Figure 8-7: P-V curves dependence on irradiance for JA-Solar JAP60S01 -P270

8.3 Monocrystalline Luxor LX-100M -P100

8.3.1 Electrical data at STC

Table 8-7: Main features for Luxor LX-100M -P100.

P_N	100 W
Power tolerance	0/+5 W
I_{SC}	8.24 A
V_{OC}	21.60 V
V_{MPP}	18.70 V
I_{MPP}	5.39 A

8.3.2 Cell temperature coefficients α , β , γ and NOCT

Table 8-8: NOCT and cell temperature coefficients for Luxor LX-100M -P100

NOCT	45+/-2 °C
Power thermal coefficient γ_{PN}	-0,49 %/°C
Voltage thermal coefficient β_{Uoc}	-0.35 %/°C
Current thermal coefficient α_{Isc}	+0.05 %/°C

8.3.3 Specifications

Table 8-9: Main specifications for Luxor LX-100M -P100

Dimensions	1194mm×542mm×35mm
Weight	7.8 kg
Type of cell	mono
Number of cells	36

In **Errore. L'origine riferimento non è stata trovata.**8, The two frontal sections of the PV module are shown

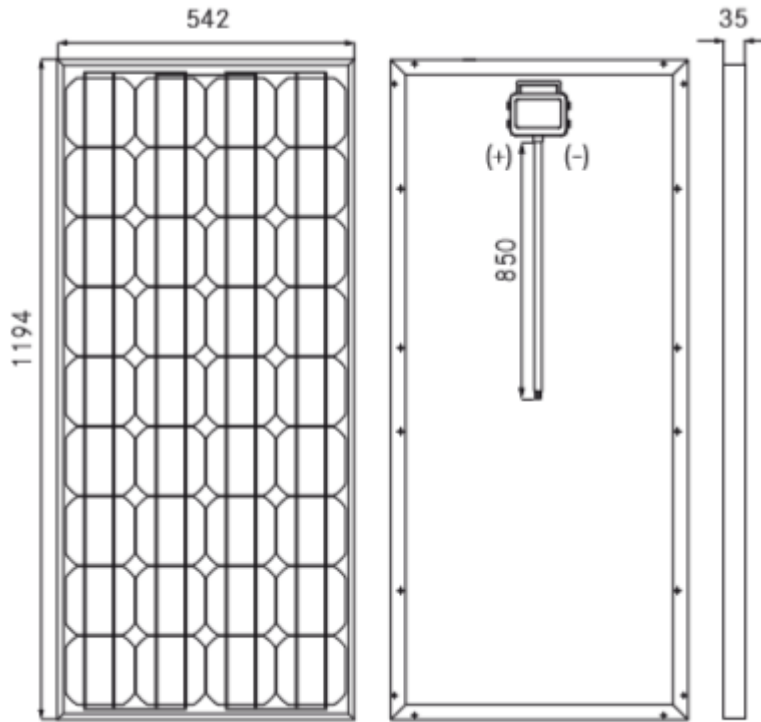


Figure 8-8: Frontal views of the two sides (front and back) for Luxor LX-100M -P100

For the for Luxor LX-100M -P100 the I-V curves and the P-V curves at different irradiance and cell temperature conditions are not reported by manufacturers.